Control of Adhesion in Carbon Fiber Reinforced Polymeric Composites

Luke Georges El Khoury

A dissertation

submitted in partial fulfillment of the

requirements for the degree of

Doctor of Philosophy

University of Washington

2023

Reading Committee:

John C. Berg, Chair

Brian Hayes

Ramulu Mamidala

Benjamin Rutz

Program Authorized to Offer Degree:

Chemical Engineering

University of Washington

Abstract

Control of Adhesion in Carbon Fiber Reinforced Polymeric Composites

Luke Georges El Khoury

Chair of the Supervisory Committee:
John C. Berg
Chemical Engineering

Fiber-reinforced polymeric composites have grown in popularity for use in structural materials due to their low weight, high specific strength, high toughness, customizability, and versatility. A critical element to the performance of composite materials is how well fiber reinforcements adhere to the surrounding polymer matrix. Different applications can benefit from different levels of adhesion, so its control is a crucial element in the design of a composite. One general drawback to the widespread use of composites is that their production with the desired adhesion level is tedious and time-consuming. It was therefore useful to investigate which steps of production might be shortened and what effects this might have on composite properties. It was found that when controlling for the degree of cure, higher temperature and faster curing schedules lead to an increase in fiber-matrix adhesion due to a freezing of internal squeezing stresses. However, the superficial increases of interfacial adhesion would return to baseline levels, but not below, if the polymer matrix was given time at elevated temperatures to anneal, decreasing internal stresses. Additionally, it was found that tertiary cure-accelerating

compounds increased curing speed while having no deleterious effect on adhesion. Lastly, it was found that fiber handling agents, or sizings, had no noticeable effect on adhesion.

Polyolefins have garnered interest for use in fiber-reinforced composites because of their low cost, high toughness, high impact strength, and excellent corrosion resistance. However, they adhere poorly to most substrates, including carbon fibers, leading to poor composite properties. Thus, different techniques to increase polyolefin-carbon fiber adhesion were explored. While most produced only modest improvements, the most promising were the addition of maleic anhydride block co-polymers to the polyolefin (polypropylene) together with the use of 6-azidosulfonylhexyl triethoxysilane to treat carbon fiber surfaces.

While increases in interfacial adhesion generally improve composite performance, there are instances where excessive adhesion can result in undesirable properties such as brittleness. Therefore, methods were investigated to tailor interfacial adhesion in carbon fiber-reinforced thermoset composites in an inexpensive, scalable manner. Treatment of the carbon fibers by a room-temperature vulcanizing (RTV) silicone dispersion in a paraffinic solvent (Isopar^{TM} L) produced reductions in adhesion and corresponding increases in toughness in a controlled manner depending on the amount of silicone added. “Charpy” impact toughness for 12k carbon fiber composite tows was approximately doubled with the addition of silicone to the interface, with only limited losses in modulus.

TABLE OF CONTENTS

LIST OF FIGURES

LIST OF TABLES

ACKNOWLEDGEMENTS

I am incredibly grateful to the following groups and people.

Dr. John Berg for his help and guidance over the years. His unwavering support and advocacy for students serve as an inspiration for us all.

The helpful insights and conversations with my committee: Dr. Brian Hayes, Dr. Benjamin Rutz, Dr. Ramulu Mamidala, and Dr. Anthony Dichiara.

My lab mates, coworkers, and friends, whom I worked with over the years: Ben, Harrison, Kyle, and Julius.

All the students from ChemE 455 and ChemE 499 whom I worked with over the years.

The technicians and device managers: Kameron, Ben, and Bill.

The people at Materials Sciences, LLC, Adherent Technologies, Inc., and U.S. Army research centers.

Financial support by subcontract from Materials Sciences, LLC. (Horsham, PA) under U.S. Army SBIR A18-115, and the Surfaces, Polymers, and Colloids center (SPC) at the University of Washington, Seattle.

DEDICATION

To my parents, Rebecca and Georges, my brothers, Dimitri and Constantino, and my dog, Wally.

Thank you for your unconditional love and support.

Chapter 1. INTRODUCTION

1.1 Document Outline

The first chapter of this thesis will deliver a brief introduction into the motivation of each project completed and will additionally describe some of the phenomena and commonly used terms for the materials discussed.

Chapters two through five will discuss the control of adhesion in different testing systems. While all address composite production and interfacial adhesion, each is distinct in its own way. Therefore, in place of a total literature review for chapter one, each chapter will contain its own literature review regarding the project of focus.

Lastly, chapter six will provide the motivations and suggestions for any future projects that can be of interest to future researchers.

1.2 Overview

Desirable structural materials which are lightweight, strong, tough, and durable have been increasingly sought after for the essential modernization and growth of our economy and infrastructure. Given that polymeric composite materials (Figure 1.1) meet most of the above criteria by minimizing weight and sharing both strength (through reinforcing fibers) and flexibility (through suitable matrix properties), they serve as promising candidates for the growing demand for better performance. Ideally, composites will continue to permeate different facets of industry. However, the pace of future advancements can only occur if further plans for the optimization of composite properties, fabrication, and processing are rigorously elucidated. The themes of this work are to illuminate and investigate processes for the optimization of composite properties in both thermosets and thermoplastics through the lens of interfacial

adhesion. While many factors can influence the mechanical properties of fiber-reinforced polymeric composites, one of the most critical is fiber-matrix adhesion, and therefore, will be given nearly the entirety of attention throughout this thesis.

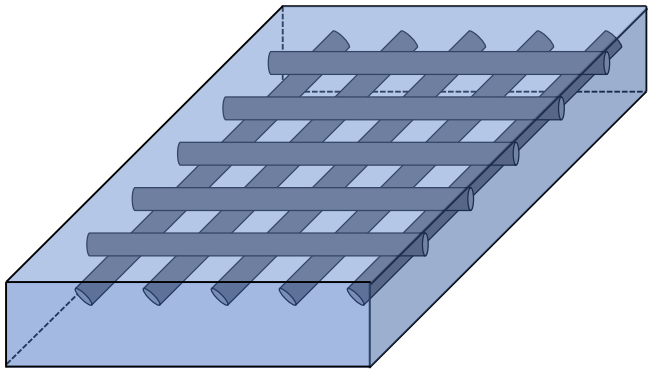

Figure 1.1: Graphic of fiber-reinforced composite.

An important goal for many manufacturers is to pursue increased production speed with minimal depreciations in physical properties. The act of curing thermoset polymers for composite fabrication and processing can prove to be one of the timeliest, and therefore costly, stages for product output. The first set of work aims to study how altered curing schedules for thermoset polymer composites alter interfacial adhesion and, by inference, the physical properties of the composites. The general effects of higher temperature cures, multi-stage cures, curing accelerants, fiber handling agents, and residual stresses are important aspects to study. However, to make proper comparisons, it is imperative to relate properties of composites that have undergone the same degree of cure or cross-linking, in contrast to earlier studies. Overall, it was found that higher temperature curing elicited higher apparent adhesion due to rapid cross-linking and freezing of internal stresses. Nevertheless, much of the observed increase in apparent adhesion dissipated with sufficient thermal relaxation above the glass transition temperature. In

addition, it was found that commonly used curing accelerants, while increasing the curing rate, did not ultimately cause residual stress accumulation of sufficient magnitude to alter the apparent adhesion, regardless of the curing temperature. Next, it was found that isothermal curing, compared to traditional two-stage curing, did induce larger residual stresses, which led to higher apparent adhesion. Lastly, it was found that typical handling agents had sufficient time during the curing process to, presumably, diffuse from the fiber surface into the bulk matrix and consequentially did not affect interfacial or adhesive properties.

While thermosets still lead in popularity for many high-performance applications, there has been a growing market need for lower-performance thermoplastic polymeric composites in applications such as boats and sporting equipment. Therefore, the second piece of work was undertaken to examine methods to enhance interfacial adhesion between polyolefins and carbon fiber. It was initially reconfirmed that polyolefin-carbon fiber systems exhibit profoundly low adhesion. Methods to enhance adhesion were generally modest but pointed to avenues for future research, such as using maleic anhydride paired with appropriate silane coupling agents, pairing strong peroxides with vinyl-silanes, and altering the interphase modulus.

The exploration of methods for tailoring and optimizing interfacial adhesion is equally important for improving polymer composites and is addressed in the third set of work. Generally, higher interfacial adhesion can lead to improved physical properties, but there are cases where excessive adhesion can lead to premature failure and brittle fracture. Furthermore, because interfacial debonding can act as a mechanism for stress relief, when removed through excessive interfacial bonding, an important avenue for energy release is hindered.

It was found that varying concentrations of room temperature vulcanizing silicone and paraffinic solvent (Isopar^{TM} L) could be applied to carbon fiber surfaces and result in the

tailoring and effective control of interfacial adhesion. For single fiber studies, silicone was added to fiber surfaces in a layer-by-layer fashion, and interfacial adhesion was directly correlated with the number of silicone layers added to the fiber surface. Since interfacial adhesion has been shown to affect the mechanical properties of composites, they were therefore of interest to be examined. Composites comprised of 12k unidirectional fibers were created and tested for mechanical properties. For fabrication, fiber tows were dip coated in solutions of varying concentrations of silicone, dried, soaked in an epoxy-hardener mixture, and cured. Different mechanical properties were tested, such as tensile, flexural, and impact strength. It was found that tensile properties all linearly degraded with increasing amounts of silicone. However, flexural properties had mixed results of increases and decreases in mechanical properties as the amount of interfacial silicone increased. “Charpy” impact toughness of fiber tow composites was tested, and as expected, it was found that increases in interfacial silicone resulted in linear increases in impact toughness. The rheological properties of pure cure silicone were tested and found that significant values of $\tan(\delta)$ and G” were likely to contribute to such increases in impact toughness.

Lastly, the derivation and use of curing kinetic models for thermoset polymers may prove helpful when designing curing schedules. Additionally, their use may give insight into improving curing schedules. Traditionally, curing kinetic models require prior knowledge of the reaction system itself (i.e., reaction order, speed, geometry, and activation sites). Given the complexity of thermoset curing, paired with the relative inaccessibility of the aforementioned reaction characteristics, accurate modeling can become an increasingly difficult task. An attempt at alleviating such drawbacks has been the introduction of “model-free kinetics,” which removes the need for a theoretical reaction model by allowing Arrhenius parameters to take different

values as the reaction progresses. Many iterations have been developed since the inception of model-free kinetics, where the most recent and commonly used is the “advanced isoconversional” method developed by Dr. Sergey Vyazovkin.

Overall, the advanced isoconversional technique is an empirical modeling method that postulates that regardless of the curing temperature path for a complex reaction, the speed of reaction progression will be linearly proportional to the activation energy of that isoconversional step. Therefore, a mathematical analysis of multiple empirical temperature sweeps in a thermogravimetric analysis device or differential scanning calorimetry device can deliver activation energy as a function of reaction completion, regardless of the temperature path. These values can then be used for kinetic predictions for any arbitrarily chosen temperature path.

Even though its use is present in many modeling software packages, there is a relative deficiency of succinct explanations for its mathematical underpinnings. Therefore, an in-depth walkthrough of the advanced isoconversional method is completed to be a possible reference for future researchers.

1.3 Polymer Plastics

1.3.1 *Thermosets*

Thermoset polymers are considered to be a subgrouping of plastics that start as a liquid mixture of monomers and irreversibly transform into a solid after the addition of energy through heat, UV, or electron beam irradiation[1] through a process known as cross-linking[2]. Their curing times can vary from the order of seconds to days. Typically, thermoset mixtures are comprised of a larger molecule, such as epoxies, phenols, esters, and urethanes, and a smaller hardener, such as cyclic amines or anhydrides.

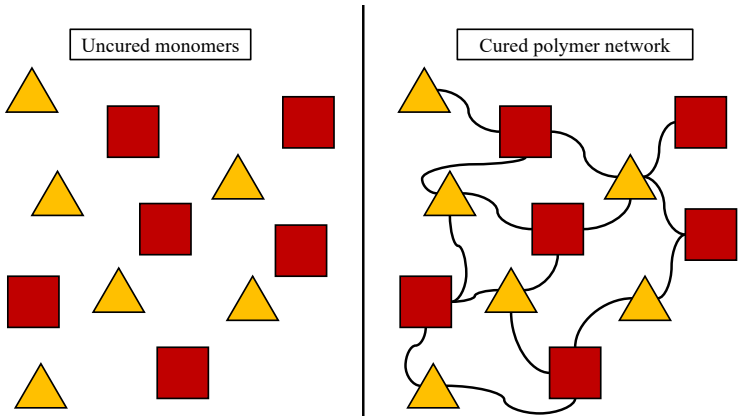

Figure 1.2: Cartoon of a pre-cured thermoset (left) and a fully cured thermoset (right). The orange triangle and red squares represent two different monomers that make the thermoset, and black lines represent chemical linkage.

As shown in Figure 1.2 above, after fully reacting, referred to as cross-linking, the homogeneous mixture of monomers becomes a polymer chain where every monomer is connected through a network of covalent bonds. Theoretically, no two monomers are separated, and the ultimate molecular weight of the fully cured polymer approaches infinity.

The curing process of thermosets is intricate and can undergo many different phases depending on the degree of cross-linkage and curing temperature. Conversion temperature transformation (CTT)[3] or time temperature transformation (TTT) diagrams are often used to map each specific region. In general, there are five main phases that the polymer network can take during a cure path, and are shown below in Figure 1.3.

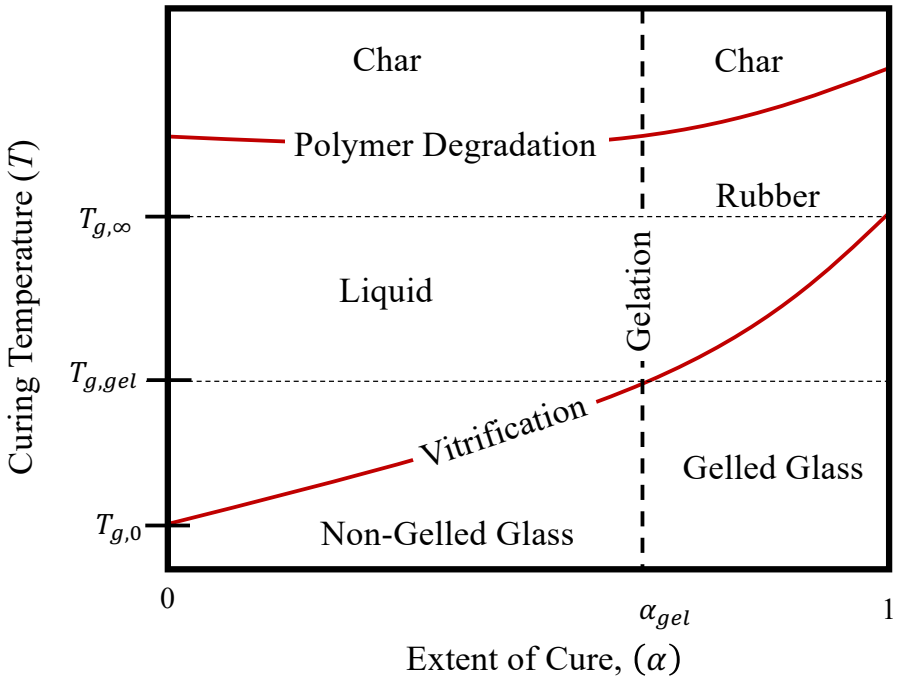

Figure 1.3: Illustration of conversion temperature transformation graph.

As shown above, the extent of cure or cross-linkage, α, is represented on the x-axis, and the curing temperature, T, is displayed on the y-axis[1]. As the polymer network approaches a fully cured state ($\alpha = 0 \rightarrow 1$), there is a critical extent of conversion, α_{gel}, where the polymer network grows large enough to transition the material from liquid-like to solid-like. This can be rheologically estimated as the point where the storage modulus, G', grows to equal the loss modulus, G". More precisely, it is defined as the point where the ratio of G" to G', otherwise known as $\tan(\delta)$, becomes independent of rheological testing frequency[1].

The second important transition that a thermoset polymer undergoes is called vitrification. When scanning from a low to high ambient temperature, the polymer network will undergo a significant change in storage modulus, G', and transition from a rubber or liquid into a glass[1]. The temperature of this transition is denoted as the glass transition temperature, T_g, and can change in value depending on the polymer composition and degree of cure. At the glass

transition temperature, polymers achieve greater mobility and rotational freedom[4], giving the polymer more rubber or liquid-like characteristics. Three distinct glass transition temperatures are recognized on the CTT diagrams. The first is $T_{g,0}$, which represents the glass transition temperature of a completely uncured mixture of monomers ($\alpha = 0$). The second value is $T_{g,gel}$, and represents the glass transition temperature at which the solid-like behavior of the polymer system is approximately equal to the liquid-like behavior ($G''/G' = tan(\delta) \approx 1$). The final value, $T_{g,\infty}$, is the glass transition temperature of a completely cured thermoset polymer system ($\alpha = 1$). Additionally, above a defined temperature, the polymer will begin degrading char.

Because they are liquid before any curing has occurred, thermosets are often easier to use for manufacturing than thermoplastics (section 1.3.2) and can flow into complex geometries before any curing is needed. Compared to thermoplastics, however, they are difficult to recycle[5] and can pose environmental and health challenges. Attempts are currently underway to develop bio-based thermosets, however they are still relatively nascent[6–8] .

1.3.2 *Thermoplastics*

Thermoplastics are a separate subgrouping of plastics, and unlike thermosets, differ because they are purchased in a solid rather than liquid form, and do not require any chemical reactions or cross-linkage for their use. Rather, only physical phase changes are required for fabrication with them. Specifically, heating above their glass transition temperature, T_g, to become pliable. Some common examples of thermoplastics are polypropylene, polyethylene, polyvinyl chloride, polyester, polystyrene, nylon, and poly methyl methacrylate.

The selection of thermoplastics varies widely both in chemical makeup and physical properties, depending on the application. They can be single macromolecules or block-copolymers made from links of multiple different monomer chains[9]. Additionally, their

molecular weight (directly related to chain length) can also vary widely and can affect properties such as modulus and T_g. Important parameters used to assess a thermoplastic's chain length and the variance of its chain length are the number average molecular weight, M_n, weight average molecular weight, M_w, and the polydispersity. These parameters are pictured in Figure 1.4.

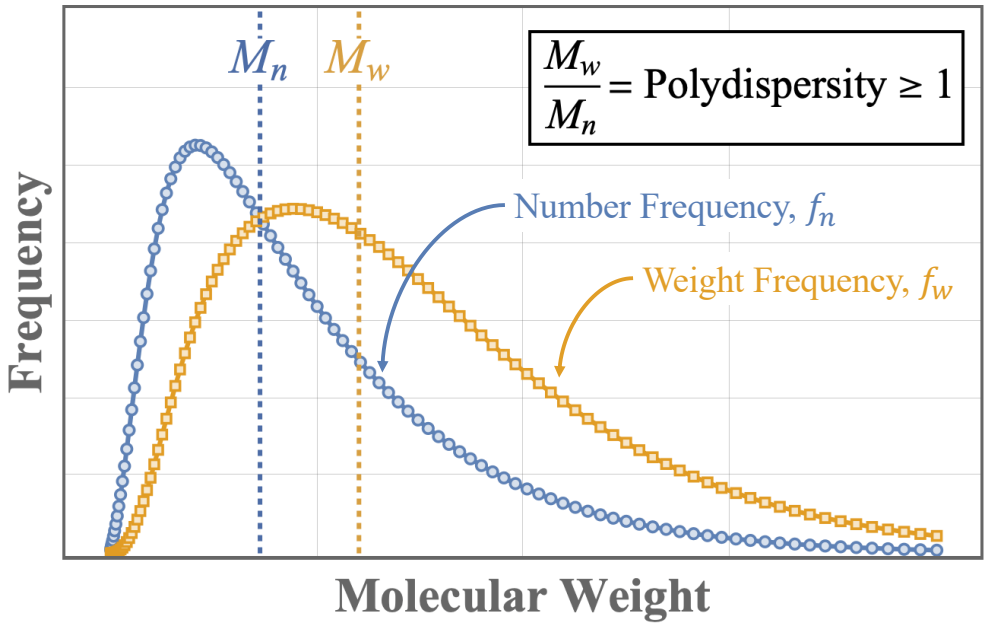

Figure 1.4: Sample graphic of the number frequency (blue circles) and weight frequency (orange squares) distribution of a polymer versus its molecular weight.

As shown above, any grouping of polymers will contain a distribution of chain lengths and molecular weights. Additionally, depending on the type of frequency function, the distribution can change in shape. Two commonly used relations for categorizing polymers are the number-average molecular weight and the weight-average molecular weight, and their mathematical representations are shown below[10,11]. The number-average molecular weight describes the average molecular weight for the group of polymers based on the total number of polymers in each size bin and is described in Eq. (1.1).

$$M_n = \frac{\sum N_i M_i}{\sum N_i} = \sum X_i M_i \tag{1.1}$$

Where N_i and M_i are the total number and molecular weight of polymer length *i*, respectively. And X_i is the mole fraction of polymer length *i*. Additionally, M_n can be understood as the point which bisects the integral area under the frequency curve into two equal parts.

$$\int_{M_{min}}^{M_n} X_i dM = \int_{M_n}^{M_{max}} X_i dM = \frac{1}{2} \int_{M_{min}}^{M_{max}} X_i \, dM \tag{1.2}$$

Where M_{min} and M_{max} are the minimum molecular weight and maximum molecular weight, respectively.

Second, the weight-average molecular weight is based on the average molecular weight of the group of polymers based on the proportion of the total weight of polymers in each size bin. Mathematically, the function is described in Eq. (1.3).

$$M_w = \frac{\sum (N_i M_i) M_i}{\sum (N_i M_i)} = \frac{\sum w_i M_i}{\sum w_i} = \sum W_i M_i \tag{1.3}$$

Where the quantity $(N_i M_i)$ is equal to w_i and is the total weight of polymer length *i*, and W_i is the weight fraction of polymer length *i*. A similar analysis, such as in Eq. (1.2) can be used to find M_w by substituting W_i for X_i.

It should be noted that the weight-average molecular weight will always be greater than or equal to the number-average molecular weight because weight averages give greater influence to larger polymer chains (as pictured in Figure 1.4). Furthermore, the dispersion or variation of molecule size for a group of polymers is directly related to M_w/M_n, which is known as the polydispersity index (PDI)[12], and will always be greater than or equal one. As the PDI for a mixture approaches one, it signifies that all the polymers have a smaller variance in size and

approach a monodisperse distribution. Practically, mixtures with a PDI near one will generally be more expensive and difficult to manufacture.

In contrast to thermosets, thermoplastics are more ubiquitous in lower-performance products such as Tupperware, water bottles, automobiles, and clothing. The production of thermoplastic materials often involves elevated-temperature injection molding and the use of hot-presses. However, compared to thermosets, thermoplastics also offer the advantage of being recyclable in most cases.

Due to being solid at room temperature and highly viscous when melted, thermoplastics also pose difficulties for composite production, particularly regarding the complete saturation of plastic throughout the fiber reinforcement[13–15]. However, they have recently received more attention for composite production due to the introduction of higher-performance thermoplastic polymers, faster production techniques, their recyclability, and the possibility of being blended with thermosets[16–18].

1.4 Carbon Fibers

Carbon fibers, as their name suggests, are small fibers in the size range of 5-10μm that consist primarily of elemental carbon with small amounts of oxygen, nitrogen, hydrogen, and other trace elements[19]. Their mounting popularity is due to physical properties such as high modulus, high strength, and low weight[19–23]. Structurally, they are comprised of a small crystalline network of hexagonal carbon rings, where the nature of the microstructure itself can affect properties such as the fiber modulus[23]. Current industries which use carbon fibers include sporting, defense, wind energy, and aerospace[21]. Even though the demand for carbon fibers has been increasing rapidly[21], their production is intricate and complex, which can hamper higher throughput production.

While there are different types of carbon fibers, such as those made from pitch[24], fibers fabricated from polyacrylonitrile (PAN) are the most widely used today[25]. The production of PAN-based fibers begins with the polymerization acrylonitrile[20] to a final molecular weight of approximately 100,000g/mol[26]. Afterwards, the slurry is cleaned, dried into a powder, reconstituted into an organic solvent, and spun through extruding holes to make PAN (also known as acrylic) fibers. Then, the PAN fibers pass through multiple drawing and cleaning stages to further reduce their diameter.

After the spinning and drawing stage, the fibers are then heat treated through a sequence of different temperatures and environments[19,20,26]. First, they are oxidized in air with a temperature range of 200-300℃. During this step, triple-bonded CN groups covalently react with their nearest neighbor to form carbon rings. Finally, the fibers are carbonized in an oxygen-free environment at temperatures from 1000℃ to as high as 2000℃, depending on the desired carbon content. If even higher carbon content is desired, then carbonization will be followed by graphitization, which can occur at temperatures of approximately 2000℃-3000℃. This process can be further visualized in Figure 1.5.

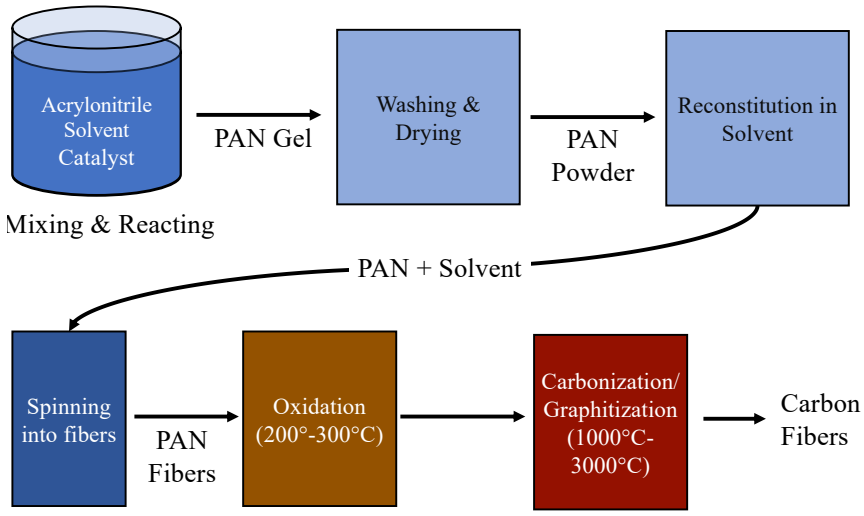

Figure 1.5: Block diagram for the creation of polyacrylonitrile-derived carbon fibers

After fabrication, the surface of carbon fibers is relatively bare and non-reactive. Given that there is a deep relation between carbon surface energy, adhesion, and carbon fiber reinforced composite performance[27], the fiber will finally undergo surface treatment. Carbon fibers can also be electrochemically oxidized in an acid bath with other electrolytes to increase the surface energy through oxygen functional groups.

Finally, PAN carbon fibers are surface treated with either commercial or custom 100-200nm coatings, often referred to as "sizing"[28,29]. Sizings can be covered on the fiber surface in the form of a solution or emulsion of polymers[30]. Additionally, the functional groups supplanted onto fiber surfaces will vary from system to system, contingent on the application and resin system being used. Overall, by increasing the functionality and the polar surface energy of carbon fibers[28], sizings are hypothesized to aid in resin wettability and promote adhesion. They are also hypothesized to protect carbon fibers from handling damage and unwanted reactivity[29].

The intricate production process of carbon fiber manufacturing, coupled with the wide array of surface treatments available, makes carbon fibers a valuable tool for current composite production and the future of materials research. Furthermore, new frontiers for carbon fiber production are also underway to aid with sustainability, decreasing cost, and increasing production throughput. Among them are the fibers made from biomass such as lignin and cellulose[31–34] rather than the traditionally used petroleum products.

1.5 ADHESION

The overwhelming majority of work presented in this document is centered around fiber-matrix adhesion. This is of particular importance because, as discussed in the sections below, adhesion, or "stickiness," between carbon fiber reinforcements and the surrounding polymer

matrix can significantly affect the composite's performance. Therefore, before discussing fiber-matrix adhesion, it may be found useful to preemptively discuss the broader topic of adhesion.

Currently, there is no universally accepted definition of adhesion, and different scientific sources all describe it somewhat differently. However, all definitions of adhesion describe the same themes. For example, Lacombe[35] attempts to define adhesion as the degree of the tendency for two materials to stick to each other that can be derived from qualitative, semiquantitative, or quantitative measurements. Whereas Butt et al.[36] quantitatively define adhesion as "the energy required to dismantle the interface between two materials."

However, adhesion is a complex phenomenon, and it is often observed that derivations of the magnitude of adhesion based purely on thermodynamic principles can widely differ from adhesion measured through physical experimentation. In other words, there exists a significant difference between thermodynamic adhesion predictions and real-world tests. Therefore, Mittal[37] defines two distinct types of adhesion. The first being thermodynamic or reversible adhesion, and the second being experimental or practical adhesion.

Thermodynamic adhesion between two surfaces (A and B) is mathematically defined in Eq. (1.4) as the sum of the two free surface energies subtracted by their shared interfacial surface energy[37].

$$W_{AB} = \sigma_A + \sigma_B - \sigma_{AB} \tag{1.4}$$

Where W_{AB} is the work of adhesion, σ_A and σ_B are the free surface energies of materials A and B, respectively, and σ_{AB} is the shared interfacial energy.

However, practical adhesion is not as easily quantified, and is often test and application dependent. This is because during delamination (the uncoupling of two materials), plastic and

other deformations must also be accounted for in addition to intermolecular forces[38]. Therefore, the total magnitude of adhesion can be shown in Eq. (1.5)

$$G = W_{AB} + W_{other} \tag{1.5}$$

Where G is the total fracture energy required to separate two surfaces at their interface, W_{AB} is the work of adhesion, and W_{other} is the remaining additional work dissipated during the deformation of the testing samples. Interestingly, it has been shown that because the W_{other} term can be orders of magnitude[38] higher than W_{AB}, there is often little information on how intermolecular forces affect the total adhesion. Additionally, it is sometimes difficult to disambiguate between adhesive (at the interface) and cohesive (through one of the materials) failure. Consequently, using different testing methods, even on the same material system, can elicit different values of apparent adhesion, all of which are contingent on the modes of failure and extent of plastic deformation. Therefore, it is commonly understood that when testing adhesion, different testing methods rarely deliver the same values of adhesion, and this leads authors such as Hull[39] to state that "no single, reliable method of testing thin film adhesion exists." This leads to the necessity of choosing adhesion tests that match the desired application of the materials.

The complexities of adhesion can be more easily comprehended when factoring in its different causes. According to Berg[40], adhesion has three other mechanisms outside of just contact/intermolecular interactions: diffuse interphase adhesion, mechanical interlock, and electrostatic adhesion. A sample illustration of these mechanisms can be seen in Figure 1.6.

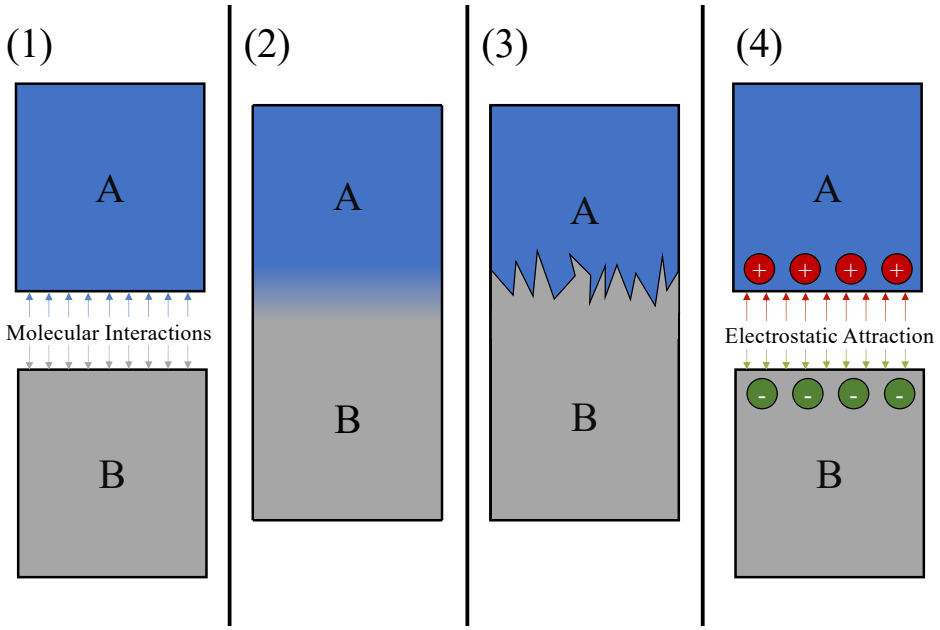

Figure 1.6: Different methods of adhesion through 1) molecular attraction, 2) diffuse interphase interlock, 3) mechanical interlock, and 4) electrostatic attraction. (Reproduced from illustrations by Berg[40])

As described above, adhesion has multiple mechanisms, and two or more often give meaningful contributions to the overall adhesion of the system. Therefore, no single method of increasing adhesion will work across different systems. However, there are general principles that can be used when optimizing the adhesion of a system.

Wettability is closely related to adhesion[41–43] because it determines the intimacy of contact between the two surfaces. Thus, while each case requires specific knowledge to best maximize adhesion values, high-energy surfaces (such as oxides) generally elicit better wettability and adhesion. Additionally, increasing surface roughness (when baseline contact angle is already less than 90°) will further increase wettability[44]. So methods to enhance adhesion and increase surface energy can include plasma treatments[45,46] or certain silanes. Conversely, the opposite is also true where decreases in surface energy and roughness (when

baseline contact angle is less than 90°) will decrease adhesion. This can be completed by supplanting a layer of low-energy material on the surface of the substrate.

In summary, adhesion is a complex and multifaceted topic where not only the thermodynamic properties of each material but also the physical characteristics of the system itself determine the effective or practical adhesion. Moreover, because of its intrinsic test-based variability, thermodynamic adhesion is a relatively inaccessible quantity. Therefore, attention should be given to the fact that even for identical material systems, different testing methods can give different absolute adhesion measurements. Regardless, trends for modifications of adhesion should remain consistent across different testing methods.

Chapter 2. THE EFFECT OF CURING SCHEDULES ON FIBER-MATRIX ADHESION IN CARBON FIBER – EPOXY RESIN COMPOSITES

*Sections of this chapter come from the journal publication:
ElKhoury L, Berg JC. The effect of curing schedules on fiber-matrix adhesion in carbon fiber epoxy resin composites. *Journal of Composite Materials* 2021; 56: 699–712.

2.1 CHAPTER SUMMARY

Fiber-reinforced polymeric composites are used in a large and growing number of applications, all requiring different property sets including the nature of the fiber-matrix adhesion to which the present work is addressed. Specifically, the number of curing cycles, curing temperature and schedule, degree of cure, use of accelerants, annealing, and the use of fiber handling agents are investigated for systems of Hexcel IM7 carbon fibers embedded in Epon862 (resin) and Epikure Curing Agent W (hardener) using the single-fiber-fragmentation method. The fractional extent of cure is monitored using differential scanning calorimetry (DSC), so that comparisons are made at the same degree of cure (99%). Single-stage curing at the highest temperature produces the highest apparent adhesion, and the use of accelerants significantly increases the curing rate while maintaining the same level of adhesion. Accelerants in some cases, however, decrease the plastic yield strength of the specimens. Annealing reduces induced residual stress and apparent adhesion, but not below the baseline achieved at lower curing temperatures. Plastic yield strength and apparent adhesion decrease for any degree of cure lower than 95%, while the use of handling agents shows no effect on adhesion.

2.2 INTRODUCTION

Fiber-reinforced polymeric composites are used in an enormous and growing number of applications, all requiring different property sets. The latter depend on the properties of the fibers and the matrix, the geometry of the lay-up, and on the nature of the fiber-matrix adhesion, to which the present work is addressed. The influence of interfacial chemistry on adhesion[47–51] in carbon-fiber reinforced thermoset composites has received wide coverage in the literature, and the influence of thermoset curing schedules [52–55] on the final properties of the material has been investigated. An important observation is that increasing curing temperature can decrease gelling time and thus hasten product throughput while also delivering increased strength and performance. In particular, literature on the accumulation of residual stresses[56,57]and thermal shrinkage [58–61] in the resin phase due to curing conditions has been compiled, revealing many effects of interest. A study by Jakobson et al.[62] showed that residual stresses are caused mainly by cure shrinkage from the cross-linking of polymers, rather than thermal expansion and contraction, while other studies[63] suggest that thermal expansion plays a more significant role. Regardless, both can therefore result in the "freezing in" of internal stresses. An interesting result of such resin shrinkage for fiber reinforced composites can be observed by the phenomenon of fiber waviness, which has been both observed and described mathematically.[64,65] Since residual stresses play a large role in the properties of composite materials and stem from curing conditions, it follows that they must influence fiber-matrix adhesion. An unpublished study by Kalantar and Drzal[66] suggested that curing time and temperature schedules may indeed have a significant effect on adhesion in such systems, and other related studies[67,68] have also shown that curing schedules can have secondary effects on the molecular architecture of thermoset polymers resulting in discernable differences in mechanical properties.

Studies done by Haider et al.[59] and Li et al. [23] showed that curing temperatures themselves do not affect the final cure shrinkage of a thermoset material; rather, shrinkage depends directly on the degree of cure. Therefore, it is reasonable to assume that all resins brought to the same degree of cross-linking would exhibit equivalent residual stress. However, since higher temperature cures gel more rapidly, both polymer mobility and time allotted for rearrangement towards a stress-free state are restricted, resulting in different degrees of stress accumulation. An important study performed by Wang et al.[61] elucidated this point by presenting how curing temperature and therefore curing speed, directly alter the residual stress state in an epoxy resin, and that rapid curing leads to higher internal stress.

In terms of mitigating the effects of residual stress accumulation, interest has also formed around post-cure heating (sometimes regarded as annealing). A study produced by Parlevliet et al.[63] displayed that post-process annealing of a cured polyurethane ("turane") significantly reduced residual strain by decreasing thermal expansion coefficients and strain-free temperature. Additionally, a study from Wang et al.[69] has shown that post-process annealing of thermoplastic composites may significantly influence apparent adhesion through the process of internal stress development, so it appears that the thermal history of polymers should also be taken into account in the design process.

In summary, as thermosets cure, they cross-link and undergo varying degrees of transformations, such as changes in modulus, thermal expansion coefficient alterations, expansion paired with contraction, resulting in increases or decreases in toughness and/or plasticity. Therefore, with the possibility of multiple confounding variables throughout the curing process, it is difficult to fully comprehend how curing schedules themselves affect

adhesion unless there is outside knowledge of the resin's apparent degree of cure or cross-linking.

Lastly, studies on the effects of resin-to-hardener ratio on cured thermoset properties such as residual stresses, adhesion, glass transition, and thermal expansion have been extensively explored[70–76]. In an important contribution to literature, Minty et al.[77] investigated the topic of how the ratio of amine groups to epoxy groups (Araldite 506 epoxy and triethylenetetramine system) affects the above stated physical properties in resin as well as the effect on interfacial strength between the polymer and glass fibers. The findings showed that amine/epoxy ratio significantly affected thermal expansion coefficients for both epoxy rich and amine rich mixtures above and below T_g. Also, while the mixture ratio greatly impacted cured polymer T_g itself, the effect on interfacial strength (for amine/epoxy ratios between approximately 0.5 and 2) was less affected. This effect on interfacial strength was also corroborated by Petersen et al.[76] In conclusion, amine/epoxy ratios affect residual stresses and can impact interfacial strength for composite systems.

During high temperature curing, particularly the early stages where fewer molecules are polymerized, and overall molecular weight is lower, the possibility for hardener volatilization can alter the original amine/epoxy ratio. Consequentially both polymer and composite interfacial properties can be affected by the type of curing schedule employed. Since competing phenomena such as rapid curing and stress accumulation, coupled with the possibility for stoichiometry alterations, a study into how curing schedules (number of stages and temperature) affect properties, specifically adhesion, is sought.

One difficulty in the quantitative interpretation of the results of the above-cited and related studies is that attention was not always given to the final extent of cure at which

comparisons were made. Since the extent of cure itself has a strong effect on thermoset composite properties, a standardized protocol is required in which the ultimate degree of cure is monitored and controlled, permitting comparison of different time-temperature schedules only between samples at the same degree of cure. The presence of accelerants has also been found to have profound effects on the curing process itself [78], but its influence on the level of adhesion obtained in samples cured to the same extent appears not to have been reported.

In addition to the importance of curing schedules to the properties of the composite is their importance to the economy of the production process. Curing protocols for some common thermosets such as epoxies and phenolic resins may require from 15 min to 20 h. Thus, resin curing can pose a costly, rate-limiting step in the manufacture of composite materials. Optimizing the curing schedule therefore may significantly reduce the cost of production.

The present study seeks to examine the effects of curing schedules on adhesion for unsized (unless specified otherwise) Hexcel IM7 carbon fiber (d = 5.2μm) - Epon862 (resin) and Epikure Curing Agent W (hardener) systems. In contrast to earlier work, the fractional extent of cure (α) is set to 99% in all cases, as monitored using differential scanning calorimetry (DSC), so that comparisons are made only between specimens at the same degree of cure. Fiber-matrix adhesion was measured using the single-fiber-fragmentation method outlined by Drzal.[79]

2.3 METHODS AND MATERIALS

2.3.1 *Differential Scanning Calorimetry (DSC)*

Differential scanning calorimetry was used in this study to determine curing times, total enthalpies of reaction, curing kinetics, glass transition temperatures, and other thermal properties during controlled heating schedules. In summary, the technique records the difference in heat required to maintain a set temperature between two pans, where one is a blank reference, and the

other contains the active sample. The endothermicity or exothermicity of the reaction will cause such differences in heat and are recorded. When the reaction is complete, there is no longer a difference in the heat required to maintain the temperature in both pans. The study was conducted using the TA Discovery DSC 2500 and TA Instruments Tzero Pans (TA Instruments, New Castle, DE). All tests were conducted with open pans under dry nitrogen. TRIOS software by TA instruments was used for analysis of results. For this study, a $5-10$ g stoichiometric mixture of EPON 862 and Curing Agent W (resin + hardener) were combined, well mixed, and then degassed for approximately 60 min. Both compounds have very low vapor pressures, so it was assumed their stoichiometric ratio remained constant during degassing. Once prepared, approximately $3-10$ mg of the resin was carefully placed into a TZero DSC pan (TA Instruments, New Castle, DE), loaded into the TA Discovery DSC 2500, and run with an open lid under dry nitrogen. Curing times were evaluated by running each sample in the DSC device through its respective curing cycle. The exotherm readouts from the DSC (Watt/g vs. time) were integrated over time to give a total energy of reaction vs. time graph which was then transformed to a plot of apparent percent cure vs. time by normalizing to the total energy of reaction term. The reaction was considered to be complete once the sample had asymptotically approached a value near zero. It was assumed that reaction kinetics for curing in the DSC were equivalent to those of oven curing used in the preparation of samples for adhesion testing. DSC exotherms were interpreted using Eq. (2.1)[80].

$$\alpha_i = \frac{\Delta H_i}{\Delta H_{rxn}} \rightarrow \frac{1}{\Delta H_{rxn}} \int_0^{t_i} H_i dt \tag{2.1}$$

Where α_i is the fractional degree of cure; ΔH_i is the cumulative heat evolved to reaction time *i* (J); ΔH_{rxn} is total the heat of reaction (J); and t_i is time point *i* (min), and H_i is heat flow (J/s).

The overall plan of experiments is detailed in Table 2.1. First, the curing kinetics were mapped out to provide knowledge of degree of cure to make direct comparisons between samples. After preparing samples at a standardized degree of cure ($\alpha = 0.99$), the effects of thermal history were investigated, including how the curing temperature and number of curing stages might play a role in fiber-matrix adhesion. Given the possibility of residual stress accumulation through a variety of compounding factors, annealing was also investigated to understand its effects on apparent adhesion. Next, the curing kinetics in the systems with accelerants were mapped out. Lastly, systems in which fiber-handling agents (sizings) were present were investigated.

Table 2.1: Overall plan of study.

Isothermal cure	-Isothermal curing at $T = 120℃, 140℃, 160℃, 180℃, 200℃$ -All cures to $\alpha = 0.99$
Two-Stage cure	1. Ramp 25°C → 93°C at 5°C/min 2. Isothermal $\alpha \rightarrow 60\%$ (214 min, 93℃) 3. Ramp to T_{final} at 5°C/min 4. Isothermal cure to $\alpha \rightarrow 99\%$ at T_{final}
Annealing	-Post curing for 0.5, 2.5, and 5 hours at 177℃
Accelerants	-Anchor 1115 (Evonik, Parsippany, NJ) -Epikure 3253 (Miller-Stephenson, Sylmar, CA) - EPON862/Accelerant ratio of 100: 3
Degree of cure	- Cure to $\alpha = 0.7, 0.8, 0.9, 0.99$
Effects of handling agents	-IM7-R sized fibers compared to unsized IM7 fibers and compared against multiple curing schedules -Short Curing Schedule 1. Ramp 25°C → 93°C at 2.3°C/min 2. Isothermal 93℃ (2 hours) 3. Ramp 25°C → 121°C at 2.3°C/min 4. Isothermal 121℃ (8 h) -Long Curing Schedule 1. Room temperature for 3 days 2. Repeat short curing schedule -Short Cure, Post Annealing Schedule 1. Repeat short curing schedule 2. Cool to room temperature 3. 25℃ → 177℃ at 2.3℃/min 4. Isothermal 177℃ (2.5 hours)

2.3.2 *Resin preparation*

The two-part thermoset system was comprised of a resin, Miller-Stephenson EPON 862 (bisphenol F diglycidyl ether, DGEBF) (Miller-Stephenson, Sylmar, CA) and the hardener, Epikure Curing Agent W (diethyltoluenediamine, DETDA) (Miller-Stephenson, Sylmar, CA). For a stoichiometric mixture, the parts were added in a weight ratio of 100 : 26.4. The fibers to be used in the study were un-sized Hexcel IM7 fibers and Hexcel IM7 R-sized fibers (Hexcel, Stamford, CT). The two accelerants used with the resin system were Epikure 3253, (2,4,6-tris(dimethymaminomethyl)phenol) (Miller-Stephenson, Sylmar, CA) and Anchor 1115 Accelerant (2-propanamine compounded with boron-trifluoride and butyl glycidyl ether) (Evonik, Parsippany, NJ).

2.3.3 *Isothermal and two-stage curing*

For isothermal curing, samples were ramped as quickly as possible to the selected isothermal curing temperatures of 120℃, 140℃, 160℃, 180℃, or 200℃ to minimize any curing during the ramping stage, and then held until the end of the curing time. The oven (Model 825F, Fisher Scientific, Hampton, NH) was then turned off, and samples were removed. For two-stage curing, samples were ramped from 25°C to 93°C at a ramp rate of 5°C/min and then held at 93℃ until $\alpha = 0.60$ (apparent), after which the temperature was ramped once again to the final values of 120℃, 140℃, 160℃, 180℃, or 200℃ until a curing degree of $\alpha = 0.99$ was reached. Again, the oven was turned off and samples removed. Cooling rates were not directly measured.

2.3.4 *Glass transition temperature*

The glass transition temperature, T_g, of the resins was measured in the DSC by initially following the protocol mentioned above to create cured samples. Once the cured samples were

cooled to room temperature, they were then ramped in temperature at a rate of 10°C/min until a noticeable jump (inflection point) in the heat flow was observed, a point identified as the glass transition temperature. An example exotherm is shown in Figure 2.1.

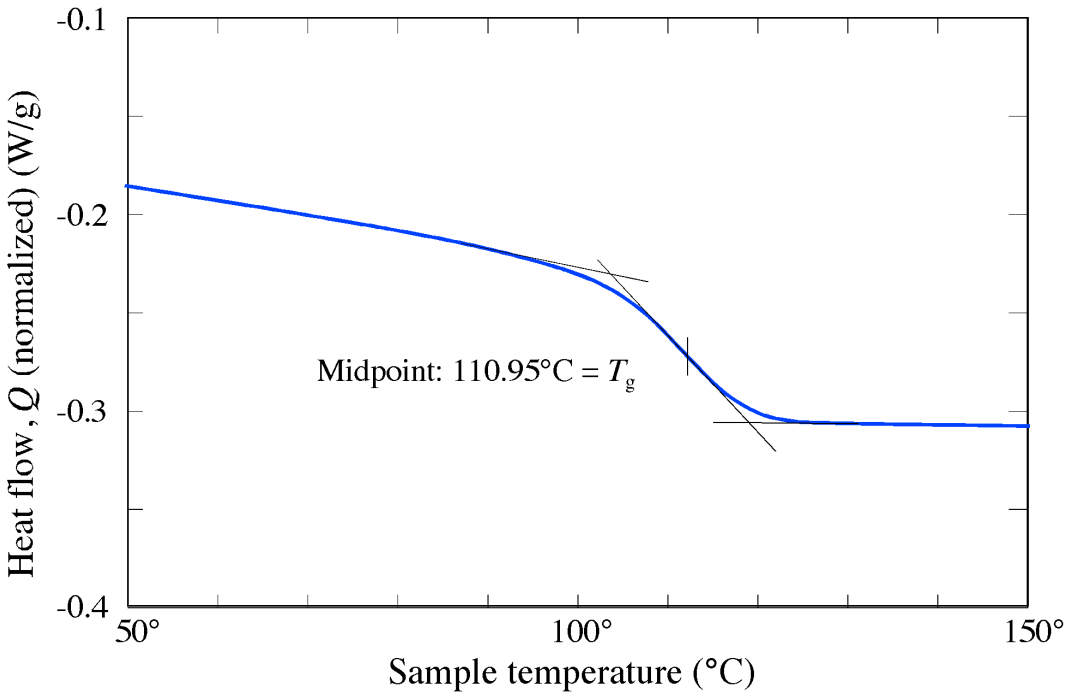

Figure 2.1: Example exotherm showing net heat evolved during DSC temperature trace at 10°C/min for EPON862 with Epikure curing agent W (ratio 100 : 26.4 w/w) following a two-stage cure with 180°C end temperature. T_g is extracted in the usual way as the temperature corresponding to the point of inflection in the exotherm.

2.3.5 *Sample Preparation*

A variety of different specimen types were prepared to investigate the effects of different curing schedules on fiber-matrix adhesion. In all cases, dog-bone shaped samples for adhesion testing, in accord with the Round Robin Assessment of the Single Fiber Fragmentation Test[79] were prepared as follows. Unsized Hexcel IM7 fibers were placed in empty, inverse silicone

molds following the dimensions of Figure 2.2 then pre-strained with a weight of 5.5 g to ensure that saturation of breaks will occur at 12% strain. Then approximately one gram of resin (Miller-Stephenson EPON 862 and Epikure Curing Agent W) was mixed (100:26.4 ratio w/w), added to the mold (Figure 2.2) and then degassed under vacuum for approximately 60 min. All samples were then doctored to ensure they had a relatively uniform amount of resin within each mold. Then using differential scanning calorimetry data, each resin was cured to the desired degree of completion in the oven.

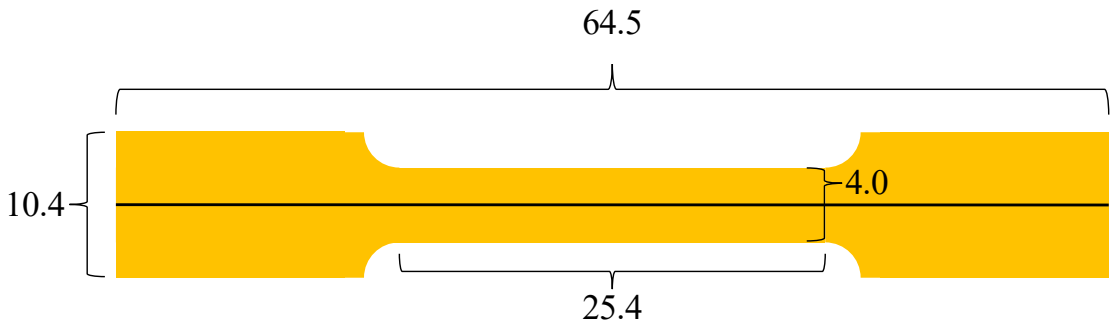

Figure 2.2: Dog-bone testing sample specifications, numbers in mm and thickness is 1.5mm. Image not to scale.

To investigate how the apparent degree of cure may affect adhesion, samples were isothermally cured (as described in the procedure above) and then taken out of the oven at the proper times to achieve apparent degrees of cure $\alpha = 0.7, 0.8, 0.9$ and 0.99.

2.3.6 *Internal stress development; annealing*

Since different temperature curing schedules may elicit different internal stresses, particularly at the interphase region between the fiber and resin[81], its effects on apparent adhesion are observable. A set of samples were isothermally cured as described above, cooled to room temperature, and then placed back into the oven for post curing/annealing. The annealing

treatment increased the temperature of fully cured samples from roughly room temperature to 177℃ (higher than reported resin T_g, and the highest documented curing temperature according to resin manufacturer[82]) in time intervals of 0.5, 2.5 and 5.0 h. The purpose of using different time intervals was to examine how stress relaxation over differing periods of time may have occurred.

2.3.7 *Use of Accelerants*

In the preparation of thermoset composite materials, additional components, termed *accelerants*, are added to the resin to reduce the required curing times. While the use of curing accelerants for thermoset resins has been studied[78,83], their effects on adhesion are yet to be extensively reported. Two separate curing accelerants, Epikure 3253 and Anchor 1115 were used in this study.

While there are no specific stoichiometric ratios for adding accelerants, ranges can be determined by the manufacturers[84,85], using DSC analysis, and using literature heuristics[78]. The ratio of EPON 862 to accelerant was chosen to be 100:3 (w/w). Once selected, the system was characterized, and cure times were calculated by using DSC. Otherwise, the samples were cured isothermally as described above.

2.3.8 *Single fiber strength testing*

Weibull statistical analysis was employed to determine the un-sized Hexcel IM7 fiber strength values. Thirty single fibers were separately mounted and tested in a SAETEC T1000 tensile device (Instron – previously SAETEC, Norwood, MA). Each fiber was strained until ultimate failure, and the stress value was recorded. Each fiber's tensile strength was rank-ordered

from lowest to highest. A probability-of-fiber-failure model was created using Eq. (2.2), the Weibull distribution[86], and fitted (by modulating σ_0 and m) to the data.

$$P_{f,model}(\sigma_i) \approx 1 - \exp\left[-\left(\frac{\sigma_i}{\sigma_0}\right)^m\right] \tag{2.2}$$

Where $P_{f,\text{model}}$ is the probability of failure model[87] (for low strain-to-failure fibers); σ_i is the tensile stress of specimen *i*; σ_0 is the Weibull strength parameter (scale); and *m* is the Weibull modulus (shape). Data were prepared using:

$$P_{f,emiprical} = \frac{i - 0.3}{n + 0.4} \tag{2.3}$$

Where: $P_{f,empirical}$ is the probability of failure; *i* is the fiber number ranked from lowest to highest ultimate tensile strength; and *n* is the total number of tests completed. Failure probability results for the IM7 fibers are plotted in Figure 2.3, and the Weibull parameters were calculated to be m = 4.62 and σ_o = 4713.32 MPa.

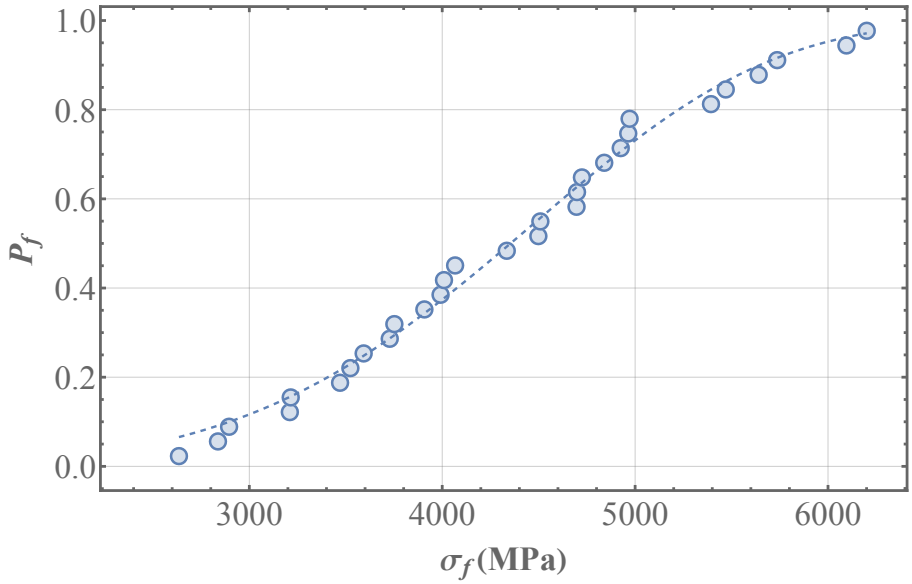

Figure 2.3: Weibull plot for unsized IM7 fibers: Probability of fiber failure, P_f vs. stress, σ_f.

2.3.9 *Adhesion testing*

Single fiber fragmentation was used to study interfacial shear strength. Tensile testing of the dog-bone specimens was conducted by using either a Drzal testing rack (Saint John's Computer Machine, St. John, MI) similar to that used by Feih et al.[87] or a SATEC T1000 tensile testing device. The test subjects a dog-bone sample of the resin, in which a single fiber is embedded, to a linear strain. As strain increases, stress transfers from the polymer matrix to the single fiber, resulting in fiber breaks. The fiber continues to break until the segments have reached a length below which they cannot support sufficient stress to cause a further break. Overall, the ultimate average fiber fragment length is inversely proportional to the interfacial shear strength (IFSS). Because observed practical adhesion is not solely a thermodynamic property, no two testing methods are expected to yield the same adhesion values. However, changes in observed adhesion from one system alteration to the next should be comparable across testing methods.

The interfacial shear strength (IFSS) for the system in this study was tested using the procedure described by Feih et al.[87] with slight modification. The samples, with a gauge length of 25.4mm, were strained at room temperature until reaching 12% elongation, which was manually tested and later assumed sufficient to reach saturation in the number of breaks. In general, eight to sixteen samples were prepared for each case, and usually three to six (but at least two) survived to saturation. The samples that reached 12% strain were examined under a microscope (Olympus IX70, Tokyo, Japan) using cross polarized light to determine the average break length allowing determination of the apparent IFSS value.

The theoretical basis for adhesion calculation, as described by Kelly et al.[88], assumes perfectly-plastic deformation. Adhesion (τ, IFSS) for the fiber fragmentation method is given by Detassis et al.[89] as Eq. (2.4):

$$\tau = IFSS = \frac{\sigma_f(l_c)d}{2l_c} \tag{2.4}$$

where: τ is the interfacial shear strength; l_c is the critical fiber length; $\sigma(l_c)$ is fiber stress at the critical length, and d is the fiber diameter. In addition, the critical length, l_c is taken as[90]

$$l_c = \frac{4}{3}\frac{L_g}{(n+1)} \tag{2.5}$$

where L_g is the dog-bone gauge length, and n is the number of fiber fractures confined within the gauge length. Lastly, fiber stress for any length can be computed using[87],

$$\sigma(l_i) = \sigma_0\left(\frac{L_0}{l_i}\right)^{1/m} \tag{2.6}$$

where: $\sigma(l_i)$ is the fiber strength with length l_i; σ_0 is the Weibull strength; L_0 is the fiber gauge length used when conducting single fiber strength tests, and m is the Weibull modulus. When all combined Eq. (2.4) will take the form of:

$$\tau = \frac{d\ \sigma_0\left(3^{1+\frac{1}{m}}\right)\left(4^{-3-\frac{1}{m}}\right)\left(\frac{(n+1)L_0}{L_g}\right)^{1+\frac{1}{m}}}{125L_0} \tag{2.7}$$

Where to get units of MPa for τ, the units of d are in μm, σ_0 is in MPa, and L_g and L_0 are in mm.

Importantly, effective adhesion is not exclusively a thermodynamic property; therefore, different testing methods may result in different adhesion values for the same system. However, changes and trends in adhesion should be similar regardless of the testing methods used.

2.3.10 *Notes on the single fiber fragmentation technique*

It should be noted that even though the single fiber fragmentation technique (SFFT) as presented above is widely used as a standard for testing interfacial shear adhesion in many applications, it has also received criticism for oversimplification. For this section, a high-level overview of some criticisms will be addressed. If additional detail on single fiber fragmentations is needed, please refer to the work by Rutz[91], who provided an in-depth discussion on the micromechanics and mathematics of fiber fragmentation testing.

Firstly, the original SFFT model fails to incorporate fiber-matrix debonding and assumes the two surfaces are perfectly adhered across the interface with constant shear[88,92]. Therefore, in the event of fiber fracture, the interfacial area is assumed to be precisely that of the surface area of the fiber. However, this is not entirely true because delamination or debonding can occur near the tips of fiber segments[93,94]. This assumption also becomes additionally complex when considering friction, elasticity, and total strain[95]. In effect, the fiber-matrix interfacial area may be smaller than when calculated solely from the fiber length.

Secondly, for all fiber segments, it is assumed that stress linearly builds from each end, and the next break will randomly occur in the region[90] between each endpoint plus a distance of $l_c/2$, this can further be visualized in Figure 2.4.

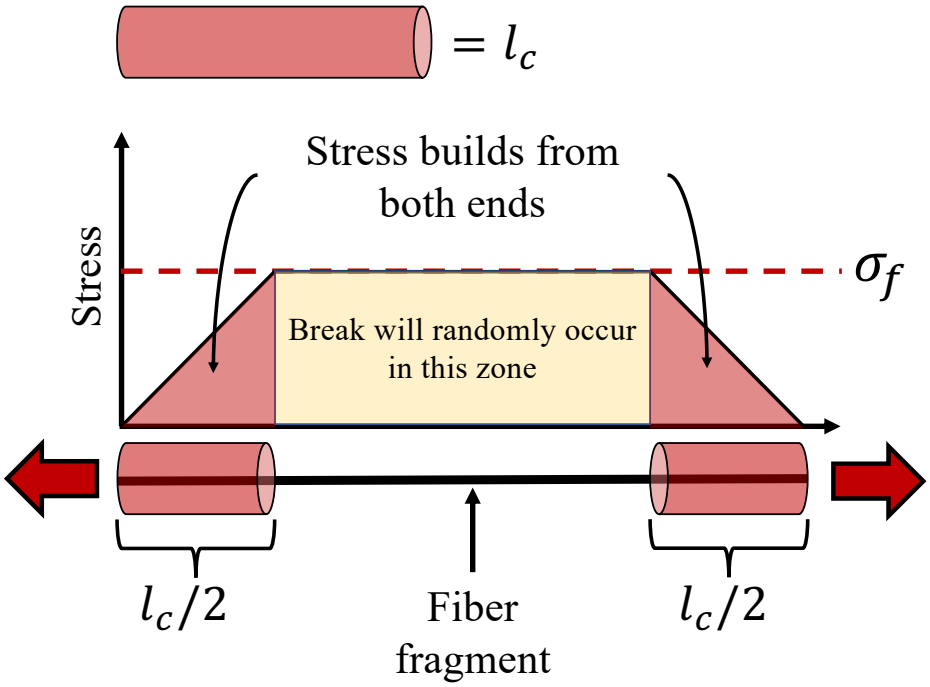

Figure 2.4: Visualization of stress accumulation in a single fiber segment. Stress builds from each end and after a distance of $l_c/2$, enough stress has built in the middle section for a break to randomly occur.

As stated by Ohsawa et al.[90], the nature of fiber fracture events dictates that the final fiber break lengths will be a random array of lengths between $1/2l_c$ and l_c. Therefore, the average fiber length will be $3/4l_c$ (making $l_c = 4/3l_{avg}$). However, among other criticisms[96,97], this assumption fails to recognize the innate material flaws which may cause stress concentration factors. Given this, the fibers are more likely to break following a Weibull distribution than a random one. An attempt at incorporating the Weibull distribution into determining the critical length was completed by Drzal et al.[98] and can be seen in Eq. (2.8).

$$l_c = \frac{\sigma_0 d}{\Gamma\left(1 - \frac{1}{m}\right)} \tag{2.8}$$

Where $\Gamma(x) = \int_0^\infty t^{x-1} e^{-t} dt$, σ_0 is the Weibull Strength (scale) parameter, d is the fiber diameter, and m is the Weibull modulus (shape) parameter.

Lastly, the SFFT model above does not consider Poisson effects (when materials contract perpendicular to the direction of strain) because it does not differentiate between frictional and interfacial adhesion[95]. If a mismatch of the Poisson ratios between the fiber and matrix is present, then squeezing or mode-I delamination may occur at the interface. If perfect adhesion across the entire fiber length were the case, then Poisson contractions would not have a meaningful effect on measured adhesion. However, since delamination or squeezing of the fiber can occur, then other forces such as friction[99] may begin to have a material effect on the overall observed adhesion.

As stated by Rutz[91], despite the limitations that the SFFT may have inherent in its assumptions, the methods as described in section 2.3.9 are still widely used throughout academic studies due to their relative simplicity. Accordingly, researchers generally use the SFFT for comparative studies where only one independent variable is changed across the same fiber, matrix, and test system. Given this, reported adhesion values that come from the SFFT are either explicitly stated or tacitly assumed to report "apparent adhesion" rather than "absolute adhesion." Practically, this implies that it is difficult to compare adhesion values from single fiber fragmentation testing to any other testing system. However, trends for changes in adhesion should be evident regardless of the test used.

2.3.11 *The effect of handling agents*

Handling agents are typically added to the surfaces of carbon fibers to reduce the frequency of fiber frays or tangling during the manufacturing and subsequent handling of fiber creels. It is thought that the presence of such fiber coatings may have adverse effects on the interfacial properties of the composite by interfering with the development of the fiber-matrix adhesive bond. To address such issues, manufacturers will sometimes de-size the fibers with solvents[100] such as acetone, or partially cure the fiber/resin systems at moderate temperatures with resin at a high enough temperature and low enough viscosity to elicit diffusion from the fiber interphase region to the bulk. To determine whether such costly treatments may be avoided, experiments were conducted with both sized and un-sized fibers. Coated (sized) fibers were compared to unsized fibers by subjecting them to three different curing schedules.

To examine how the presence and type of fiber handling agents may affect adhesion, IM7-R sized fibers were compared to un-sized IM7 fibers. The "R" sizing is composed of both epoxy and polyester material[101] and is assumed to be coated on rather than covalently attached. Interphase alterations were attempted by following three separate curing schedules, all shown in Table 2.1. The "long" cure samples were left at room temperature, allowing for a relatively small amount of polymerization to occur while still being at a low enough temperature to reduce diffusion of fiber sizing into the bulk resin and possibly cause the handling agent to be sequestered to the fiber surface. After three days at room temperature, the samples were placed in an oven following the cure cycle in Table 2.1. Results for the extended room temperature cure were compared to those that were placed directly in the oven as well as to those which were post-cure annealed.

2.4 Results and Discussion

2.4.1 *Curing times vs. temperature*

The times required to reach 99% apparent cure for isothermal curing at different temperatures are shown in Figure 2.5. Curing time decreases approximately linearly with temperature, with the slight deviation from linearity at 160℃ due possibly to either varying volatility of the resin hardener (indicated by perceptible fuming and amine odor), homopolymerization, or a stepwise change in reaction kinetics for a particular rate-limiting step. Samples isothermally cured at 200°C underwent a weight loss of 12.3%, suggesting that substantial volatilization of the hardener occurs, leaving homopolymerization to complete the cure.

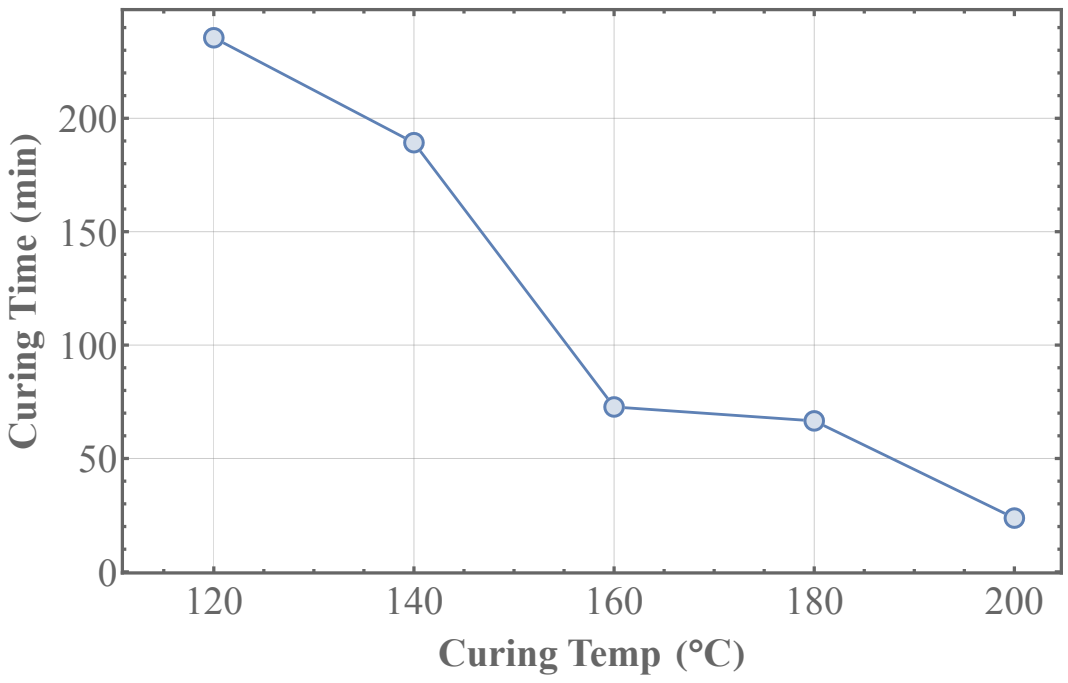

Figure 2.5: Curing time vs. isothermal curing temperature. ($\alpha = 0.99$).

Curing times, again for a final apparent cure of 99% for the second isothermal curing stage of a two-stage curing schedule, were determined as shown in Figure 2.6. Differential scanning calorimetry results showed that the initial curing phase at 93 ℃ took 214 min to reach $\alpha = 0.60$.

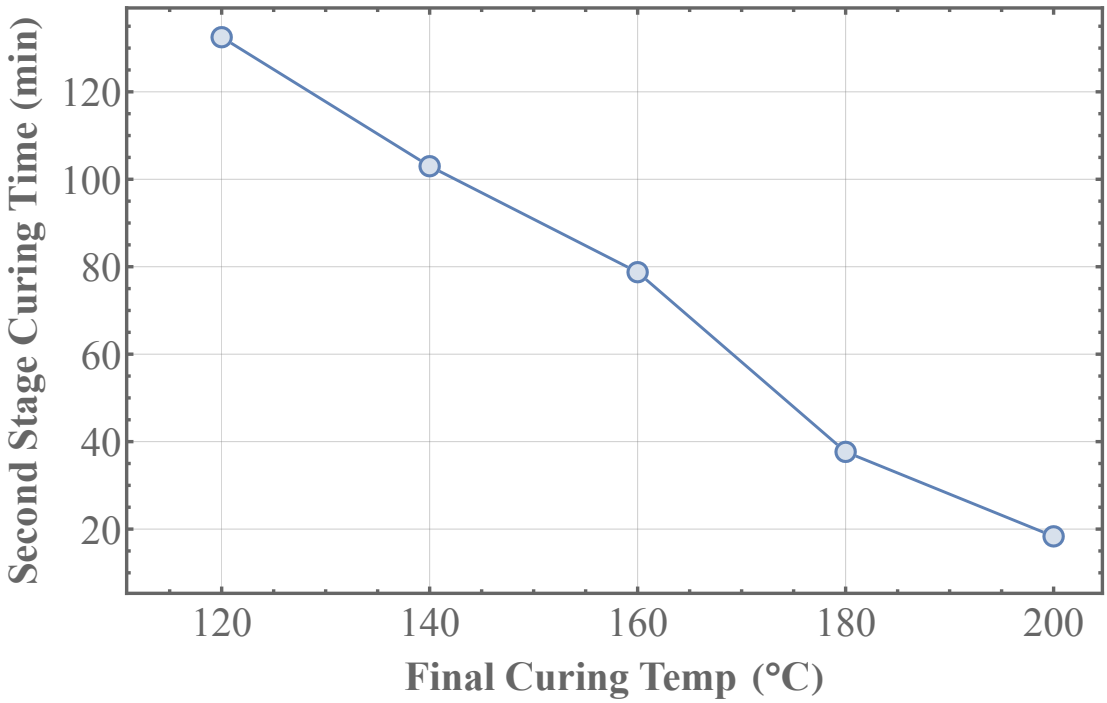

Figure 2.6: Curing time vs. final curing temperature for two-stage cure (α=0.99). The first curing stage was 214 min at 93°C (to reach apparent α=0.60)

Again, the linear decrease in curing time with final temperature suggests that the lower temperature (93℃) during the first curing stage allowed for sufficient polymerization to reduce the volatility of the hardener. Then the second stage of the cure most likely proceeded without vaporization of the hardener to the same extent as in isothermal curing.

2.4.2 *Adhesion vs. temperature for isothermal and two-stage curing processes*

Figure 2.7 shows adhesion results for both the single stage (isothermally cured) and the two-stage cured samples. The measured level of adhesion (IFSS) depends strongly on the curing temperature, increasing from approximately 89 to 139 MPa as the isothermal curing temperature is increased from 120°C to 200°C, similar to results obtained by Kalantar and Drzal[66] who used a resin system comprised of diglycidyl ether of bisphenol A and diethylene triamine. Additionally, the two-stage cure increased adhesion from about 73 to 112 MPa. To control the degree of cure and final curing temperature, all samples were brought to $\alpha = 0.99$ and finished their respective cures at the same temperature. The dependence of apparent adhesion to the curing temperature, as well as the smaller increase of apparent adhesion for the two-stage cured systems compared to the isothermal ones may relate to the importance of internal stresses. It is known that internal stresses develop during curing and affect properties of thermosets[102,103], and may thus constitute an important part of the apparent adhesion that is observed. More rapid curing of the resin system (as occurs at higher temperatures) leads to higher residual stresses, which can considerably increase the resin modulus, leading in turn[81], to a more efficient transfer of stress from the resin to the fiber across the interphase boundary. Internal stresses result from cure shrinkage and coefficient of thermal expansion (CTE) mismatch of the resin and fiber. Another important variable is the temperature at which the fiber attaches to the resin. When epoxy–amine resins are rapidly cured, less time is available for chain extension through reacting with the faster primary active hydrogens relative to cross-linking from secondary active hydrogens. Therefore, the resin spends less time as a liquid, and once gelled (attached to fiber), starts to build internal stress. As long as a resin system is in the liquid state, no stress is developed.

The reduced effect of residual stresses in the two-stage-cured systems may be due to the majority (60% apparent conversion) of the reaction occurring at a lower temperature, leading to more time near or above resin T_g to rearrange from high stress to low stress states.

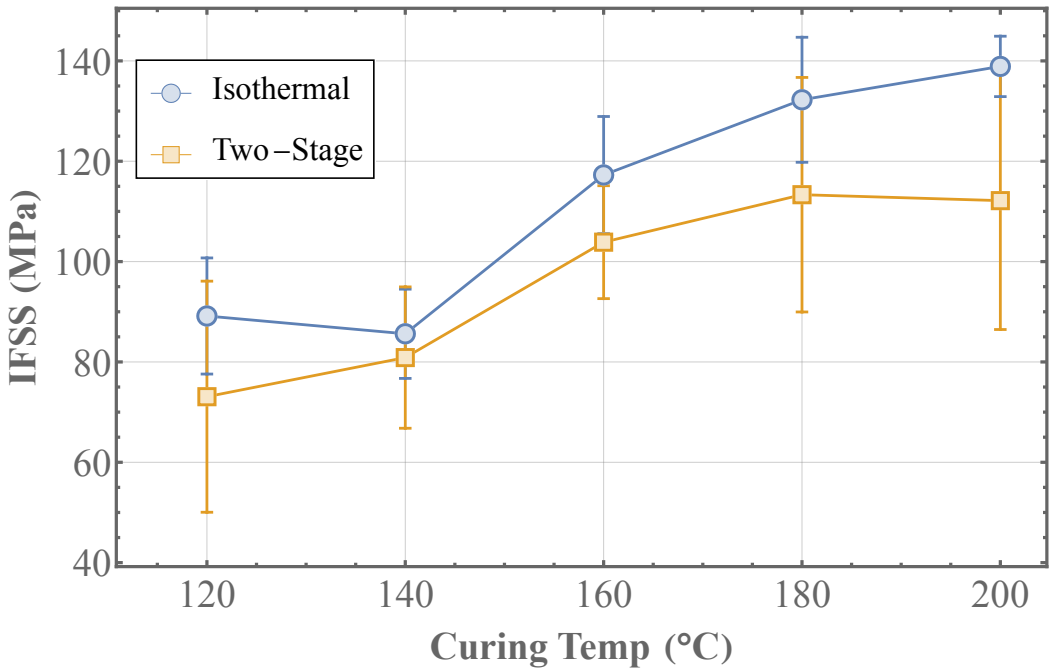

Figure 2.7: Adhesion for isothermal curing vs. two-stage curing (Mean ± SD) Blue circles represent isothermal curing, and orange squares represent two-stage curing.

Other theories[89,103,104] have also been proposed to explain why the adhesion in this type of system could increase with cure temperature, such as an increase in mismatch of fiber-resin thermal expansion coefficients and increasing differences in testing temperature compared to the stress-free temperature, T_g. If the difference in temperature between T_g and the testing temperature were to continue to grow as a consequence of curing procedure, then so would the apparent adhesion. However, T_g data for cured samples, presented in the next section, suggest that it remains relatively constant with cure temperature. Therefore, physical thermal expansion

may not play a major role in the changes in apparent adhesion for this system, if T_g is the stress-free temperature rather than the temperature of fiber attachment. It appears more likely that the increased rate of the cross-linking reactions with temperature, and higher gelation/attachment temperature, leads to an increase in residual stress. Lastly, when the resin attaches to the fiber (at gelation) above T_g, large residual strains can develop while cooling. Even though the resin is still rubbery, sufficient stresses can develop to cause fiber buckling.

2.4.3 *Effects of degree of cure on adhesion*

Even though the effects of degree of cure on thermoset properties have been tangentially reviewed in other studies[105,106], in-depth analysis of its effects on carbon fiber epoxy adhesion is lacking. However, after isothermally curing each fiber-resin system from $T = 120℃ \rightarrow 200℃$ at varying apparent degrees of cure ($\alpha = 0.7 \rightarrow 0.9$), few of the samples exhibited satisfactory mechanical properties to undergo interfacial shear strength testing. Specifically, the samples exhibited low plastic yield strength, so they were unable to support the required 12% strain to reach saturation of fiber breaks. Consequentially, no definitive adhesion results could be collected. In contrast, fully cured samples ($\alpha = 0.99$) maintained relatively robust physical properties and maintained elasticity for much longer strain ranges, allowing for reasonable tests to occur.

2.4.4 *Glass transition temperature*

To further examine the cause for the increase of apparent adhesion as isothermal curing temperature increases, we examined how the resultant glass transition temperature (T_g) of the resin changed with different curing cycles. Figure 2.1 shows a sample exotherm from which T_g is determined. Figure 2.8 shows glass transition temperatures of isothermal and two-stage cured

resins. The T_g for the isothermal curing schedule remained relatively constant throughout the different curing temperatures, as expected when curing to the same degree of cross-linking [107,108].

In comparison, the T_g for the two-stage curing cycle continually increased from one temperature step to the next. This result was unexpected, since the two resins have the same degree of ultimate cure, but as other studies have shown[4,67], thermal history and curing schedules can have significant effects on a range of macroscopic properties. This may be due to volatilization of curing agent. Also, T_g increases slightly with curing temperature above 180°C possibly due to homopolymerization or etherification. Since there is a lack of curing agent, epoxy-epoxy or epoxy-hydroxyl bonds are formed.

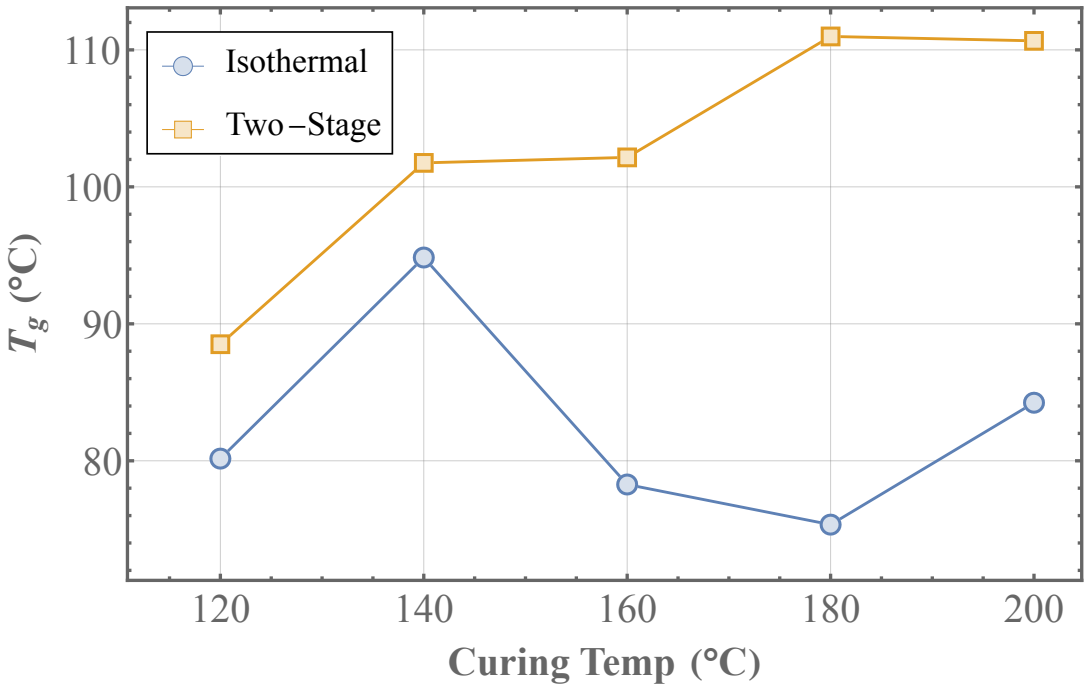

Figure 2.8: Different glass transition temperatures of cured resins. Blue circles represent isothermal cure cycle, orange squares represent two-stage cure cycle.

Below about 180° C, these reactions are slow. This suggests that the structure of the final polymer network and therefore properties such as T_g can be influenced by cure history.

A comparison of Figure 2.7 and Figure 2.8 suggests that T_g does not correlate directly with interfacial strength. There may be two reasons for this. First, as discussed above, increased isothermal cure temperatures resulted in an increase of hardener evaporation, creating an epoxy-rich resin. As noted by Minty et al.[77]and Petersen et al.[76], the epoxy/amine ratio heavily influences the T_g of the resin, but has much less effect on interfacial strength, even at amine/epoxy ratios as low as 0.5. Secondly, isothermal curing is more likely to induce greater residual stresses than the two-stage one.

It should also be noted that during the curing process, as tracked by DSC, two competing processes are taking place: first, the vaporization of the hardener (endothermic), and second, the cross-linking between the hardener and epoxy, or epoxy and epoxy (exothermic). Because there was no direct knowledge of the extent to which either process had advanced as a function of time, we could not decouple one from the other. Therefore, the best that could be done was to consider the point at which no change in enthalpy is occurring as the "end" of the combined process. At that point, no further increase in cross-linking density or hardener vaporization will occur. Because the final enthalpy evolution is asymptotic, a value of 99% was chosen to be the best endpoint to use.

2.4.5 *Annealing*

Given the increase of apparent adhesion with curing temperature as shown in Figure 2.7, it was sought next to examine how heat treating (annealing) the samples post cure, above T_g, might affect internal stress relaxation. Samples were cured isothermally as described above, then allowed to cool down to room temperature. Resin shrinkage was evident upon microscopic

examination of the cooled specimens, an example of which is shown in Figure 2.9, revealing noticeable waviness, as observed by earlier invstigators[64,65]. Volume changes that are not matched between the fiber and matrix may cause stress buildup and axial loading in the fibers, which can lead to fiber waviness[65]. For annealing, samples were then placed in an oven at 177°C (above the glass transition temperature) for 2.5 h. Glass transition is commonly understood as the temperature region where a polymer network loses glass-like properties and more closely resembles a rubber. In the rubbery state, greater molecular motion and rotational freedom are allowed[4]. Therefore, if volume shrinkage were the main reason for stress accumulation, then time above resin T_g should allow rearrangement of the polymers from high to low stress configurations, ultimately reducing apparent adhesion.

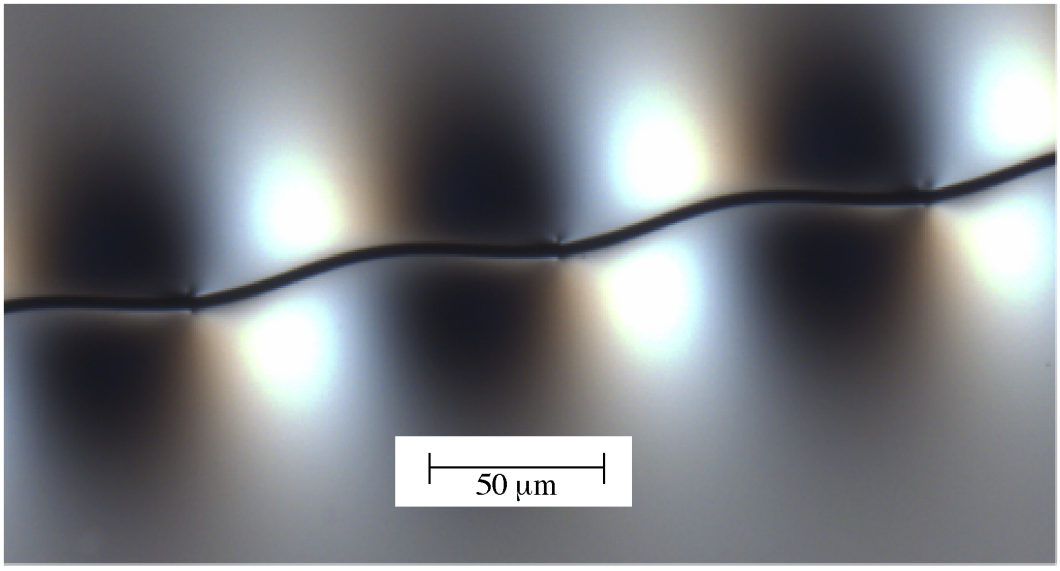

Figure 2.9: Fiber sample cured isothermally at 177°C and cooled to room temperature, showing the effects of resin shrinkage.

As shown in Figure 2.10, the apparent adhesion exhibited in the annealed samples was less than that of their non-annealed counterparts. This is attributed to the decrease in internal radial compressive stress on the fiber.

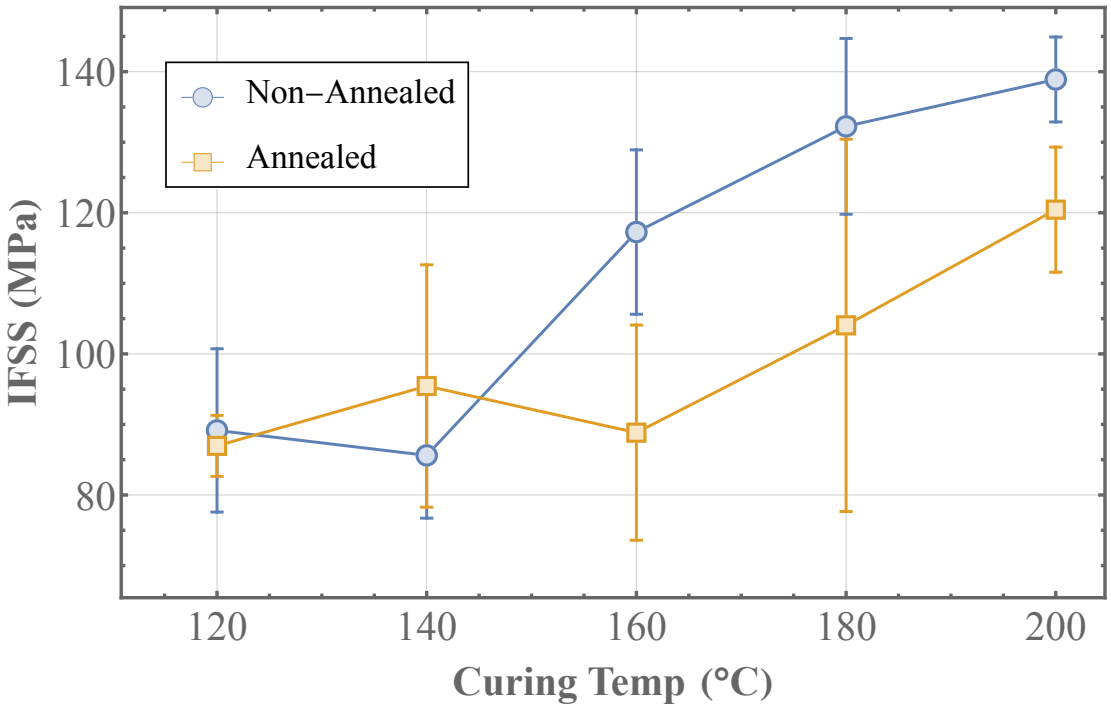

Figure 2.10: Adhesion vs. isothermal curing temperature (Mean ± SD). Blue circles represent non-annealed, isothermally cured specimens, and orange squares represent annealed samples. Annealing was performed at 177°C for 2.5h.

A second explanation for the drop in adhesion upon annealing could be thermal degradation [109,110] of the resin itself, which could lead to degraded physical properties, but since the annealing temperature used, 177C, was equal to the maximum curing temperature as reported by the manufacturer, it was not suspected of playing a role in the decrease in adhesion for the annealed samples.

Figure 2.11 shows results for the effect of annealing time on samples that were cured (isothermally) at two different temperatures (180°C and 120°C). Annealing time at 177°C

appears to have no effect on the apparent adhesion level produced with the lower temperature cure, reinforcing the idea that molecular mobility is one of the reasons for reductions of internal stress and apparent adhesion in samples prepared at higher temperatures.

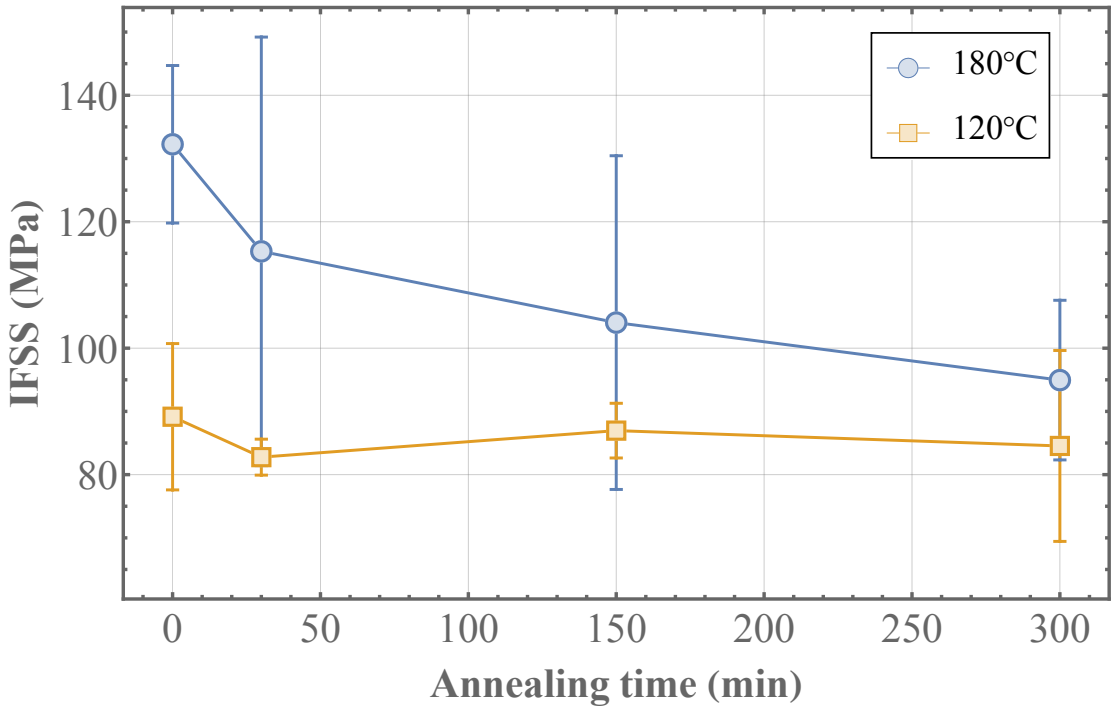

Figure 2.11: Effects of annealing time on adhesion (Mean ± SD) for isothermally cured systems. Blue circles represent 180°C isothermal cure, orange squares represent 120°C isothermal cure.

2.4.6 *Curing accelerants*

As noted earlier, while the use of curing accelerants for thermoset resins has been studied,[78,83] their effects on adhesion are yet to be extensively explored. Epikure 3253 and Anchor 1115 were used with the resin systems in this study to determine their effects on adhesion. As shown in Figure 2.12, both Epikure 3253 and Anchor 1115 significantly decreased curing time for the resin system for all isothermal curing temperatures. It is of interest that

significant differences of DSC exotherms, as shown in Figure 2.13, were produced by the presence of Epikure 3253. Typical DSC exotherms for epoxy-amine resins contain only one distinct peak. In contrast, resin systems containing Epikure 3253 displayed three distinct peaks, suggesting that the accelerant promoted separate polymerization reactions. As suggested by Burton[83], tertiary amines such as Epikure 3253 are most compatible with epoxy-anhydride resin systems, in contrast to the epoxy-amine system in this study.

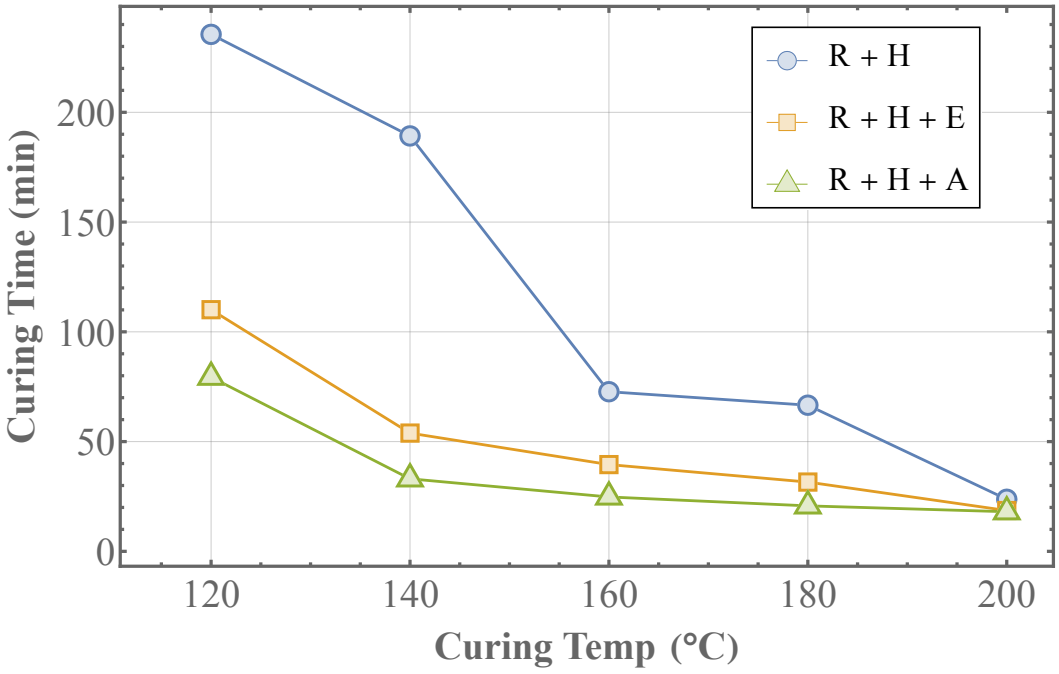

Figure 2.12: Isothermal curing time for resin systems ($\alpha = 0.99$). Blue circles represent EPON 862/Epikure Curing Agent W (100: 26.4), orange squares represent EPON 862/Epikure Curing Agent W/Epikure 3253 (100: 26.4: 3), and green triangles represent EPON 862/Epikure Curing Agent W/Anchor 1115 (100: 26.4: 3).

Since DEDTA reacts with epoxy at a relatively low rate, the presence of tertiary amines (Epikure 3253) can induce both epoxy homopolymerization and etherification[111] between epoxy

and hydroxyl groups, which would account for the first and third major peak shown in Figure 2.13.

In contrast, the resin cured using Anchor 1115 did not exhibit multiple peaks in the exotherm. This suggests that Anchor 1115 was well matched with the current resin and hardener system and did not lead to large quantities of side reaction products. In addition, the peak exotherm for the system with Anchor 1115 shifted to the left by approximately 50℃, indicating that the activation energy for the reaction to occur was significantly lowered. Curing with Epikure 3253 caused the mechanical properties of the resin to deteriorate substantially, i.e., susceptible to plastic deformation at much lower strain. Due to this, most samples were not able to exhibit the requisite 12% strain to complete the interfacial shear strength testing protocol.

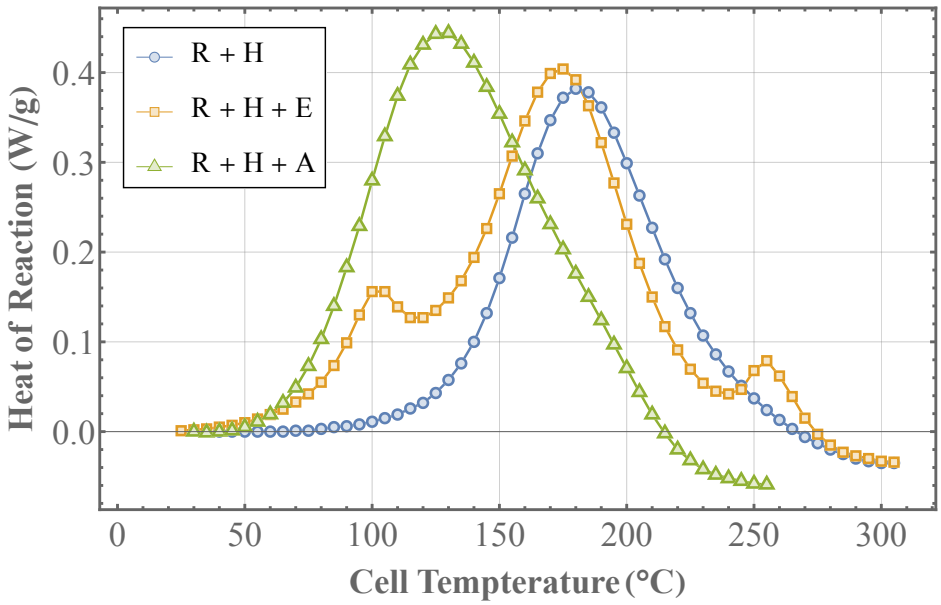

Figure 2.13: DSC exotherms for resin systems undergoing 5°C/min ramp from 25℃ → 325℃. Exotherm plots were cut off before degradation of the polymer occurred. Blue circles represent EPON 862/Epikure Curing Agent W (100: 26.4), orange squares represent EPON 862/Epikure Curing Agent W/Epikure 3253 (100: 26.4: ~3), and green triangles represent EPON 862/Epikure Curing Agent W/Anchor 1115 (100: 26.4: ~3).

Due to the altered physical properties, insufficient tests were conducted to determine any meaningful analysis of interfacial shear strength. Moreover, the few samples that were able to reach sufficient tensile strain without showing plastic failure had approximately 60% lower adhesion than the non-accelerated systems. Overall, the use of Epikure 3253 resulted in significantly accelerated curing times, at the cost, however, of weakening adhesion to the carbon fibers and resin properties. This accelerant, therefore, would not be optimal for use in the polymeric composite systems studied.

Anchor 1115 on the other hand, while still significantly reducing the overall yield strength of the composite, did so to a much lesser degree and therefore adhesion test results could be extracted. Secondly, it should be noted that while the presence of Anchor 1115 reduced the plastic yield strength of the resin for all curing temperatures, reductions in toughness were particularly exaggerated for lower temperature cures. Interestingly, as seen in Figure 2.14, the apparent adhesion of the isothermally cured composites with Anchor 1115 did not increase as curing temperature increased. While there can be many possible reasons for this, the most likely explanation would be that the presence of Anchor 1115 altered the curing volume shrinkage, resulting in lower compressive stress development. An example of a cooled fiber specimen in resin with Anchor 1115 is shown in Figure 2.15 showing an absence of the waviness present in the absence of the accelerant, indicating a decrease in the amount of resin shrinkage.

As seen in Figure 2.9, composites cured isothermally at a high temperature in absence of Anchor 1115 undergo significant cure shrinkage, resulting in a wavy fiber. However, as seen in Figure 2.15, composites isothermally cured at similar temperatures with Anchor 1115, although still somewhat in evidence, did not result in nearly as much cure shrinkage and wavy fiber

structure. The lack of thermal residual stress buildup resulting in lower apparent adhesion should be taken into consideration when manufacturing composite systems with this accelerant.

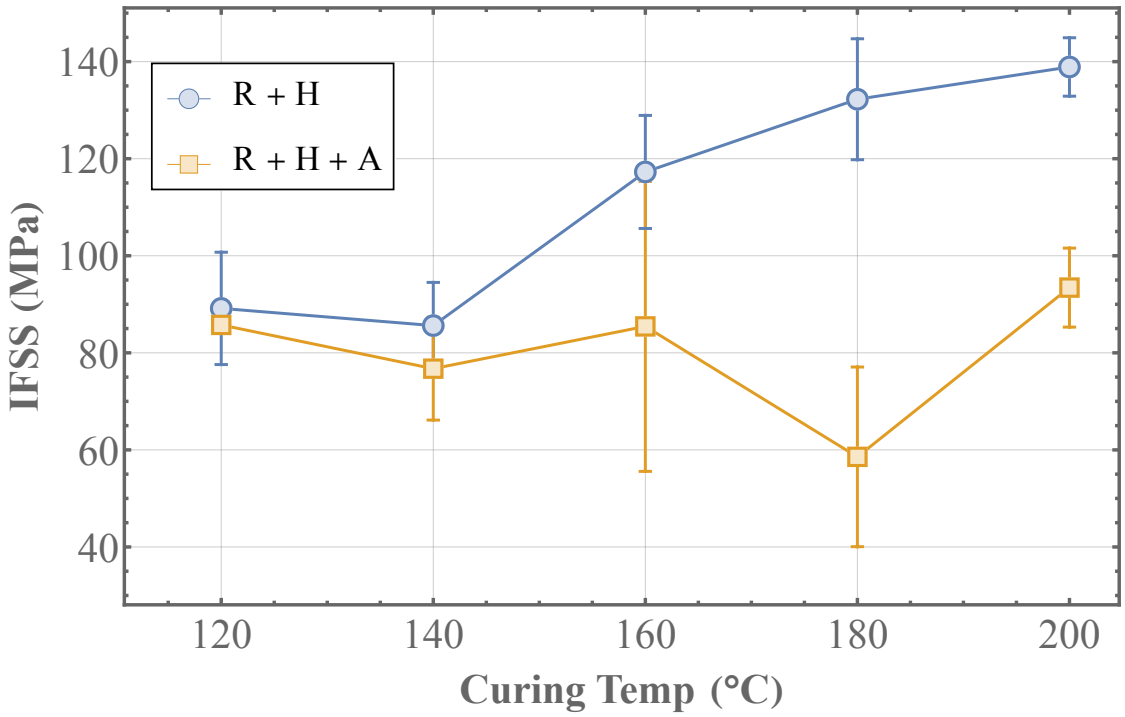

Figure 2.14: Adhesion vs. isothermal curing temperature (Mean ± SD). Blue circles represent EPON 862/Epikure Curing Agent W (100: 26.4), and orange squares represent EPON 862/Epikure Curing Agent W/Anchor 1115 (100: 26.4: 3).

Thus, even though the curing accelerant greatly decreased the throughput time for composite production, it may come at the cost of a reduction in composite plastic yield strength. The latter effect may be mitigated to some extent by increasing final curing temperature.

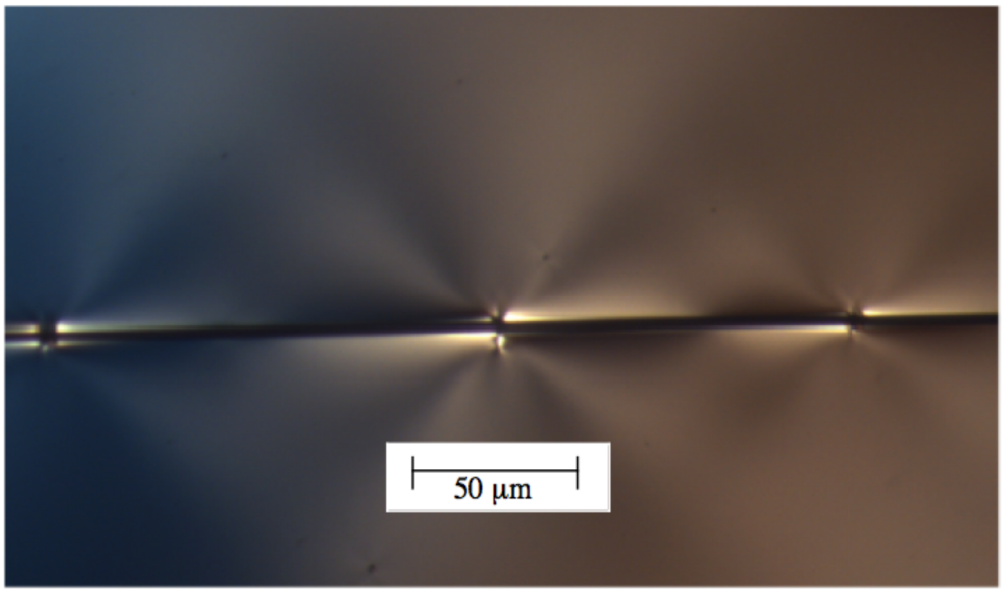

Figure 2.15: Cooled fiber sample in resin + Anchor 1115.

2.4.7 *The effect of handling agents*

Lastly, the effects of handling agents on the apparent adhesion of the system were to be inspected. Figure 2.16 which compares the unsized IM7 fibers to the IM7-R fibers, shows marginal changes in adhesion, if any, between the two sample sets for all three curing cycles.

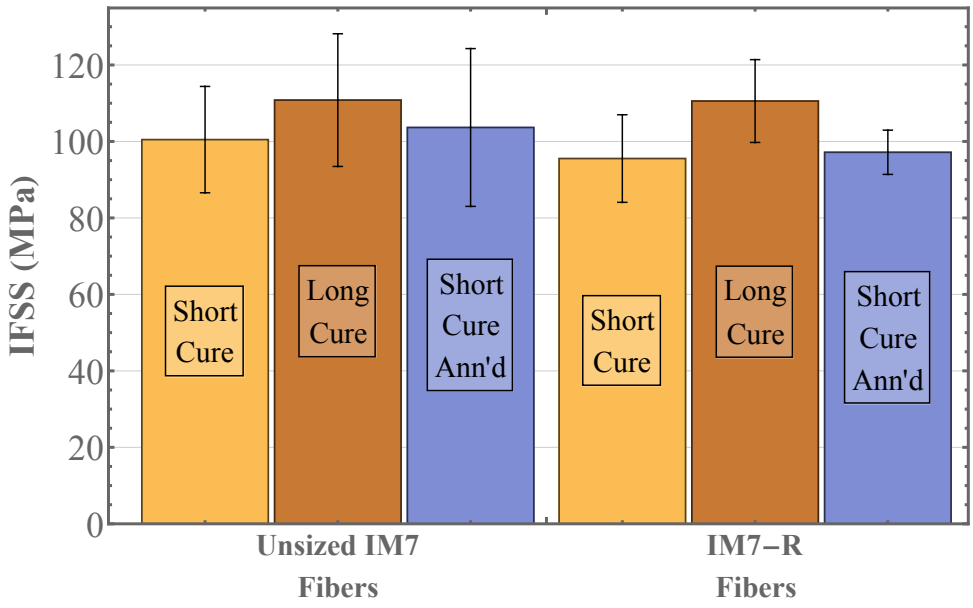

Figure 2.16: Adhesion differences for (Mean ± SD). Yellow bars represent the "short" curing schedule, brown bars represent the "long" curing schedule, and blue bars represent the "short cure, post annealed" curing schedule.

Thus, for reasonable periods of time at room temperature and for different curing schedules, the presence of the "R" handling agent does not clearly affect interphase mechanics and apparent adhesion for this resin system. Therefore, it appears that the need for chemical treatments to strip the handling agent is unnecessary for this system and these curing schedules.

2.5 CONCLUSIONS AND RECOMMENDATIONS

A large number of conclusions can be drawn from the reported studies of curing schedules and other factors on fiber-matrix adhesion in carbon fiber-reinforced thermoset composites. It should be noted that the single fiber test results may not be indicative of what occurs with "multiple fiber" composites

- Effects of curing temperature on adhesion and physical properties

    - Measured (apparent) adhesion is proportional to the curing temperature for the polymeric composite system used in this study. Higher curing temperatures yielded higher adhesion values.
- Effect of the number of curing stages on adhesion and internal stress
    - Isothermal curing exhibited higher apparent adhesion than the typical two-stage curing cycles often used industrially. This is believed to be due to the slower polymerizations at lower temperatures in the two-stage curing cycle, delaying internal stress accumulation as compared to isothermal curing at the higher temperature.
- Effect of annealing samples post-cure on internal stress states
    - Post-cure annealing resulted in significantly lower apparent adhesion for isothermally cured samples. Heat-treating samples at temperatures above the glass transition temperature allowed internal stresses to relax, resulting in reduced radial pressure on the fiber. Thus, it could be concluded that rapid curing at high temperatures and subsequent volume shrinkage upon cooling led to high internal compressive stresses that are the primary reason for increased adhesion obtained using high curing temperatures.
    - A baseline level of adhesion was achieved at a low curing temperature, 140°C. Curing above this temperature, residual stresses cause proportional increases in apparent adhesion. Post-cure annealing reduced the residual stress buildup, but not to the extent of causing apparent adhesion to decrease below the values of the low-temperature cure.

    - The high initial value of apparent adhesion obtained can be reduced, even without polymer degradation, when subjected to high enough temperatures.
- Effect of the degree of cure
    - Any degree of cure less than that of roughly 95% produced a resin system of low plastic yield stress, lower modulus, and reduced toughness, causing premature sample failure and low adhesion.
- Effect of accelerants on curing times and sample properties.
    - Epikure 3253 significantly increased the resin curing speed, however degraded physical properties, and reduced adhesion by a factor of roughly 60%. In addition, the accelerant caused three separate reactions resulting in phase separation.
    - Anchor 1115 significantly increased resin curing speed and did not decrease the apparent adhesion of the system to a large extent. Accumulation of residual stress did not occur to the degree of that for the non-accelerated system. Importantly, the increase of curing speed with the maintenance of baseline apparent adhesion also leads to a significant decrease in resin toughness. This effect can be mitigated to some extent by curing the resin at higher temperatures.
    - If curing accelerators are to be used, it is advised to cure at a higher temperature to partially mitigate the decrease in plastic yield strength.
- Effect of fiber handling agents/sizing on adhesion and system properties.
    - Fiber handling agents did not significantly affect adhesion when provided sufficient time to diffuse from the fiber surface into the bulk resin. A two-stage curing cycle with a lower temperature first stage allowed for sufficient diffusion to occur.

- Aging at room temperature up to three days post cure did not affect overall adhesion in the system. Therefore, any curing that occurs at room temperature for this system has negligible effects on the effective adhesion of the handling agent.

Chapter 3. STRATEGIES FOR THE ENHANCEMENT OF ADHESION BETWEEN CARBON FIBERS AND POLYOLEFIN MATRICES

*Sections of this chapter come from the journal publication:
ElKhoury L, Berg JC. Strategies for the enhancement of adhesion between carbon fibers and polyolefin matrices. *Journal of Adhesion Science and Technology* 2022; 0: 1–16.

3.1 CHAPTER SUMMARY

Carbon fiber reinforced polyolefin (polyethylene, polypropylene, etc.) composites would be attractive materials for many applications, including aquatic sporting equipment, if fiber-matrix adhesion could be brought to acceptable levels. The present work explores a variety of strategies for adhesion promotion in these types of systems. The use of conventional (silane) and unconventional (titanate and zirconate) coupling agents, matrix additives, surface treatments producing interphase modulus graduation, and combinations of the above is examined using fiber pullout tests for T700 GC-12k-91 carbon fibers embedded in both polyethylene and polypropylene matrices. Only modest enhancements were achieved in all cases using coupling agents and other surface treatments, with azidosulfonyl silanes producing interfacial shear strengths (IFSS) to levels approaching 15 MPa for low-density polyethylene (LDPE). The use of maleic anhydride graft copolymer matrix additives achieved similar results. The combination of azidosulfonyl silane surface treatment with maleic anhydride additive produced IFSS values approaching 30 MPa.

3.2 INTRODUCTION

Fiber-reinforced composite materials consist of long, load-bearing fibers embedded in a polymeric matrix. Their mechanical properties depend not only on the properties of the fibers and the matrix but also on the adhesion at their interface[81,112–114]. In recent years, sports equipment and automobile manufacturers and others have taken interest in transitioning from thermoset to thermoplastic resins[115,116]. Polyolefins, such as polypropylene and polyethylene, are principally appealing due to their high toughness, low cost, resistance to chemical erosion, high impact strength, and rapid manufacturing time. Their chemical inertness,[117] however leads to inadequate fiber-matrix adhesion in almost all applications. The fiber surfaces (with oxygen-containing surface groups) can be functionalized using coupling agents, so that with the right choice of organofunctional group, there may be the possibility of physical interdigitation or reaction with the matrix, providing enhanced adhesion. In their extensive review of silane coupling agents used for natural fiber/polymer composites, however, Xie et al.[118] reported only modest improvements in the mechanical properties of the composites using such strategies, and the improvements achieved may be attributed more to improved distribution of the fibers in the polymer than to enhanced adhesion. While most studies only inferred the effects of surface treatments on adhesion from measured changes in the bulk properties of the composites, Park et al.[119] measured changes in the interfacial shear strength (IFSS) of single jute fibers in polypropylene using the microdroplet micromechanical test. Surface treatments with aminopropyl silane (APS) produced only modest increases in IFSS. Any covalent linkage to the matrix is precluded by the lack of chemical reactivity of the polymer. Even simple interpenetration or interdigitation is difficult to achieve due to the physical incompatibility of virtually any organofunctional group with the polymer.

Other physical enhancements might be produced by fiber surface roughening (providing mechanical interlock). For example, Luo et al.[100] tried attaching graphene-oxide to carbon fiber surfaces for enhanced physical interlock, but achieved only moderate increases in adhesion. Another strategy to improve, or at least to alter, the interaction between fiber surface and matrix might be softening of the matrix material adjacent to the fiber, producing a visco-plastic inter*phase*.

Matrix additives, i.e., materials containing functional groups that may be more amenable to interdigitation or even chemical interaction by coupling agent organofunctional groups but are still adequately miscible with the polyolefin matrices. Felix and Gatenholm[120], for example, obtained measurable improvements in the properties of cellulose fiber/polypropylene composites using maleic anhydride/polypropylene copolymers additives. Liu et al.[48] combined a fiber coating with epoxy rings on the outer group with polypropylene/maleic anhydride copolymer matrix to induce chemical bonding and moderately increased adhesion between carbon fibers and the matrix. Bikiaris et al.[121] studied a similar phenomenon by treating E-glass fibers with silane coupling agents containing terminal amino groups and reacting them with a maleic anhydride-polypropylene copolymer matrix, again achieving only small adhesion enhancements. In any case, there is at present more interest in carbon fibers[122], due to their superior mechanical properties.

A more promising approach appears to be the use of compatibilizing agents that are capable of chemically attacking the polyolefin backbone. Two such possibilities have shown success in producing property enhancements of polymer nanocomposites. These include the use of vinyl silanes with the addition of a peroxide initiator[123] which decompose at elevated

temperatures to form oxy radicals that attack the thermoplastic backbone. Another such approach is the use of azidosilane (AZS) coupling agents.

The current study is concerned with adhesion between a commercial unsized carbon fiber (Toray T700 GC-12k-91) and a polyethylene or polypropylene matrix. It seeks to provide side-by-side direct measurements of adhesion (IFSS) using a single test method, viz., fiber pullout. Results for all the physical and physico-chemical methods named above are sought as well as those for a number of situations that appear not yet to have been examined. These include the use of titanate and zirconate coupling agents, two new matrix additives, combinations of surface roughening and interphase formation, and combinations of matrix additives with peroxide/vinylsilane and azidosilane treatments.

3.3 MATERIALS AND METHODS

3.3.1 *Fiber sample preparation*

Commercial carbon fibers T700 GC-12k-91 (Toray Composite Materials America, Tacoma, WA), nominal diameter 7 μm, tensile strength 4,900 MPa were used in this study. The fibers, which are unsized, are electrolytically oxidized in a proprietary process, and are assumed to possess ample carboxyl and hydroxyl groups on their surfaces. Single fibers were extracted from a fiber tow and glued to a 1x2 cm manila paper cutout, with approximately 3 mm of the fiber protruding from the edge of the paper. A hole was punched through the opposite end of the mounted sample to allow it to hang from the force sensor, as shown in Figure 3.1. All samples that did not have a nearly 90° angle to the fiber edge were discarded.

3.3.2 *Interfacial strength testing*

The fiber pullout[124] method, using a lab-made testing device shown schematically in Figure 3.1, was used to conduct the study. It measured interfacial strengths (IFSS) by embedding a single fiber (as described above) into a globule of the matrix, then pulling it out once cooled. A mode-II shearing force is imparted to the interface between the fiber and matrix. If the fiber cleanly debonds from the matrix before either the fiber or the matrix fails, then maximum interfacial strength can be deduced. The device was created using a micro controller (Arduino, Somerville, MA), a stepper motor (Sure Step, Automation Direct, Cumming, GA), and a load cell (LSB200 Miniature S-Beam Jr. Load Cellsile, Futek, Irvine, CA).

For testing, a roughly 30 mg ball of polyethylene or polypropylene was placed on a tray and heated to elevate the temperature to roughly 25°C above the described glass transition temperature. In the rubbery state, greater molecular motion and rotational freedom are allowed[4], so that a single fiber can be inserted into the plastic at this point. After fiber insertion to the desired depth, cooling water (at 0°C) was run through the plate until the testing temperature of 25°C was reached. The tray was then slowly moved downward until debonding occurred, and the force and the embedded length were recorded. A typical force trace of the pullout event is shown in Figure 3.2. The embedded length was taken to be the displacement from the onset of force accumulation until the force reached zero. The interfacial shear strength (IFSS) is obtained as[124]

$$IFSS = \sigma = \frac{Peak\ Force}{Surface\ Area} = \frac{F_p}{\pi dl} \tag{3.1}$$

where F_p is the peak pullout force, d is the fiber diameter, and l is the embedded length. It should be noted that for this test to occur properly, the ultimate fiber strength must be higher than that of the system adhesion. Therefore, the fiber pullout test is well suited for low-to-moderate adhesion systems, as might be expected for polyolefin-carbon fiber composites.

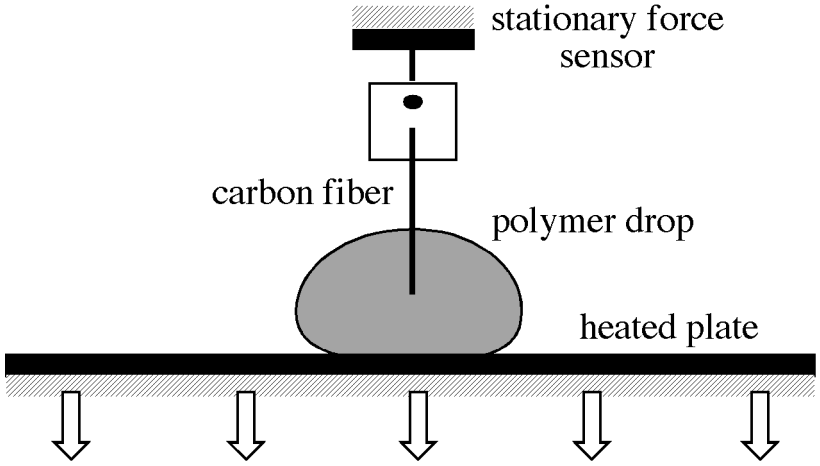

Figure 3.1: Schematic of single-fiber pullout device

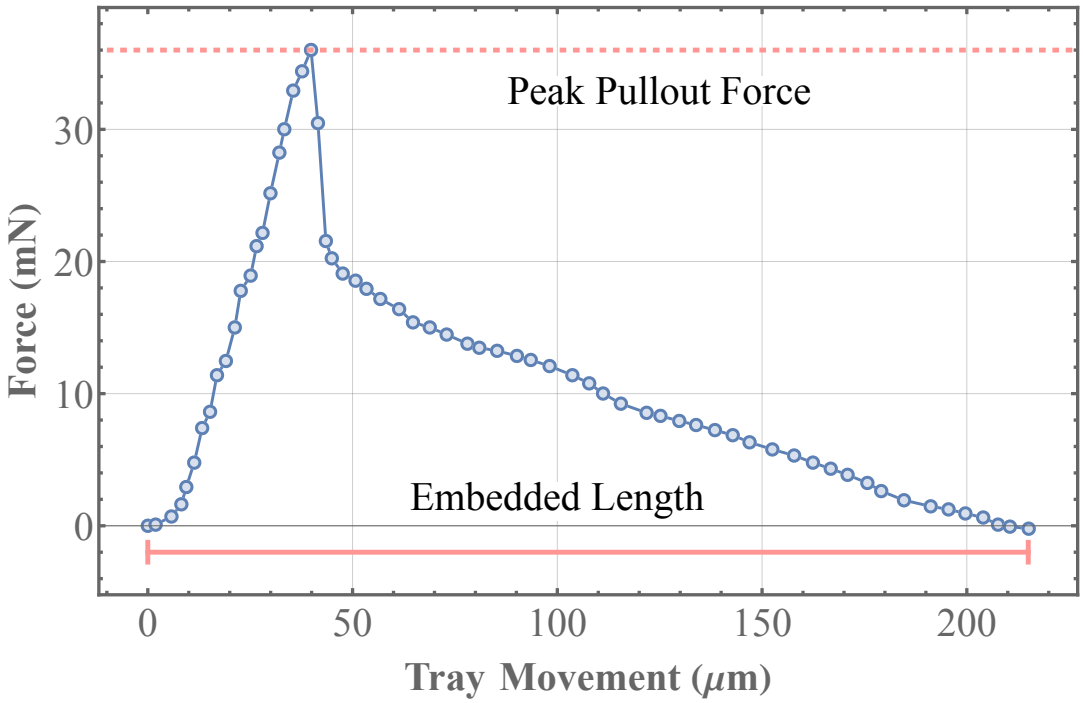

Figure 3.2: Example force *vs.* displacement curve for fiber pullout test. Carbon fiber with VTS surface treatment, embedded in low-density polypropylene.

3.3.3 *Matrix materials*

Three different polymer systems were used: polyethylene (melt index 25g/10min, Sigma-Aldrich Inc, St. Louis, MO) (LDPE), isotactic polypropylene (M_n ~ 5,000) (Sigma-Aldrich Inc, St. Louis, MO) (LDPP), and isotactic polypropylene (M_n ~67,000) (HDPP).

3.3.4 *Silane coupling agents*

The silanes used were 3-aminopropyl trimethoxysilane (APS), vinylethoxysilane homopolymer (VPS), vinyltriethoxysilane (VTS), and 6-azidosulfonylhexyl triethoxysilane, (AZS) (Gelest Inc., Morrisville, PA). Protocols for the application of silane coupling agents to carbon fibers have varied among different investigators[121,125,126], but the method employed in this study was as follows. A solution of 100 mL of 190 proof ethanol and 0.5-1.0 mL of silane was titrated to a pH of 4.5 using either glacial acetic acid or solid sodium hydroxide and stirred for 20 min to allow for hydrolysis. Then a roughly 12-in tow of the Toray T700GC-12k-91 carbon fibers was submerged in the bath and allowed to react for 60 min. Finally, the fibers were removed and oven dried at 110°C for 5 to 10 min. A slightly lower drying temperature for AZS treated fibers was used to keep the silane from reacting. All fibers were stored in a cool, dry place between tests. The amino and vinyl silanes were chosen because of the possibility of interdigitation with the polyolefin and increasing adhesion, although no direct chemical interactions with the resin were to be expected. However, the azidosulfonyl silane has been shown to directly interact with C-H bonds, thus having the possibility to create a stronger link between the fiber and matrix. The azido group can be characterized as an alkyl group attached to a nitrene, as shown in Figure 3.3. At elevated temperatures, the nitrene reacts with carbon-hydrogen bonds, performing an insertion, effectively linking the two materials. Nitrogen gas is released, and the final product can be seen with the R’ and R” groups attached, where the R’

group represents a polyolefin backbone, and the R" group represents a silane attached to a carbon fiber. After reaction, a stable chemical bridge is presumed to attach the polyolefin to the carbon fiber.

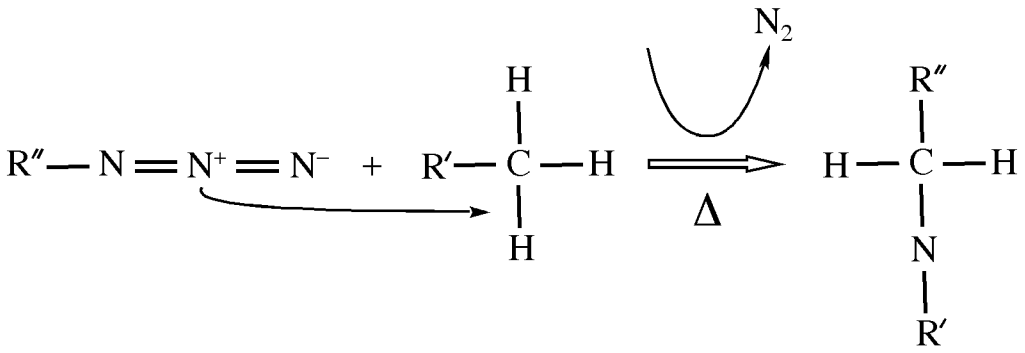

Figure 3.3: Simplified reaction mechanism for 6-azidosulfonylhexyl triethoxysilane and a polyolefin.

3.3.5 *Titanate and zirconate coupling agents*

Titanates and zirconates have received little attention for promoting adhesion in composites. Typically, they are additives to plastics that tend to migrate to the matrix-filler interface spontaneously. The titanates and zirconates of choice for this study were: NZ12: Zirconium IV 2,2(bis-2-propenolatomethyl) butanolato, tris (dioctyl) phosphato-O; LICA12- Titanium IV 2,2(bis 2-propenolatomethyl) butanolato, tris (dioctyl) phosphato-O; NZ09: Zirconium IV 2,2(bis-2-propenolatomethyl) butanolato, tris(dodecyl)benzenesulfonato-O; LICA 09: Titanium IV 2,2(bis 2-propenolatomethyl) butanolato, tris (dodecyl) benzenesulfonato-O, and NZ01: Zirconium IV 2,2(bis-2-propenolatomethyl) butanolato, tris neodecanolato-O, all provided by Kenrich Petrochemicals (Bayonne, NJ). The specific chemicals were chosen by company recommendation for their presumed compatibility with polyolefins.

The process of adding titanates and zirconates to polyolefin powder was to add 20 g of LDPP with 2 g of the titanate and zirconate of choice to a blender (Magic Bullet, Pacoima, CA) and blend for 2 min. Then the 10 wt% by weight titanate or zirconate polyolefin was once again added to the blender with clean LDPP to create a 1 wt% powder that was used as the plastic for the testing procedure with carbon fibers as described above.

3.3.6 *Surface functionalization with peroxides*

Peroxide treatment to superficially functionalize and increase adhesive properties of polyolefins has been reported[125,127–129]. The different treatment processes used have not been standardized, but typically the surface to be bonded to the polyolefin is first treated with a vinyl silane. A peroxide initiator, which decomposes at elevated temperatures creating oxy radicals can be coated onto the silanized fiber to react with carbon-hydrogen bonds of the polyolefin. The radical simultaneously reacts with the vinyl group, linking it to the polyolefin[123,127] creating a chemical bridge between the two materials. The process of peroxide initiation in this study began by adding vinyltriethoxysilane (VTS) (Gelest, Morrisville, PA) to the surface of the T700 fibers as described above. The fibers were then dipped in a room-temperature ethanol solution of approximately 5wt% dicumyl peroxide (Sigma-Aldrich Inc, St. Louis, MO). The fibers were soaked for 20 min, then extracted and air dried for 24 h at room temperature. At this point, the fiber surfaces were presumed to contain covalently bonded vinyl groups and a loosely held, evenly distributed layer of unreacted dicumyl peroxide. The treated fibers were then inserted into softened polypropylene (HDPP) and tested as described above.

3.3.7 *Fiber roughening*

Physical roughening is meant to alter the morphology of the fiber surface to increase mechanical interlock. The surface of as-received carbon fibers was relatively smooth, with shallow axial crenulations. Physical etching was effected using different methods that exposed the fibers to harsh environments such as strong acids, bases, and ozone. The first fiber roughening process used nitric acid treatment[130], in which a small coil of carbon fiber was submerged into 200 mL of concentrated nitric acid and refluxed for 2 h. The base of the column was submerged in a bath of boiling water to keep the acid temperature at 100°C. The fiber bundle was removed and soaked multiple times with room-temperature DI water and dried. In the second treatment, a small tow of the fibers was immersed in commercial bleach[18] (Clorox Company, Oakland, CA) at 100°C for 2 h, rinsed and dried, and in the third method, a fiber tow was soaked in a solution of 30% ammonium hydroxide[131] at room temperature for 120 h, and the fibers were removed, washed and dried. In a final procedure, the fiber tow was placed in a glass Petri dish and exposed to ozone by insertion into a low-pressure plasma-ozone cleaner (Deiner Electronic, Ebhausen, Germany)[132] for 15 min on maximum power. The fibers were brought out and sealed in an airtight container.

3.3.8 *Interface softening; formation of an interphase*

The interface between polyolefins and carbon fiber is generally brittle, so that debonding occurs through crack initiation and sudden growth. The mechanism of adhesive failure may be changed if the interface were replaced with an inter*phase* of finite thickness (generally less than 1 μm) and consisting of a visco-plastic softened layer of the matrix polymer. Debonding would then occur through the gradual deformation of the interphase until its yield stress is reached. While the value of this yield stress is unlikely to be larger than the stress required to debond the

brittle interface, the structure may exhibit significantly enhanced toughness, so that any small-amplitude "failure" would be capable of self-healing. To produce a visco-plastic interphase, the fiber was first dipped into molten LDPE to form a 1- 2-μm plastic sheath around the surface. The coated fiber was then dipped in toluene for approximately 100 s to soften the matrix. Finally, the solvent-treated fiber was reinserted into the plastic sessile drop on the fiber pullout device.

3.3.9 *Matrix additives*

Maleic anhydride graft-copolymers have been used as matrix additives to increase both the surface energy and reactivity of polyolefins[121,133]. Because this material, as shown in Figure 3.4 contains a polypropylene group, it mixes well with low molecular weight polypropylene, so that no phase separation is observed. The maleic anhydride graft-copolymer polypropylene (M_n ~ 3,900, 8-10 wt% maleic anhydride) (Sigma-Aldrich, St. Louis, MO) was added in various quantities to pure LDPP. Once together, they were heated to 185°C in a convection oven, stirred, and cooled at room temperature until solid. Nine different testing samples of plastic were created with their approximate weight composition of maleic anhydride of: 0%, 0.9%, 1.7%, 3.1%, 4.1%, 5.1%, 6.2%, 7.0%, and 9.0%. Testing followed the procedure described above.

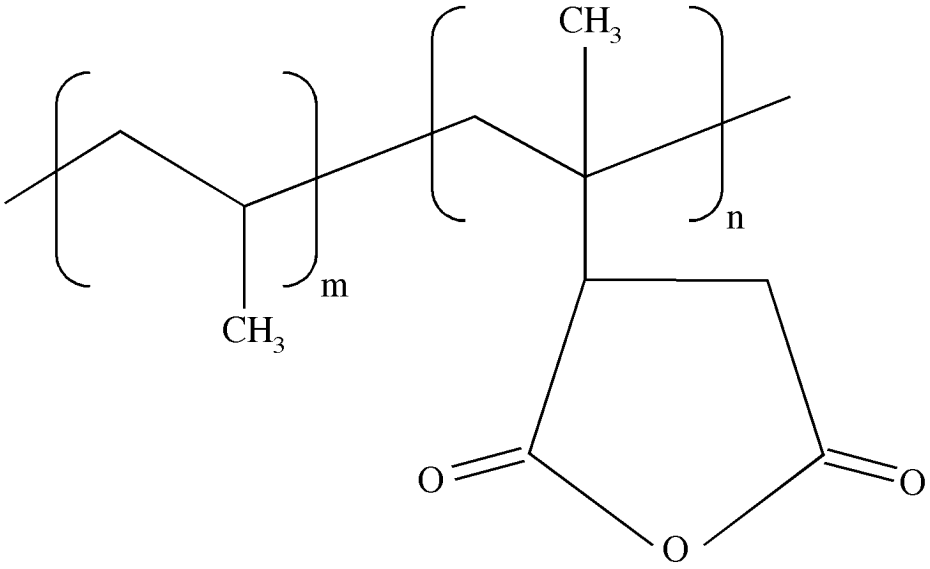

Figure 3.4: Polypropylene maleic anhydride graft copolymer.

While it would be of interest to see a similar study such as referenced above, but with maleic anhydride + LDPE or HDPP. However, it was not possible to conduct such studies because the MAPP additive was miscible only with LDPP and would not mix with higher molecular weight HDPP. Additionally, while MAPE additives did exist, their percent weight of maleic anhydride was relatively low, and therefore would not allow for a spread of different weight percentages.

Two other candidate block copolymer additives, Elvaloy PTW and Elvaloy 4170, were provided by Dow Chemical Co. (Midland, MI). Elvaloy PTW is comprised of 28 wt% butylacrylate and 5.25 wt% glycidyl methacrylate,[134] and Elvaloy 4170 contains 20 wt% butylacrylate and 9 wt% glycidyl methacrylate,[135] both with a polyethylene backbone, in contrast to the polypropylene backbone of the maleic anhydride copolymer. To elicit the strongest possible increase in adhesion, both copolymers were tested independently and compared to pure polyethylene as a control without being blended into pure polyethylene.

3.3.10 *Combination of silanes with matrix additives*

To further increase chemical linkage from the fiber to polyolefin matrix, silanes were applied to the fiber surfaces for their end groups to react with the maleic anhydride additives in the LDPP polyolefin matrix[121,136]. While pristine fibers were taken to be the control, the fibers as received already contained some reactive oxygen species, such as carboxyls and hydroxyls[137]. Since maleic anhydride can react with such groups[138,139], an increase in adhesion with maleic anhydride concentration can be expected, even in the absence of silane treatments. The effect of APS treatment was examined because it was expected that its amino terminal group might covalently bond with maleic anhydride. The AZS, i.e., 6-azidosulfonylhexyl triethoxysilane was chosen because of its purported ability to covalently attack the C-H bonds in the polypropylene backbone. The reactivity of the maleic anhydride itself, together with that of the AZS could act in parallel to increase adhesion. For testing, fibers were treated with silanes using the methods above and then tested with LDPP at varying levels of maleic anhydride, as described in the section above.

3.4 RESULTS AND DISCUSSION

3.4.1 *Baseline results*

In the absence of surface treatments or modifications, the carbon fiber/matrix adhesion (IFSS) levels obtained for the three different polymers used were: LDPE 1.9 MPa, LDPP 9.7 MPa, and HDPP 5.0MPa. The results obtained for various treatments and modifications are to be compared with these baseline values.

3.4.2 *Silane coupling agents*

Results showing the effect of the three silane treatments used are shown in Figure 3.5. The vinylethoxysilane homopolymer (VPS) and 3-aminopropyl trimethoxysilane (APS) treatments were expected to produce enhancements in adhesion due to interdigitation of the organofunctional groups into the polymer matrix, and are seen to have produced only small enhancements. The 6-azidosulfonyl hexyltriethoxysilane (AZS), however, with its ability to react directly with C-H bonds in the polyolefin itself, increased the IFSS over six-fold to a value of approximately 13 MPa.

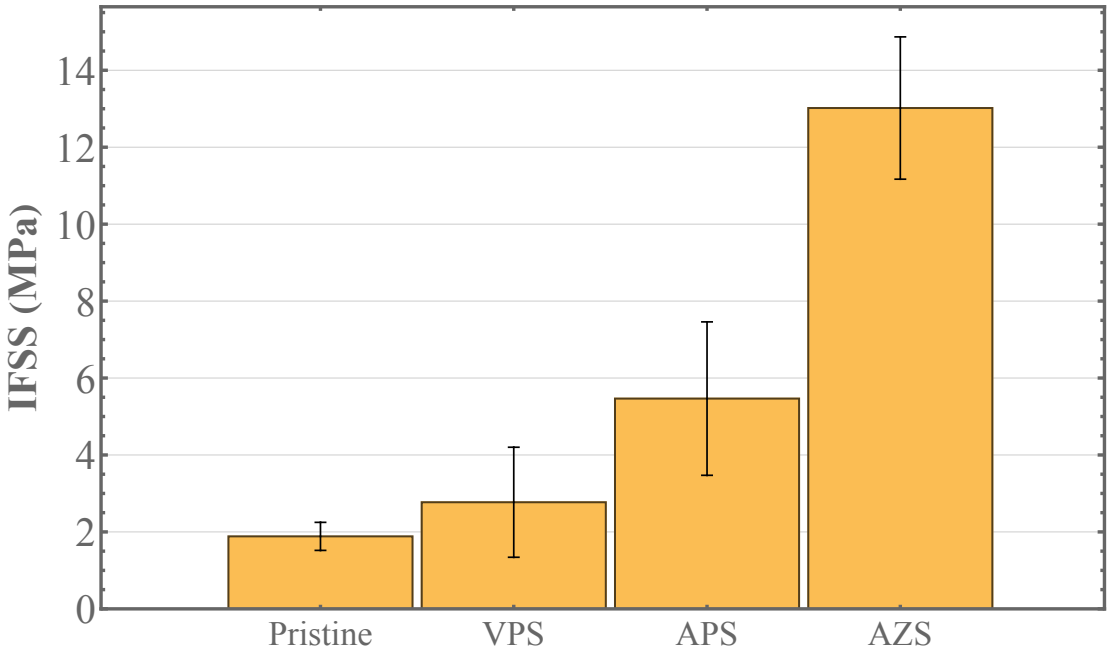

Figure 3.5: Adhesion (Mean IFSS ± SD) of LDPE to as-received T700 GC-12k-91 carbon fibers and those treated with vinylethoxysilane homopolymer (VPS), 3-aminopropyl trimethoxysilane (APS), and 6-azidosulfonylhexyltriethoxysilane (AZS).

3.4.3 *Titanate and zirconate coupling agents*

Contrary to silanes, titanates and zirconates do not require hydrolysis and attach to the surface of carbon fibers through acid-base interactions. They are thought to be more resistant to high temperatures, a concern for composite materials enhanced with silane coupling agents, and bond to a wider variety of substrates[140]. The results for the titanates and zirconates tested with a polyethylene matrix are shown in Figure 3.6 where they are labeled with their industrial names.

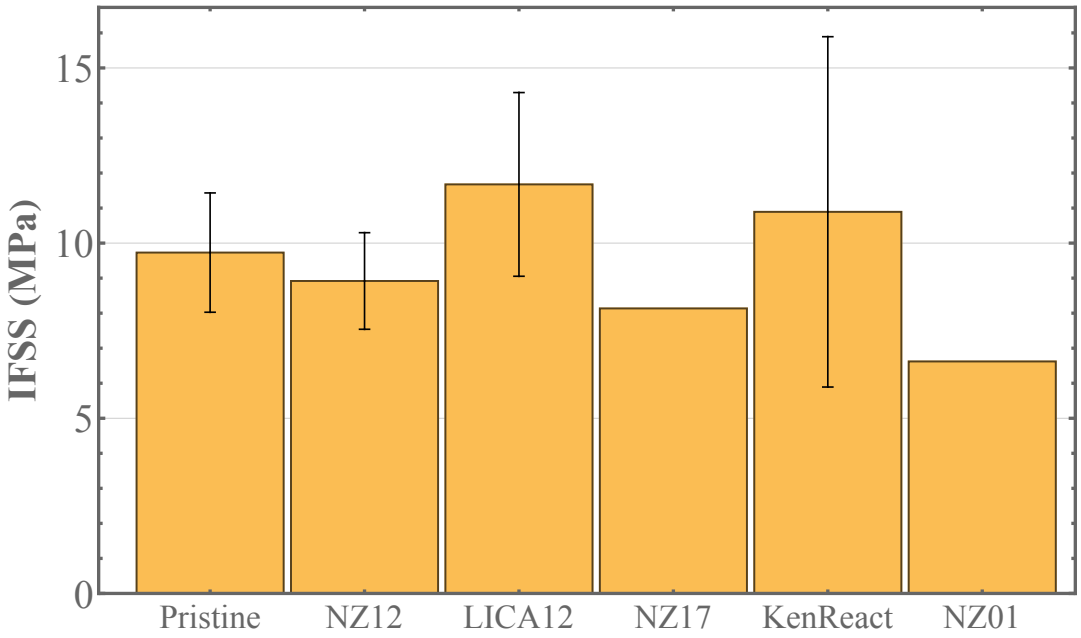

Figure 3.6: Adhesion (Mean ± SD) results for carbon fibers and LDPP mixed with 1% titanate or zirconate, identified by their industrial shorthand names.

The results show no significant enhancement in adhesion for any of the compounds tested. It appears that even if effective migration and interaction with the carbon fiber surfaces occur, the outward-facing functional groups of the titanates and zirconates, have little or no interaction with the matrix polymer LDPP. While these compounds were not effective in the system studied, they have shown promise with more reactive matrices [141,142].

3.4.4 *Surface functionalization with peroxides*

The grafting of vinyl silane (VTS) to an HDPP matrix through the use of dicumyl peroxide initiator produced the results shown in Figure 3.7. In addition, adhesion between HDPP and AZS fibers is shown. While it was anticipated that increases in adhesion with the peroxide method would elicit larger increases in adhesion, it boosted adhesion only a modest amount, from roughly 5.0MPa to 8.2MPa.

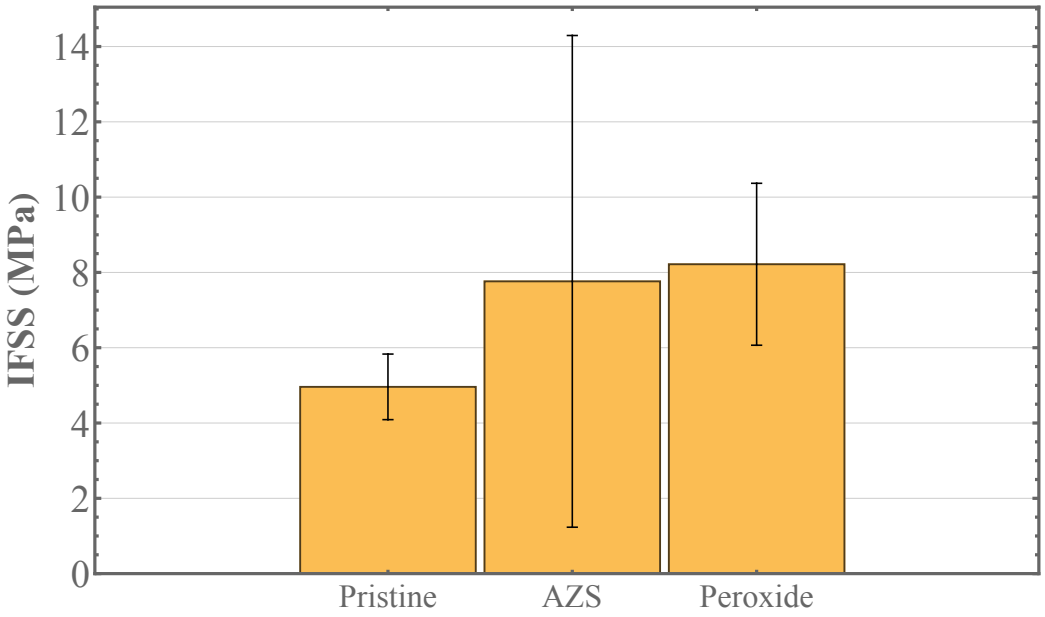

Figure 3.7: Adhesion (Mean ± SD) for pristine, AZS, and peroxide treated carbon fibers in HDPP.

3.4.5 *Fiber roughening*

Roughening treatments qualitatively had differing levels of effects on the fiber surfaces, as seen in Figure 3.8. The nitric acid treated fibers produced little to no difference in topography, in contrast to work reported by others[104,130]. Bleach treatment was seen to produce significant,

uniform roughness. The plasma/ozone had little to no effect, and the presence of bumps could be remnants of sizing or impurities that reacted with ozone to create silicon dioxide or other oxidized debris. The ammonium hydroxide treatment enhanced the axial crenulation of the fibers.

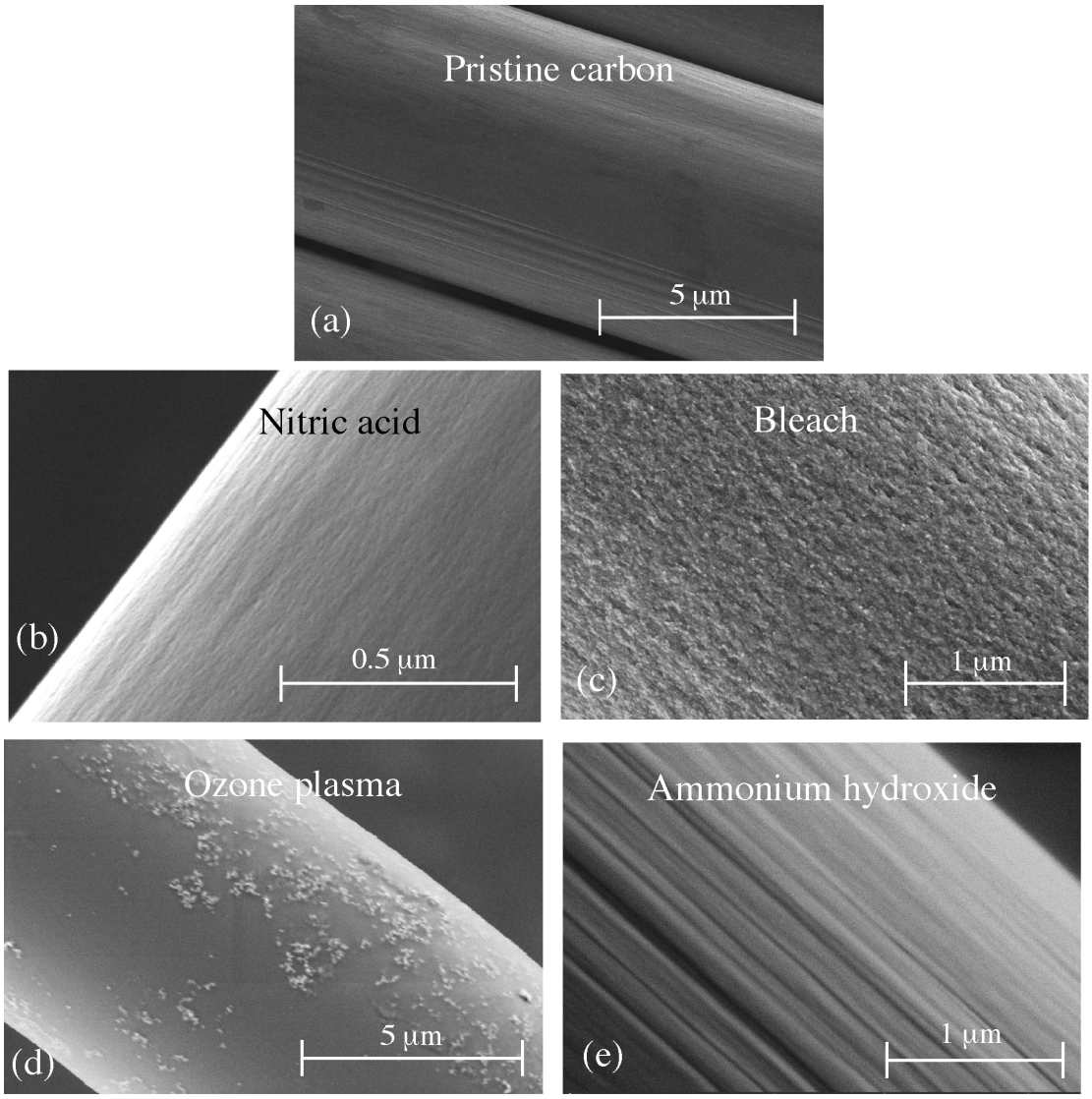

Figure 3.8: Scanning electron micrographs of (a) pristine carbon fibers, (b) fibers treated with nitric acid, (c) fibers treated with bleach, (d) fibers treated with an ozone plasma, and (e) fibers treated with ammonium hydroxide. Images were acquired using an Apreo Variable Pressure SEM (ThermoFisher Scientific, Waltham, MA), courtesy of the University of Washington Molecular Engineering & Science Institute's Molecular Analysis Facility.

Increased surface roughness might be expected to increase mechanical interlock between the resin and the fiber for low surface tension fluids such as polyolefins,[117] but the results shown in Figure 3.9 do not seem to sustain the claim that increased roughness and mechanical interlock lead to increased adhesion. This can be attributed to insufficient roughness asperities, and in the case of the ammonium hydroxide, the co-linearity of roughness features with the applied stress. A modest increase in adhesion was observed only for the bleached surfaces.

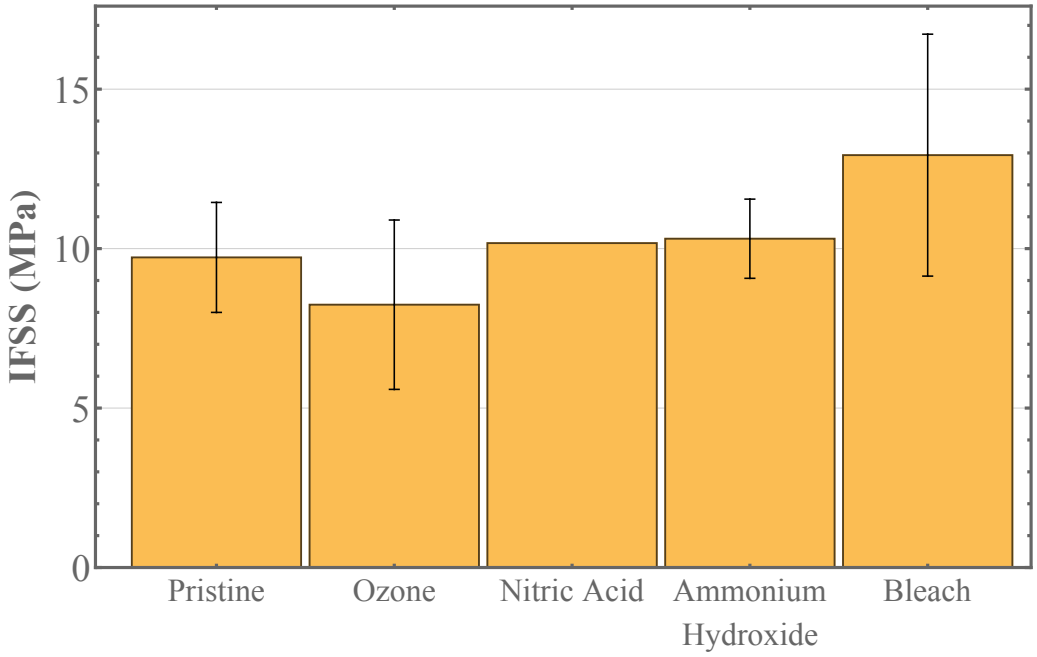

Figure 3.9: Adhesion (Mean ± SD) results for carbon fibers roughened with different treatments embedded in LDPP.

3.4.6 *Interface softening; formation of an interphase*

It was anticipated that the toluene solvent used would diffuse into the polypropylene and dissolve it in the region adjacent to the fiber surface[143,144], producing a viscoplastic inter*phase*

and a different type of adhesive failure. The type of adhesive was indeed different from that obtained without interface softening, as shown in Figure 3.10, which compares the case of a pristine fiber/LDPE interface with that of a pristine fiber toluene-softened inter*phase*. The force required to cause detachment was approximately doubled, such that the ultimate IFSS also increased (by a factor of roughly 2.8), however, the absolute IFSS for such systems was still relatively low. Therefore, while this technique could be used for modifying the interphase region and reducing its stiffness, it could not be relied upon to significantly change adhesion.

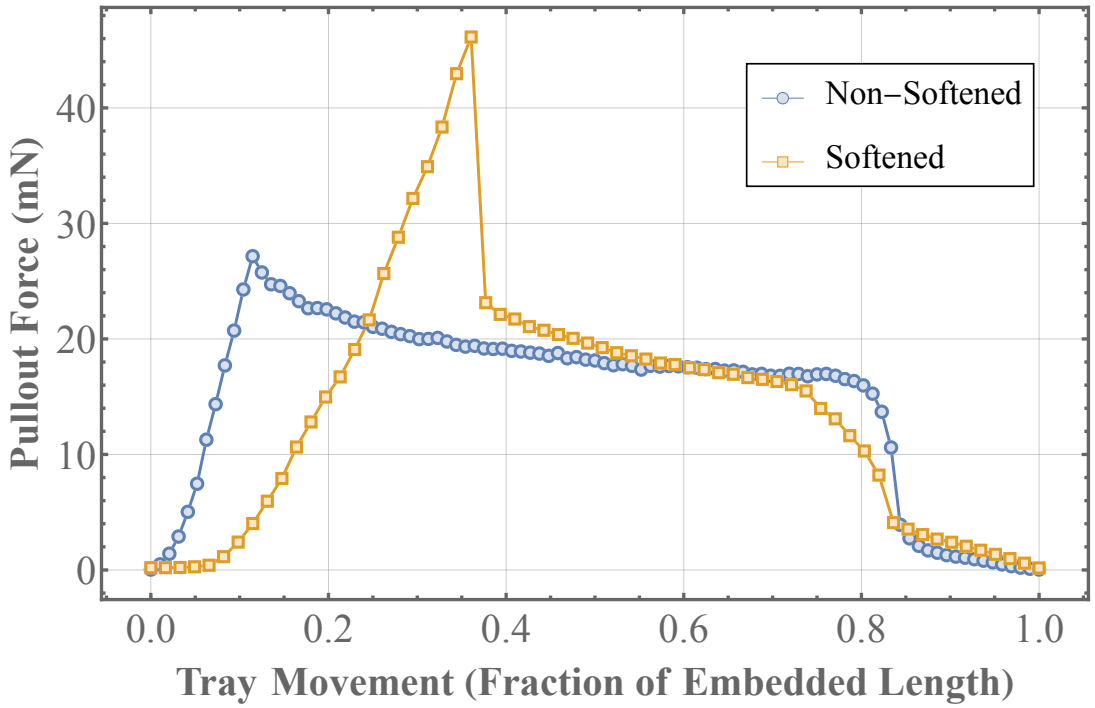

Figure 3.10: Measured adhesive force between dry LDPE and the softened LDPE against an unsized carbon fiber *vs.* tray position. Orange squares represent softened matrix, blue circles represent non-softened matrix.

3.4.7 *Matrix additives and combinations of silanes with matrix additives*

The two new candidate matrix additives tested, Elvaloy PTW and Elvaloy 4170, polyethylene terpolymers normally used as tougheners, contain butylacrylate glycidyl methacrylate groups, offered the possibility of chemically interacting with hydroxyl groups on the pristine carbon fibers. While increases in adhesion were observed, as shown in Figure 3.11, the final values remained small.

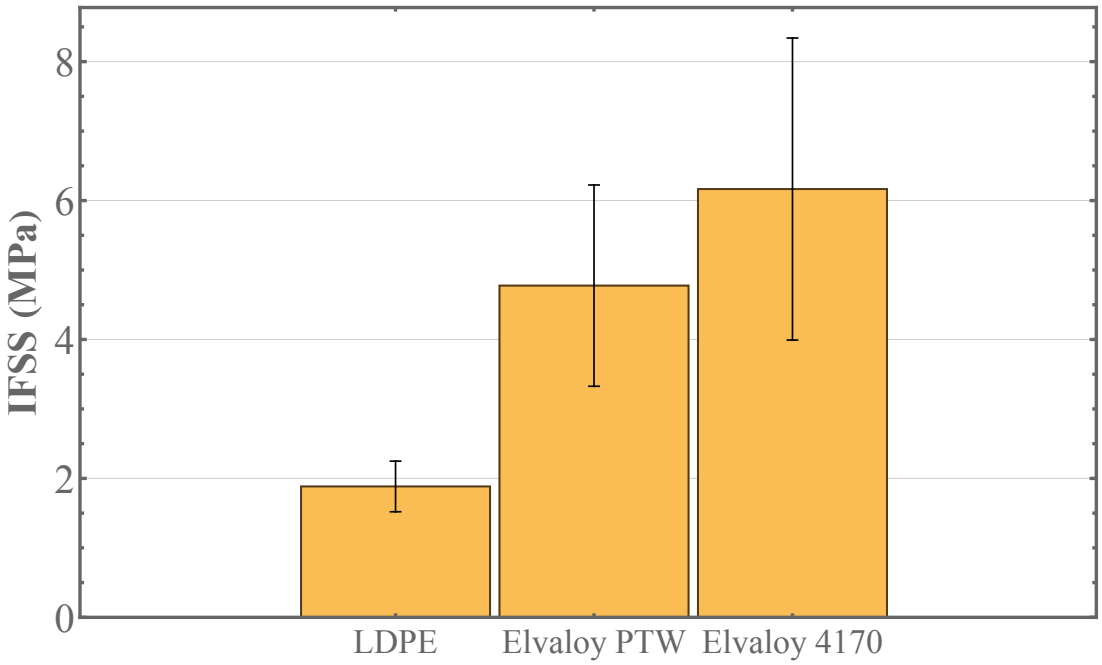

Figure 3.11: Adhesion (Mean ± SD) results for pristine carbon fiber and LDPE, and different polyethylene block copolymer matrix additives.

Figure 3.12 shows the results obtained using the maleic anhydride matrix additive to LDPP at various levels, both without and with various silane surface treatments. It is first noted that the adhesion level of the untreated fibers was increased to a level of approximately 20 MPa, twice the value in the absence of the additive. Secondly, it is seen that the presence of the amino

silane (APS) had no effect on IFSS at any concentration. The most interesting result was that obtained for the combination of 6-azidosulfonylhexyltriethoxysilane (AZS) surface treatment with the presence of the maleic anhydride matrix additive. IFSS values rose from the baseline value of nearly 10 MPa to nearly 30 MPa with the increase in maleic anhydride content.

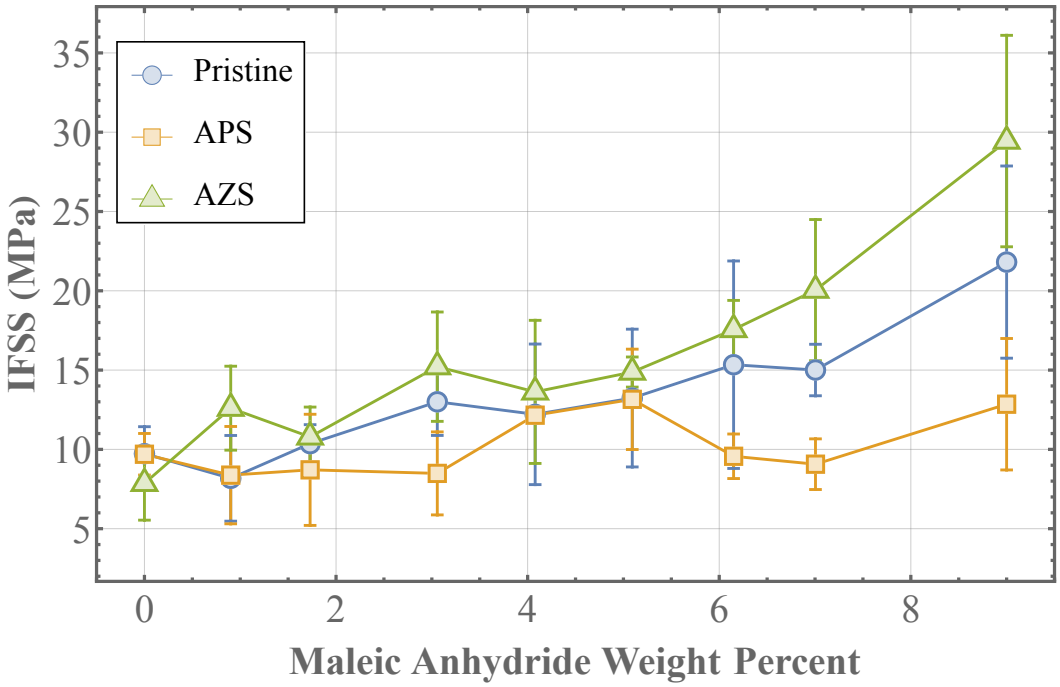

Figure 3.12: Adhesion (Mean ± SD) results for pristine carbon fiber and LDPE, and different polyethylene block copolymer matrix additives. Blue circles represent pristine fibers, orange squares represent APS fibers, and green triangles represent AZS fibers.

Even though the final increases in adhesion due to the addition of maleic anhydride suggest a promising future for industrial application, a limitation is that the final data refer to pure polymer additive. With weight percentages of maleic anhydride as high as 9 wt%, the originally robust properties of polypropylene and polyethylene, such as toughness and impact strength begin to degrade.

3.5 CONCLUSIONS

This study presents the results of adhesion testing using the fiber pullout technique for a commercial carbon fiber, Toray T700 GC-12k-91, embedded in a polyethylene (LDPE) or polypropylene (LDPP or HDPP) matrix for a variety of fiber surface treatments and matrix modifications. Adhesion levels in the absence of modifications were low, specifically in terms of interfacial shear stress (IFSS) values: LDPE 1.9 MPa, LDPP 9.7 MPa, and HDPP 5.0 MPa. Surface modifications used were treatments with 3-aminopropyltriethoxysilane (APS), vinyltriethoxysilane (VTS), vinylethoxysilane homopolymer (VPS), 6-azidosulfonylhexyl triethoxysilane, (AZS), and two titanate and three zirconate coupling agents. With the exception of the AZS treatment, all enhancements were modest, ranging from negligible to factors up to two. Similarly, modest enhancements were achieved for fiber surface roughening and for the production of a softened inter*phase*. These results suggest that whatever increases in adhesion achievable through purely physical interdigitation or interlocking are unable to produce adhesion levels needed for adequate strength of a carbon fiber reinforced polyolefin composite. AZS treatment, on the other hand, was able to achieve an increase in IFSS for the fiber/LDPE system from about 2 to 13 MPa. This significant enhancement can be traced to the chemical linkage of the azidosulfonyl group of the silane with the backbone of the polymer. The bonding of the matrix to vinylsilane-treated fibers through the use of peroxide initiators, however, produced only modest improvements. The use of maleic anhydride matrix modifiers to LDPP produced an increase of adhesion over that of the untreated fibers from 9.7 to about 20 MPa, but their use in combination with most silane treatments produced no added benefit. The most promising result was achieved with the maleic anhydride matrix additive in combination with fiber surface treatment with AZS (6-azidosulfonylhexyl triethoxysilane), which increased the IFSS to nearly

30 MPa. It may be concluded that while strategies for improving purely physical interactions will be unable to produce adequate enhancements in fiber-polyolefin matrices, there are promising techniques for achieving this goal through chemical attack and attachment to the polymer backbone.

Chapter 4. THE TAILORING OF INTERFACIAL ADHESION AND ITS EFFECTS ON MATERIAL PROPERTIES FOR CARBON-FIBER REINFORCED POLYMERIC COMPOSITES

*Sections of this chapter come from the journal publication:
ElKhoury L, Berg JC. The tailoring of interfacial adhesion and its effects on material properties for carbon-fiber reinforced polymeric composites. *Journal of Adhesion Science and Technology* 2023; 0: 1–22.

4.1 CHAPTER SUMMARY

Carbon fiber reinforced polymeric composites have long been of interest owing to their remarkable properties of high strength, toughness, and low weight. Part of their appeal comes from their customizability to fulfil a large number of applications. Controlling the degree of interfacial adhesion between the fibers and polymeric matrix is one of the important ways of optimizing composite properties for desired applications. The present study examines a simple technique for modulating adhesion, its measurement using single-fiber fragmentation, and its effects on the tensile, flexural, and impact properties of the corresponding fiber tow composites. Adhesion was modified by coating untreated Hexcel IM7 fibers to various levels with room temperature "vulcanizing" silicone dissolved in the mixed alkane solvent Isopar™ L. The matrix polymer was Epon862 with an Epikure curing agent W. Fiber tows consisted of 12k fibers, and were tensile, 3-point bend, and "Charpy" impact tested to evaluate their mechanical properties. Interfacial adhesion was reduced from 101 MPa to near zero, while impact toughness was more than doubled. The tensile modulus decreased only up to 25%, while the flexural modulus decreased by approximately 50%. Ultimate flexural strength and flexural modulus decreased. Energy to failure had no meaningful changes.

4.2 INTRODUCTION

Carbon-fiber reinforced polymeric materials are widely used in many applications due to their superior mechanical properties such as high modulus, excellent weight adjusted strength, high toughness, and robust fatigue lifetime, all dependent at least in part on the adhesion between the fibers and the polymer matrix. While it has long been recognized that static (or strain-rate independent) strength properties are optimized when adhesion is maximized, [47–50,145–147] strain-rate dependent properties, such as impact toughness, have a more complex relation to interfacial adhesion[148–155]. Impact toughness (energy needed to cause failure from sudden impact) and plasticity of the interfacial region directly affects the ability of the composite material to withstand sudden, dramatic changes in loading conditions.[81] The level of adhesion in composites also affects the way that interfacial fractures occur[47]. Maximum adhesion can elicit brittle fracture and sudden material failure due to crack tip migration from fiber breaks directly to the surrounding resin matrix while a system with relatively lower adhesion can blunt impacts by absorbing some energy at the fiber-matrix interphase resulting in mode-two debonding, i.e., delamination. Such "interfacial softening" is often used to alleviate spontaneous failure in composite materials such as bullet-proof vests, armor plating, and sporting equipment.[156]

For example, *Concept2, Inc.* (a top tier rowing oar and sports equipment company) has been focusing recently on improving the impact toughness of rowing oars, which are comprised mainly of carbon fiber reinforced thermoset polymer composites (Kevin Stevenson, Concept2, Inc., September 14th, 2022, personal communication). One of the main motivations derives from the recent increase in popularity of open ocean rowing races where blades and oar shafts commonly impact other oars, boats, docks, buoys, and submerged objects. One method used to address the poor impact toughness was to use carbon fibers of lower modulus, thus lowering the

total modulus of the composite itself. The drawback to this is that more fibers must be used to sustain typical loading conditions, increasing the weight of the oar. The effort to optimize the properties of composite rowing oars to meet impact toughness requirements is ongoing.

In another example, Jensen et al.[152] described E-glass fiber-matrix adhesion modification using different silane coupling agents to affect interfacial chemistry and different fiber roughness to affect frictional forces. While the usual tradeoff between strain-rate independent properties and impact strength existed, they found that by coupling fiber roughening with a mixture of "compatible" and "incompatible" silane surface treatments, they were able to maintain adequate structural properties while improving impact properties. Chen et al.[157] presented a method to create carbon fiber–epoxy interphase regions that increase adhesion by dip coating them in dopamine solutions creating polydopamine films. Other studies have shown a variety of other techniques to alter adhesion and the interphase such as, roughening of the surfaces through grit-blasting[158], adding core-shell particles to glass fiber surfaces[159,160] , the grafting of amino-POSS onto fiber surfaces[148], using mixed groupings of silanes to elicit optimal adhesion[161], growing carbon nanotubes on carbon fiber[162], or the grafting silicon dioxide nanoparticles.

Examples of adhesion modification in other types of systems yield similar results. Javanshour et al.[164] examined the use of thermoplastics to modify the interphase of flax-epoxy composites. Flax fibers were treated by coating them in biobased cellulose acetate of 3μm thickness, allowing more extensive plastic deformation in the interphase region. While slightly decreasing static properties such as flexural strength, substantial improvements for large impacts were also revealed. In similar work, Gassan et al.[165] and Koolen et al.[166] studied the effects of modulating the fiber-matrix interphase region using a silicone (a softer thermoset polymer) to coat flax fibers to create an interphase region for flax-polyurethane and flax-epoxy composites.

Both studies altered the silicone layer thickness by dipping fibers in a toluene solution with increasing silicone weight percentages. Gassan et al.[165] examined how the silicone interphase would affect stress transfer from the matrix to the fibers under different hygroscopic conditions. Among other findings, they revealed that the coating did not have noticeably deleterious effects on stress transfer. Koolen et al.[166] more traditionally studied how such interphases would affect strain-rate dependent properties such as impact toughness, finding that while static properties such as flexural strength and modulus dropped, impact toughness increased by a factor of two, and fatigue properties also improved. In another example, Luo et al.[100] controlled fiber interphase thickness by using a layer-by-layer technique (LBL) to alter graphene oxide and polyethyleneimine coatings on carbon fibers for polyolefin composites.

Previous work[165] has shown that the addition of a soft fiber-matrix interphase layer may be helpful for the improvement of impact strength properties. However, it has also been studied that there is an inherent tradeoff between interfacial adhesion and impact toughness[167–170]. Interestingly, even though the tradeoff in properties is proportional to the amount and thickness of the soft, interphase coating, it has also been shown that optimal amounts of coating exist where increases of impact toughness are achievable while minimizing the reductions in other strain-rate independent properties[169,171,172], underscoring the need for methods that can discreetly deposit polymer onto the fiber surface. Furthermore, not only the thickness of the interphase affects the overall properties of the composite, but also the modulus of the interphase as well. In a review paper, Labronici et al.[171] found that interphase layers with roughly one-tenth the modulus of the continuous matrix phase exhibit optimal properties[173]. Therefore, not only the amount but also the type of polymer can be used as an effective control for tailoring interfacial properties.

While the tailoring (increasing or decreasing) of adhesion in composites to achieve desired property profiles has been investigated, the results for carbon fiber reinforced polymers are not entirely satisfactory. The most widely-used method is fiber surface modifications using silane coupling agents[126,140,174], which are expensive and often difficult to bond to these substrates[126,175]. Other methods that have been examined have also been costly and tedious to complete. Even though the method of modifying composite properties through the addition of a soft, polymer interphase has been studied and discussed in the paragraphs above, such studies miss some aspects that may contribute to the total knowledge of this technique. Namely, they tend to focus on the relation of mechanical properties to interlaminar shear strength, which displays aggregate fiber-matrix adhesion rather than the more fundamental, single-fiber-matrix interfacial adhesion. Additionally, most of these studies tend to use high quality reagents for the deposition of a soft, polymer interphase. The proposed work plans to study the relationship between silicone deposition, single-fiber-matrix adhesion, and mechanical properties, all while presenting some practicality by using materials that can be purchased cheaply and in bulk rather than from a chemical vendor. Readily available sealant, viz., a room-temperature-vulcanizing (RTV) silicone, dispersed in the hydrocarbon solvent Isopar™ L, is evenly coated in a controlled manner to varying levels onto Hexcel IM7 carbon fiber surfaces before their incorporation into a matrix of Epon862 with an Epikure curing agent W. The study first seeks to quantify the adhesion strength (IFFS) using standard single fiber fragmentation tests as described by Drzal[79,126]. For single fibers, the silicone is coated layer-by-layer, thus progressively altering the interphase region. The effect of the varying adhesion levels on composite mechanical properties is examined using fiber tows for which the silicone was applied by dip coating them into solutions of varying concentration. The study investigates the impact, flexural and tensile

properties of the fiber tow composites to determine the degree of their correlation with the level of interfacial adhesion. Finally, rheological data were collected for the cured silicone to determine its various storage and loss properties under select conditions.

4.3 Experimental Methods and Materials

4.3.1 *Single fiber strength testing*

Single fiber strength testing was completed in the same manner as in section 2.3.8. For additional information, please refer to page 29.

4.3.2 *Single fiber-matrix adhesion testing*

Single fiber-matrix adhesion testing was completed in the same manner as in section 2.3.9. For additional information, please refer to page 31.

4.3.3 *Single fiber diameter measurements through wetting force analysis*

Even though the analysis for interfacial adhesion used the fiber diameter value reported from the Hexcel data sheet, and corroborated through SEM imaging, fiber diameters were also calculated through wetting measurements – which are typically referred to as the "wetted perimeter/ diameter." In theory, the wetted perimeter/diameter will have a greater value than those found through microscopy. This is due to inherent crenulations and roughness present on most surfaces, which cause a slightly larger surface area when compared to a smooth surface. This value is useful because it can be used to measure the degree of surface roughness and is also necessary to calculate surface energies through wetting measurements.

For testing, single fibers were laid flat on a small strip of manila paper and then taped down to prevent movement. After, the strips were cut into small squares with the fiber protruding

at one end. Next, single fibers were taped onto a copper hang-down wire attached to a Cahn microbalance (Cahn Scientific, Irvine, California). A small pool of Hexamethyldisilane (HMDS, σ = 16 mN/m) was positioned below the fiber. For testing, force measurements were taken with the fiber out of solution and inserted in the solution. The difference in downward force measured on the electro balance was contributed to surface tension forces (where the negligible contribution of buoyancy is discarded), which can be seen in Eq. (4.1).

$$F_{\downarrow} = P\sigma Cos(\theta) \xrightarrow{\text{cylinder}} \pi D\sigma Cos(\theta) \tag{4.1}$$

Where $F_{\downarrow}$ is the downward force on the fiber, P is the wetted perimeter of the solid, D is the fiber diameter (assuming that carbon fibers are cylindrical), σ is the probe liquid surface tension, and cos(θ) is the contact angle made between the fiber and the probe liquid. The equation can be rearranged, and fiber diameter can be calculated knowing the surface tension of HMDS and assuming that cos(θ) = 1 (corresponding to a total wet out) given the incredibly low surface tension of HMDS. A force readout used for calculation can be seen in Figure 4.1

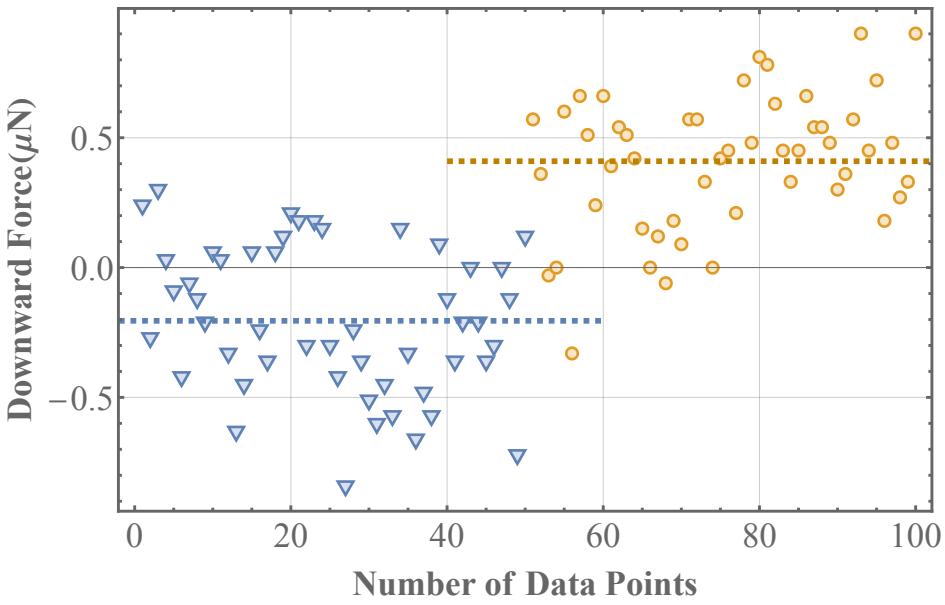

Figure 4.1: Example of downward surface tension wetting force measurements on a carbon fiber. The blue triangles represent when the fiber is out of the liquid. And orange circles represent fibers inserted in the probe liquid. The difference of the average value of both sets (shown as the dashed lines) is calculated to determine $F_{\downarrow}$.

For the carbon fibers used in this experiment, the average wetted diameter was found to be 7.2 ± 1.7 μm (mean ± SD) compared to the reported value of 5.2μm.

4.3.4 *Single-fiber silicone coating*

For single fiber coatings, a 1% (w/w) solution of silicone sealant (Liquid Nails, Akzo Nobel Paints LLC, Strongsville, OH) was dispersed in a solution of C10-C13 paraffins, Isopar™ L (ExxonMobil Chemical, Irving, TX) and stirred until fully dissolved. The silicone sealant was composed of a cross-linking agent (Methyltri(2-Butanoneoximyl) Silane), a polymer (Dimethyl (Polysiloxane)), and a filler (silica). Cross-linking and hardening of the thermoset occur when the silane (cross-linking agent) reacts with water from the atmosphere and hydrolyzes to form

silanol groups. Next, the silane and siloxane polymer undergo a condensation reaction, thus causing chain linking and extension[176].

To avoid excessive deposition of silicone on the fiber surface as well as to have a finer degree of control for coating thickness, fibers were coated with varying numbers of layers of the same silicone solution. For sample preparation, single fibers were strung on a thick paper strip and taped down to maintain their position. All samples were brushed with a cotton swab with the silicone solution on the front and back part, where each brushing was defined as one coating. The samples were placed in the oven (Model 825F, Fisher Scientific, Hampton, NH) set to 100°C for 10 min to evaporate the trace solvent, leaving only silicone. These steps were repeated until the desired number of coatings was reached.

4.3.5 *Scanning electron microscope imaging*

All electron microscopy samples were mounted on aluminum stands and adhered using black carbon tape. No conductive coating was necessary to perform imaging of single fibers, and 4 nm of platinum sputter coating was applied to image the cross sections of fiber tows. Apreo Variable Pressure SEM (ThermoFisher Scientific, Waltham, MA) was used at 2 kV and 13 pA. All samples were laid flat in SEM and images were taken in high vacuum conditions.

4.3.6 *Fiber tow composite sample preparation*

Similar to the work of other researchers[177–179], fiber tow composite samples were prepared by infusing the treated fiber tows with the epoxy resin mixture described in the materials section. After silicone treatment, as described below, significant amounts of fiber bridging were caused from the silicone during the drying process. Therefore, the fiber tows were first massaged to dislocate as many fiber bridges as possible. Next, the resin and hardener were

mixed and degassed. Afterwards, the fibers were slowly dipped into the resin mixture and tamped down with a metal spatula to ensure maximum fiber-resin contact. Then, the samples were pulled out through a 1.5mm aluminum die to aid in uniformity while removing excess resin. Lastly, the uncured tow composites were hung on a non-stick rod and weighed down with 5 g weights on each side. Once ready, all samples were cured in the oven by increasing from room temperature to 93°C at 2.3°C/min, set at 93°C for 2 h, then ramped again from 93°C to 121°C at 2.3°C/min and set at 121°C for 8 h.

4.3.7 *Fiber tow surface treatment*

For experiments involving fiber tow testing, the fibers were coated with silicone in a slightly different manner because of the inability to coat fiber bundles with a brush in a layer-by-layer fashion. Therefore, to deposit differing amounts onto the bundles, silicone Isopar™ L solutions were made with silicone weight percent ranging from a control value of 0% to a maximum value of 5%. The solutions were then stored in sealed containers. A 50-cm strip of fibers was dipped into solution and then pulled out and carefully squeezed between two fingers to remove any excess liquid. They were then hung on a rod and placed in an oven at 100°C for 5 h. The amount of silicone deposited on the fiber tows was also measured by calculating the weight difference between untreated and post-treated, dried fibers.

How the level of silicone sizing affected (if at all) the tow diameter was also a pertinent detail. It was assumed throughout this study, and verified through inspection, that the tow composites take a cylindrical shape with a circular cross-section. The average value for multiple width measurements with electronic calipers was used for future measurements. It is nearly impossible to create samples with perfect cross-section uniformity, so each set of diameters was based on no less than eight measurements.

4.3.8 *Fiber volume fraction in tow composites*

Two main methods for determining the volume fraction of reinforcements in polymeric composites have been acid digestion[180] and thermogravimetric analysis[181–183]. The volume fraction of fibers in a cured tow composite for this study was determined by thermogravimetric analysis (TGA). For all tests, small samples were placed in a ceramic pan and inserted into a TA Instruments Model Q200 TGA (TA Instruments, New Castle, DE). During testing, air was blown over the samples at a rate of 50 mL/min, and the temperature was increased from room temperature to 530°C at a rate of 20°C/min, then soaked for 60 minutes at 530°C. At this point, the test was considered complete. Then weight measurements from TGA, combined with the fiber and cured resin density values provided by their manufacturers,[82,184] were used for the calculation of fiber filling fraction.

4.3.9 *Fiber tow impact testing*

Impact testing for fiber tows was done by slightly modifying ASTM E2248 − 18, "Standard Test Method for Determining the Charpy Impact Resistance of Notched Specimens of Plastics." [185] The main reason that the ASTM could not be followed exactly was due to slight differences in sample geometry and material makeup. Specifically, this ASTM is used for notched plastics, rather than composite filament tows, which could not be notched in a reliable manner. Nevertheless, the steel striking hammer which was used for the testing was made by following the layout as put forth in ASTM E2248-18.

The testing apparatus, shown schematically in Figure 4.2 was comprised of a stiff aluminum rod with a striking hammer attached at the tip. The base of the pendulum was attached with a ball bearing to a raised, horizontal bar. Beneath the horizontal bar were two cylinders perpendicular to the base, with a clipping apparatus used to attach and hold the testing filament

while not imparting undue stress concentration factors. The span between testing holders was set to be 40 times that of the sample set's average diameter. All samples were held in place by tightening them with a torque wrench set to 5.65 Nm. A protractor was attached to the pendulum to record both the initial and final angle, which later was used to measure the energy absorbed in impact. The total mass of the kinetic pendulum was 271.1 g, and the center of mass (found by balancing the rod on a thin blade) was 380 mm away from the axis of rotation.

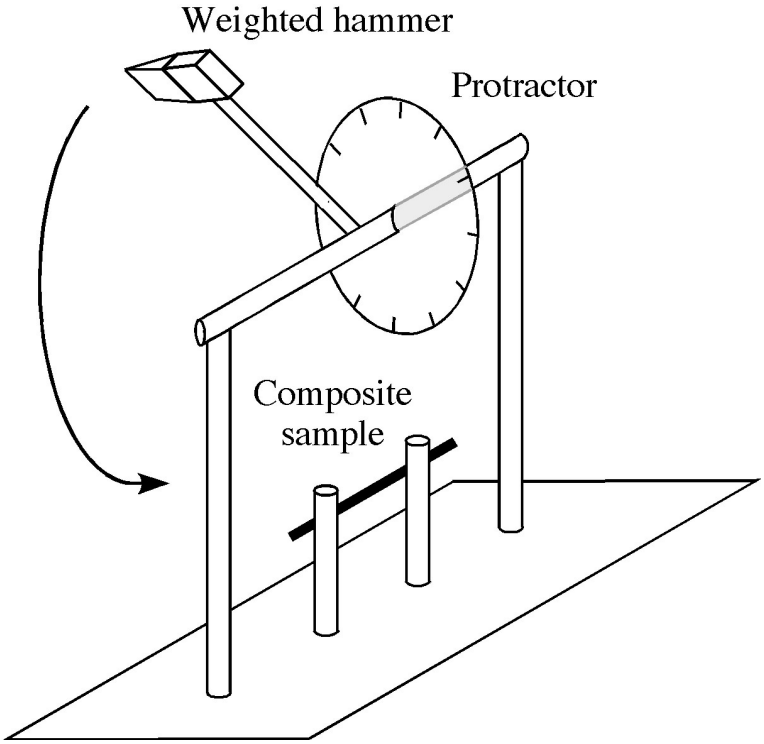

Figure 4.2: Schematic of the pendulum impact-testing device for composite fiber tows. The tip of the weighted hammer converges at a 30° angle to a ~1mm.

Testing was done by raising the pendulum to a defined angle (10° from the vertical) and then dropping it. After dropping from a standstill and becoming perpendicular to the floor, the hammer impacted and broke through the fixed composite tow sample and then continued traveling to a final height. The difference between the initial and final potential energy of the

pendulum (also accounting for frictional losses) was defined as the impact toughness. An energy balance was used to find the difference in potential energy (while also taking frictional losses into account). The schematic for which can be seen below in Figure 4.3.

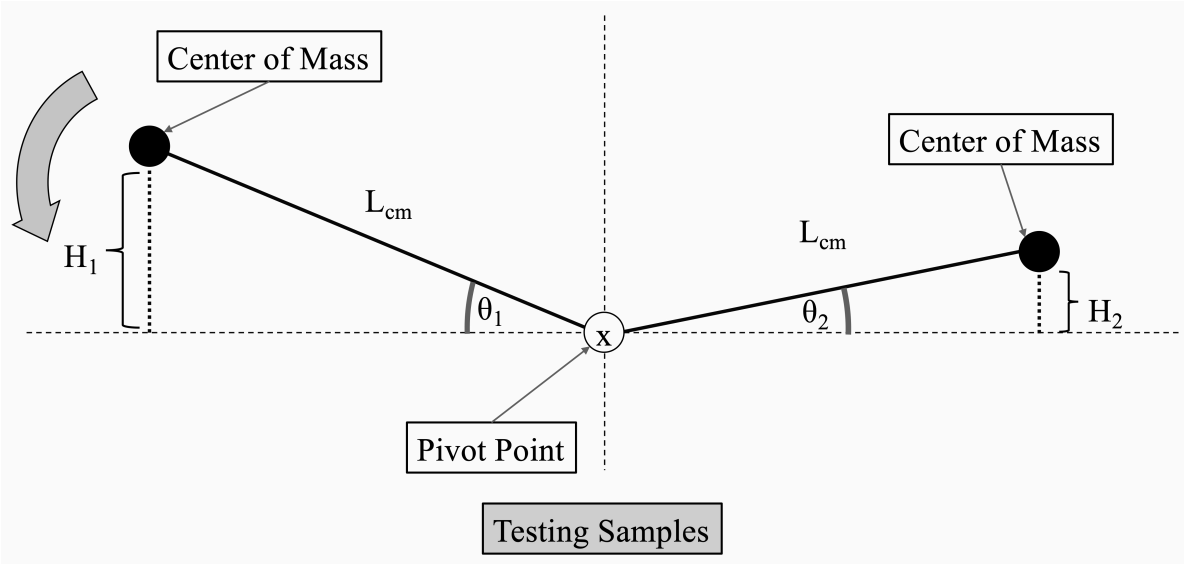

Figure 4.3: Pendulum schematic used for the energy balance to calculate impact toughness of composite fiber tows.

In Figure 4.3, a pendulum is held at an initial angle, θ_1, and is then dropped with an initial velocity of zero to rotate counterclockwise, pass through the testing sample, and then end with the final angle θ_2. These angles can be used along with center of mass measurements to perform energy balances:

$$PE_1 = PE_2 + f_{loss}(\theta_t) + E_{impact} \tag{4.2}$$

$$PE_i = mgH_i = mgL_{cm}\sin(\theta_i) \tag{4.3}$$

Where PE_i is the potential energy of the pendulum at point i, $f_{loss}(\theta_t)$ is the energy loss due to friction as a function of the total degrees of rotation for each test, and E_{impact} is the energy absorbed by breaking the composite tow sample. m is the total mass of the weighted pendulum, and g is the gravitational constant. To find the energy loss value in the system due to friction and air resistance, the testing setup was run without any composite tow in the holder, leaving the E_{impact} value to equal zero. Multiple trials were run with varying θ_1 values (10°, 20°, 30°, 45°) to determine an average θ_2 value so the $f_{loss}(\theta_t)$ term from Eq. (4.2) can be calculated. Once completed, all future tests can use a combination of Eqs. (4.2) and (4.3) to determine the E_{impact} value for a set of samples.

4.3.10 *Fiber tow tensile testing*

Tensile properties of the fiber tow composites were analyzed with guidance from ASTM D4018-17[186]. To measure how the amount of silicone on the fibers and therefore magnitude of fiber-matrix adhesion, would affect tensile properties, all sets of fiber tows were soaked in silicone Isopar™ L solutions of varying concentration and then fully dried. The tows were made into four sets of fibers soaked in Isopar™ L with 0%, 1%, 2.5%, and 5% silicone by weight. To dampen the stress concentration factors at the gripping section of a tensile device, the tow ends were tabbed at both ends by sandwiching them between two 2x5cm corrugated cardboard sheets using cyanoacrylate (Super Glue Corporation, Ontario, CA), leaving a gauge section of approximately 10 cm in length. However, individual gauge lengths were measured with electronic calipers to ensure the most accuracy. Once prepared, the samples were pressed together between two flat plates at moderate pressure until fully cured (30 – 60 min).

Tensile testing was effected using an Instron Model 5585 (Boston, MA), and relevant calculations were performed with the accompanying BlueHill® 3 software. Samples were loaded

into two separate clamps and strained at a rate of 1 mm/min until failure. All composite tow testing sets had a minimum of five samples where the measured variables were: strain-at-failure, tensile modulus, energy to failure, and ultimate tensile stress.

4.3.11 *Fiber tow flexural testing*

The effect of interfacial adhesion on tensile properties has been widely investigated using single tow composite testing, but the study of flexural properties using three-point-bend tests on fiber composite tows is less explored. Although complicated by mixed-mode strain, it may still present qualitatively useful results. The effect of interfacial adhesion on flexural properties was investigated by using three-point-bend with inspiration from ASTM D7264[187]. As in the tensile tests, the tows were made into four sets of tows soaked in Isopar™ L with silicone concentrations of 0%, 1%, 2.5%, and 5% by weight. Since the sample sets had slightly different average diameters, the testing span for each set was changed to maintain a 40:1 span-to-diameter ratio. The testing spans, rounded to the nearest mm, were: 35 mm, 36 mm, 39 mm, and 41 mm. The length of every specimen was 1.2 times the size of the three-point-bend span. The measured variables were flexural modulus, ultimate flexural stress, flexural strain at failure, and energy to failure.

4.3.12 *Silicone rheological testing*

The rheological characteristics of an interphase in composites may be reflected in their mechanical properties[188–190]. For example, Jafari et al.[191] concluded that higher values of the loss tangent (tanδ) would result in greater impact toughness in polymer matrices. Thus, the existence and magnitude of the loss modulus and loss tangent of the cured silicone coatings used in this study were investigated using oscillatory rheometry. A globule of silicone was placed on the flat

plate tool of a model MCR300 rheometer (Anton Paar, Graz, Austria) and flattened to a 1 mm thick puck with a diameter of 25 mm. The testing section was set to a temperature of 100°C for four hours to cure the silicone. After 4 h, the plate was brought down to a temperature of 20°C and maintained for the rest of the test. Next, a PP25 flat-plate attachment was set flush on top of the cured silicone puck to start measurements.

Next, a frequency sweep was conducted to determine *G′* and *G,*" the storage and loss moduli, respectively, of the cured gel. The gel was oscillated through a range of frequencies starting at 6 Hz and ending at 500 Hz, ramping at a rate of 83 Hz/min. The loss tangent was computed as the ratio of *G*"/*G*'.

4.4 Results and Discussion

4.4.1 *Interfacial adhesion (IFSS)*

Interfacial adhesion between the treated fibers and epoxy thermoset was tested to examine the possible effects of the silicone coating. Overall, it was found that for each increasing layer of silicone coating, there was a proportional decrease in interfacial adhesion (IFSS), as shown in Figure 4.4. The IFSS obtained decreased linearly with the number of coatings from a value of approximately 101 MPa for the uncoated fibers down to near zero for the fibers with ten coatings of silicone.

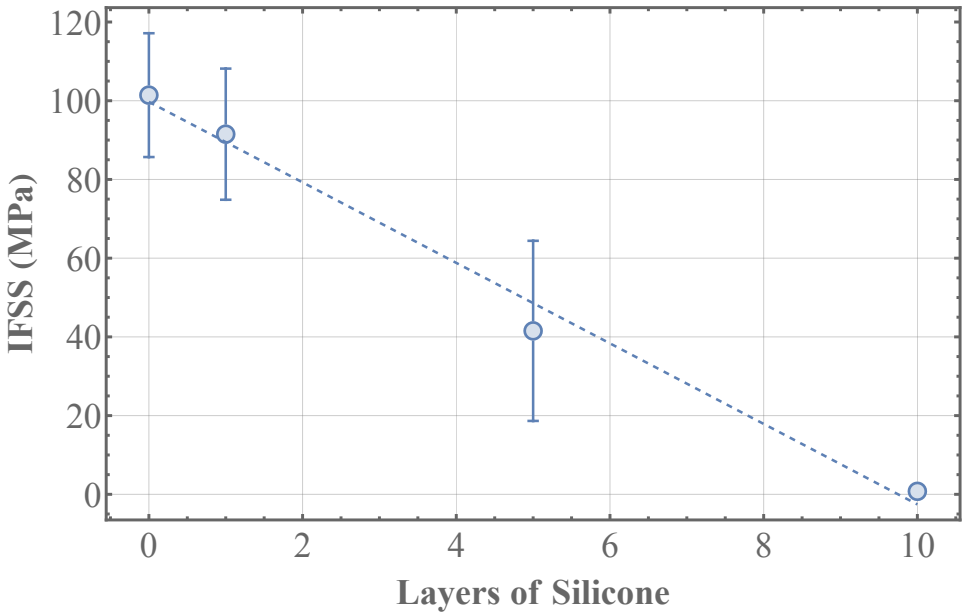

Figure 4.4: Interfacial shear strength for single carbon fibers in cured epoxy resin as a function of the layers of silicone coating (Mean ± SD).

The structure of the fiber breaks also changed as the number of silicone coatings increased. The untreated fibers, when fractured, produced long and thick dumbbell shaped cracks, but as the adhesion was reduced (amount of silicone increased), the fractures became smaller and less prominent, as seen in the optical micrographs of Figure 4.5. Changes in the shape of fiber/resin breaks are indicative of alterations to adhesion. As reported by Feih et al.[87] systems with high interfacial adhesion lead to damage and large cracks into the surrounding resin, whereas systems with lower adhesion do not damage the surrounding resin to such a degree.

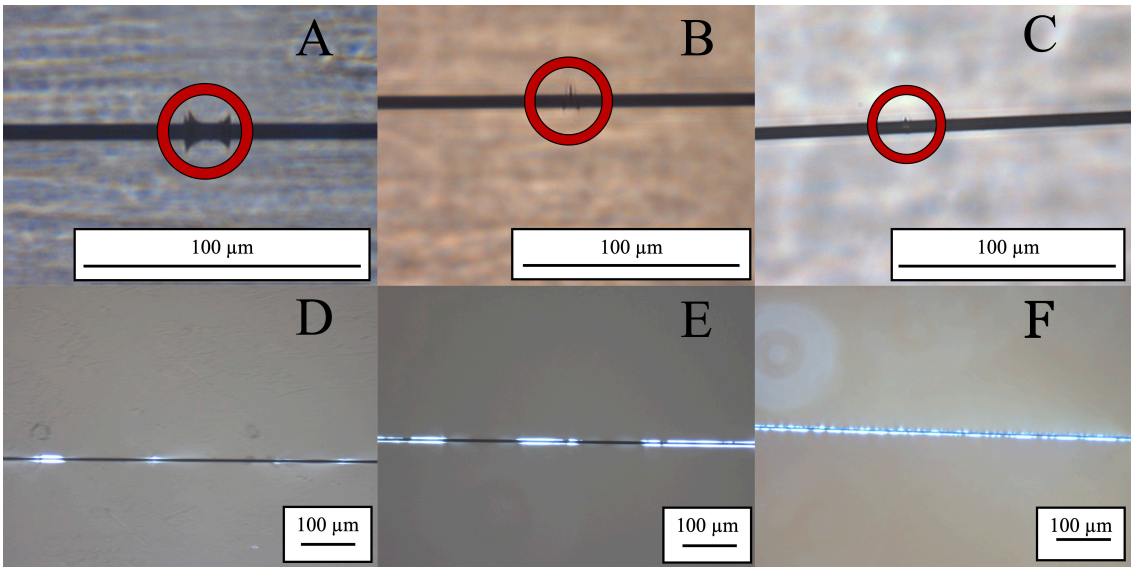

Figure 4.5: Images of fiber/matrix fractures used for single fiber fragmentation testing. The images on the top row labeled "A, B, and C" stand for fibers with one, five, and ten layers of silicone, respectively. Additionally, red circles are placed to give attention to fiber breaks. The images on the bottom row (D, E, F) represent the same fibers when viewed through cross-polarized light.

When reinforced epoxy matrices are observed through cross-polarized light, areas with large strain and stress gradients, such as interfacial debonding and fiber-matrix cracking sites, display bright spots resulting from birefringence[192]. This birefringence was observed in the present study, as shown in Figure 4.5 as bright blue spots, which highlight fiber breaks and/or fiber-matrix debonding. While the complex phenomena of fiber-matrix debonding have been extensively examined in other studies[99,193–196], in general, systems with high adhesion show small and punctuated birefringence patterns while systems with lower adhesion show elongated birefringence patterns along the surface of the fiber. These elongated patterns are typically caused by the fiber pulling away from the matrix while not necessarily cracking, and are referred to as delamination. As seen in Figure 4.5, System D has very little debonding, whereas System F

is brightly lit along the whole fiber. It is clear that the amount of silicone coating on the fibers had a direct relation to the level of interfacial adhesion and to the nature of the debonding event.

4.4.2 *Fiber volume fraction in tow composites*

Thermogravimetric analysis was used to determine the volume fraction of each constituent of the fiber tow composites. Temperature was ramped at 20°C /min and held at 530°C for 60 min, which was shown to be high enough temperature to oxidize all the remaining epoxy matrix while still low enough to protect the carbon fibers from any mass loss (Figure 4.6). The final asymptotic weight percent value for this experiment was 50.6%. The fiber volume fraction for untreated (free of silicone) carbon fiber composite tows was found to be 40.9%.

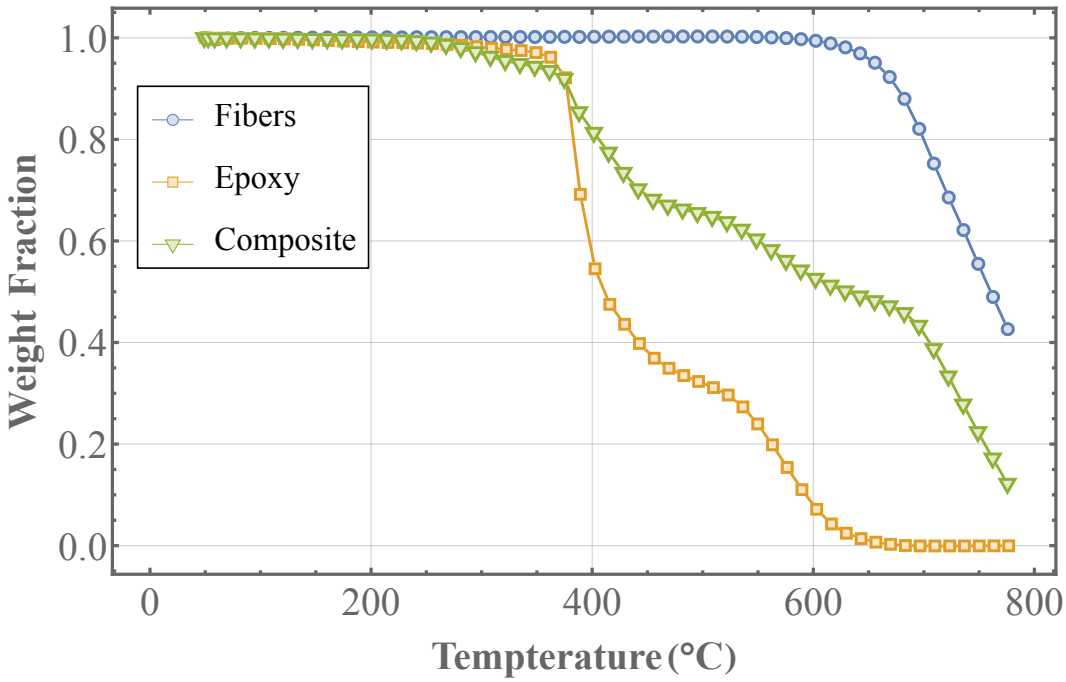

Figure 4.6: TGA results for fiber tow composite and its constituents. Blue circles represent TGA results for plain carbon fibers. Orange squares represent pure, cured epoxy. And green triangles represent results for carbon fiber-epoxy tow composite

4.4.3 *Effects of silicone treatment of fiber tows*

The weight percentage of silicone on the dried fiber tows soaked in varying concentrations of silicone solutions shown in Figure 4.7 increased linearly with the concentration of the solution. When soaked in pure Isopar™ L, minimal weight gain was observed, showing that essentially all the solvent had evaporated. When soaked in a 5% concentration of silicone in Isopar™ L, nearly a 3% weight gain of silicone was measured on the fiber tow. All other intermediate points were linearly proportional to the concentration of the silicone solution. It was also observed that, as the amount of silicone in the soaking solution increased, the diameter of the cured tow composite also increased. Composite tow diameters were 0.87 mm, 0.90 mm, 0.98 mm, and 1.03 mm for fibers soaked in solution with 0 %, 1%, 2.5%, and 5% silicone by weight, respectively.

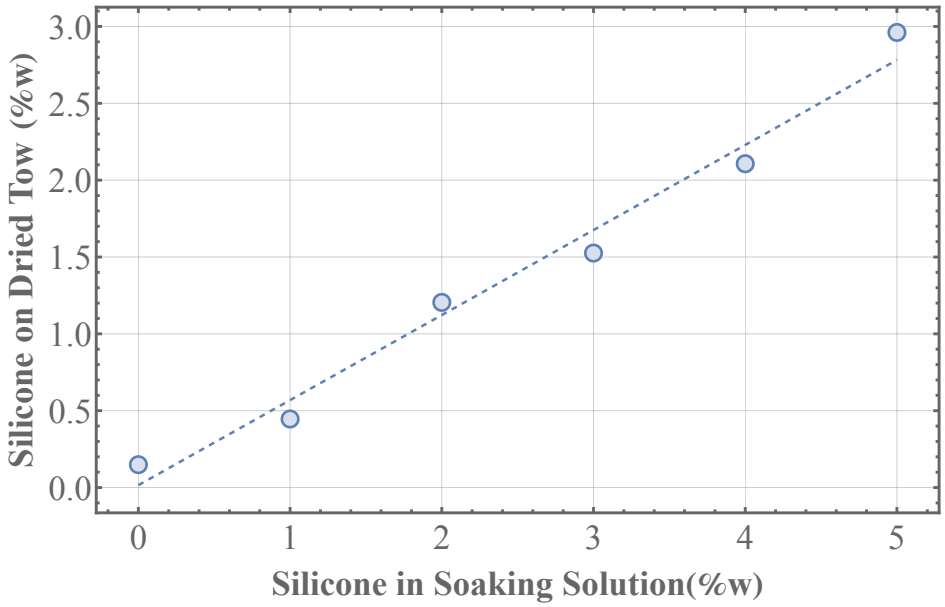

Figure 4.7: Weight percent of silicone for dried fiber tows soaked in varying concentrations of silicone solutions.

These average diameters were used for calculations of mechanical properties. Cross sections of the fiber tows with no treatment and with treatment with an Isopar™ L solution of 5%w silicone are shown in Figure 4.8 below:

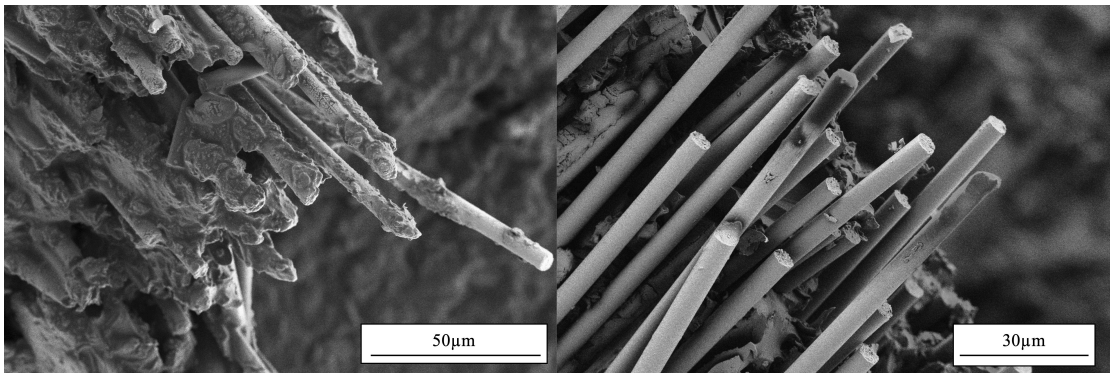

Figure 4.8: Scanning electron micrographs of sections of (left) untreated (no silicone) fiber tow composite cross-section and (right) fiber tow composite soaked in Isopar™ L solution of 5%w silicone.

As shown, the cured epoxy matrix evenly spread on the untreated fibers, leading to cohesive failure, while the composites with silicone deposited on the fiber surface showed primarily adhesive failure, leaving most fibers bare and unbonded to the matrix.

4.4.4 *Fiber tow impact testing*

As expected, increases in impact toughness with increases of silicone at the fiber-matrix interface were observed, as presented in Figure 4.9, which shows a linear trend for impact toughness increase with the extent of silicone surface treatment. Initially, fibers soaked in a solution of pure Isopar™ L had an impact toughness of 168mJ. When treated by soaking in a solution containing 5%w of silicone in Isopar™ L, the impact toughness increased to a value of 366mJ, a more than 2x increase.

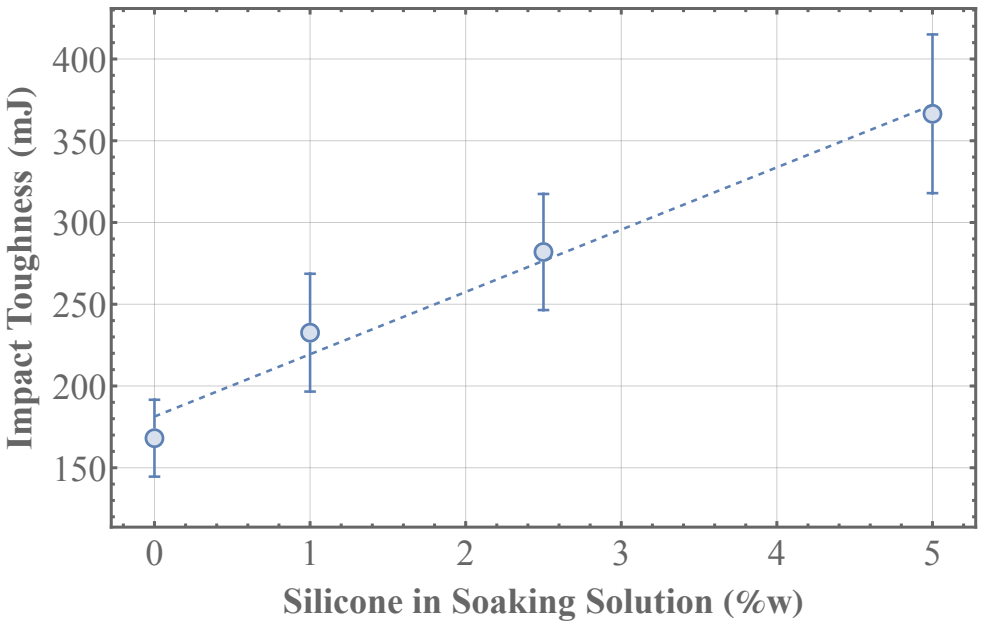

Figure 4.9: The effect of silicone soaking solution concentration on composite tow impact toughness (Mean ± SD).

4.4.5 *Fiber tow tensile properties*

It has been shown in previous work[197] that reductions in adhesion typically result in the degradation of many strain-rate independent properties, such as modulus and ultimate tensile strength and toughness, so it was expected that an increase of silicone in the interfacial region would also lead to reductions in these composite properties. Results for ultimate tensile stress (UTS), strain-at-failure, energy to failure (toughness), and tensile modulus, shown in Figure 4.10, show that as the amount of silicone increased on the carbon fiber tows, all tensile properties degraded. For fibers with no silicone, the ultimate tensile strength started at a value of 2.29 GPa, and fell to a final value of 1.06 GPa for samples soaked in a 5% silicone solution. The strain-at-failure also decreased from a value of 2.84% for fibers with no silicone to 2.2% for fibers soaked in a 5% solution. Furthermore, the energy to failure (tensile toughness) decreased from a value of

2.04 J for fibers with no silicone to 1.2 J for fibers soaked in a 5% solution. Lastly, tensile modulus decreased from a value of 90.9 GPa for fibers with no silicone to 67 GPa for fibers soaked in a 5% solution. The treatment showed a gradual linear decrease in tensile properties with the increase of silicone in the tows.

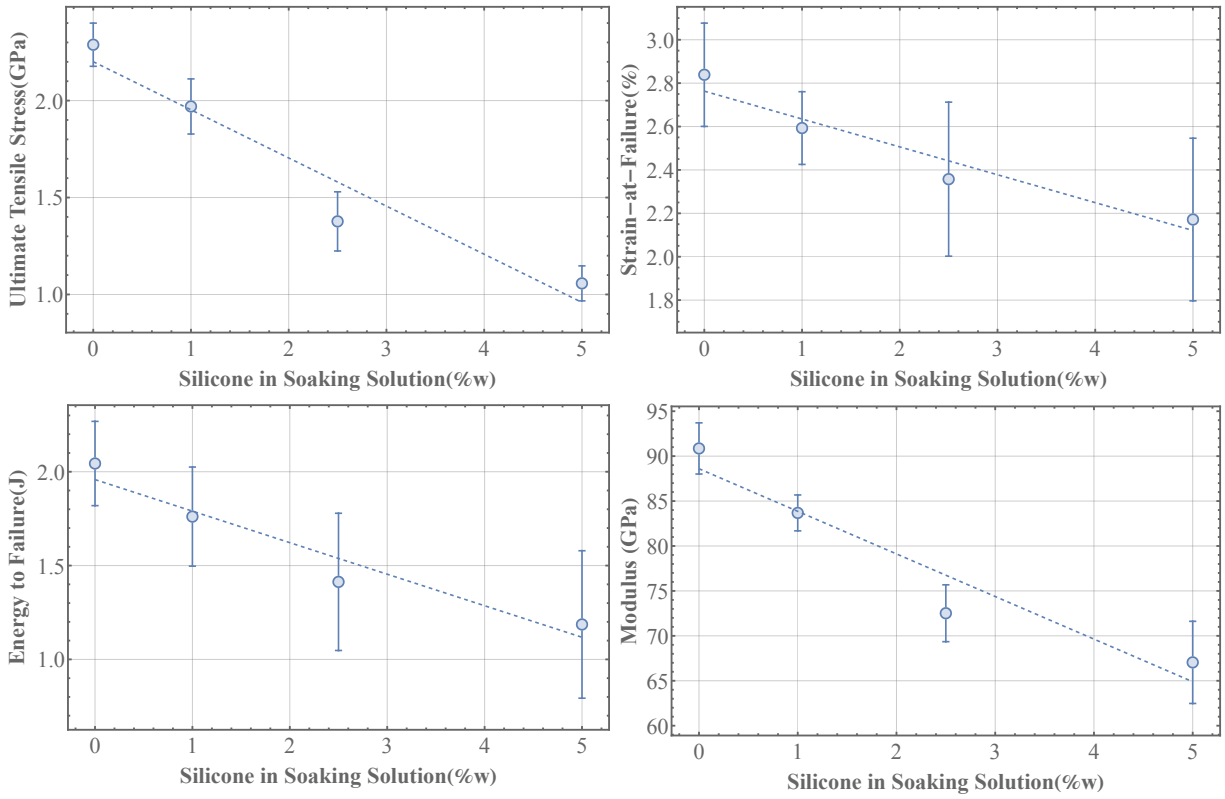

Figure 4.10: The effect of silicone soaking solution concentration on composite tow tensile properties. (top left) Effect on ultimate tensile stress, (top right) effect on strain-at-failure, (bottom left) effect on energy to failure, (bottom right) effect on tensile modulus (Mean ± SD).

When pushed to failure, fiber tows with no silicone had abrupt and chaotic failure events. The breaks were clean and flat, signifying brittle fracture. Conversely, when fiber tows soaked in 5% silicone solution were pushed to failure, the process was much different. Fracture events appeared to fray the tow rather than producing a clean, brittle break, as shown in Figure 4.11.

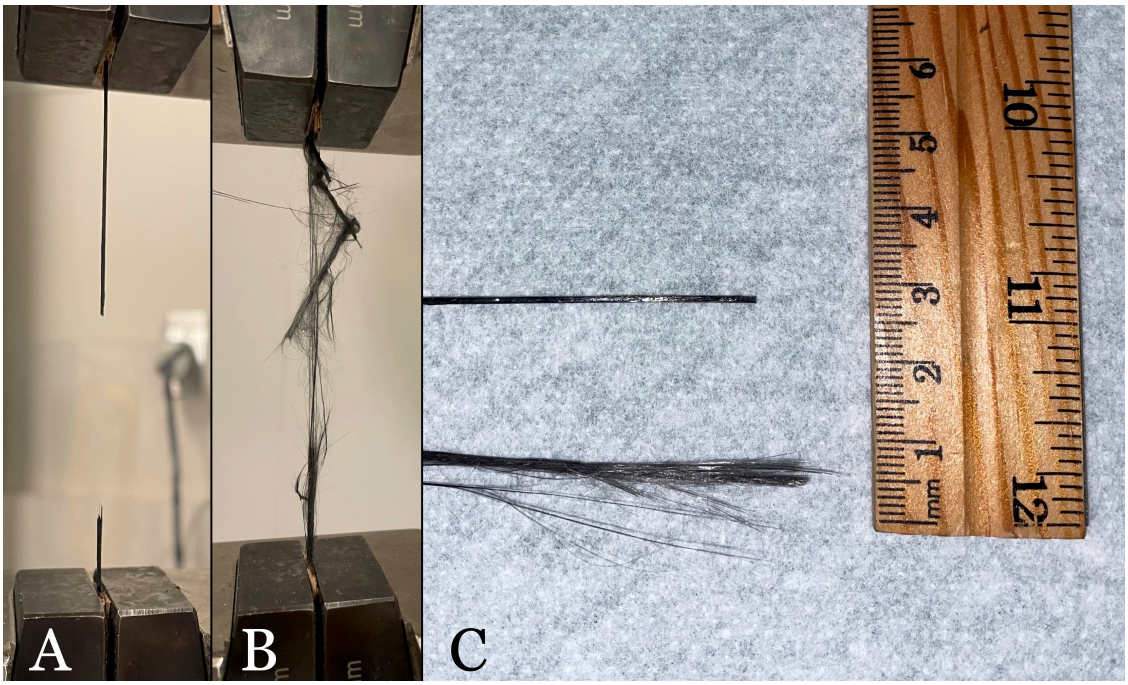

Figure 4.11: (A) Fiber tow composite with no silicone fracture after tensile testing. (B) Fiber tow composite soaked in a 5%w solution of silicone in Isopar™ L fracture after tensile testing. (C) comparison of fracture tips for fiber tow composites soaked in pure Isopar™ L and composites soaked in 5%w solution of silicone in Isopar™ L.

4.4.6 *Fiber tow flexural properties*

While increasing the amount of silicone on the fibers resulted in predictable decreases in tensile properties, the flexural properties for the fiber tows showed mixed results. Some properties, such as flexural modulus and ultimate flexural stress, decreased with the addition of silicone. The presence of the silicone had little effect on the energy to failure, and flexural toughness. Finally, the strain-at-failure had a weakly positive correlation with the amount of silicone at the interface, as shown in Figure 4.12. For ultimate flexural strength, samples with no silicone had a value of 1.54 GPa, which decreased to a value of 0.55 GPa for samples soaked in a 5% silicone solution. The flexural strain-at-failure increased from a value of 1.7% for samples

with no silicone to a value of 2.3% for samples soaked in a 5% silicone solution. The energy to failure showed little difference after the addition of silicone. Samples with no silicone started at a value of 23 mJ to cause failure and samples soaked in a 5% silicone solution needed 25mJ on average.

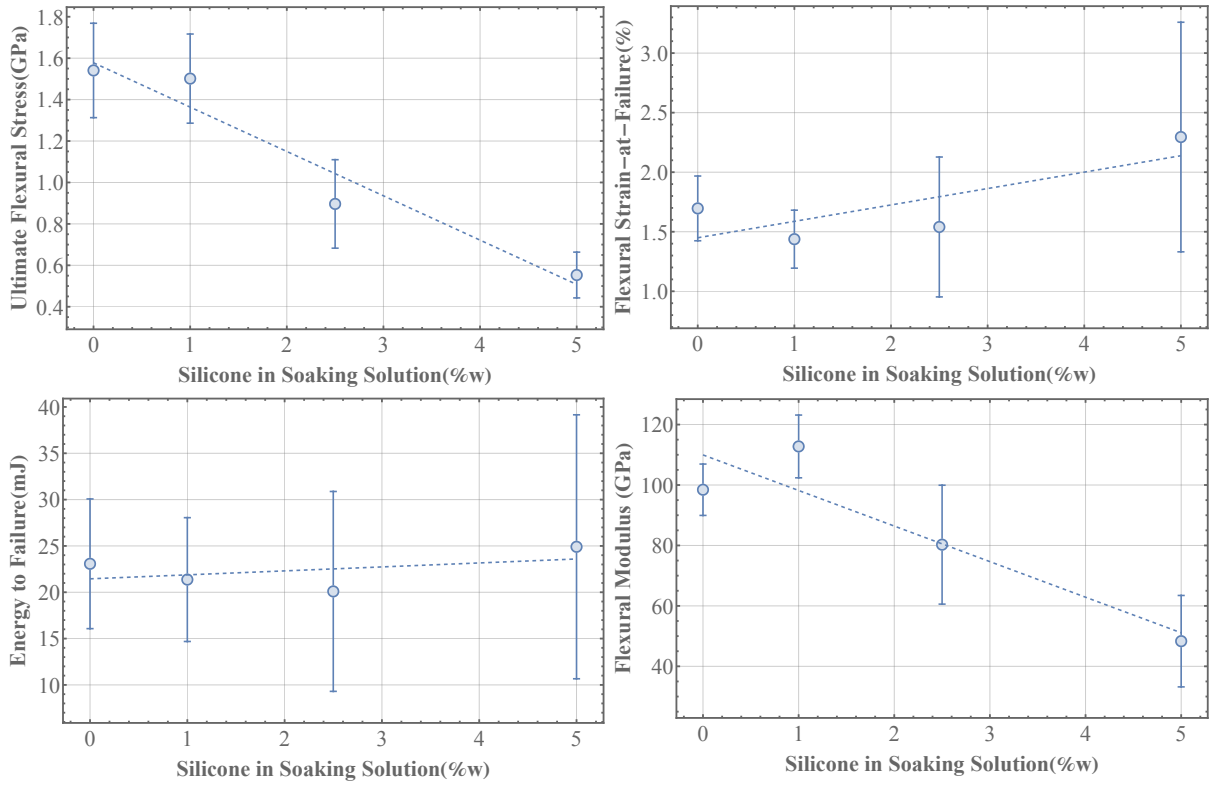

Figure 4.12: The effect of silicone soaking solution concentration on composite tow flexural properties. (top left) Effect on ultimate flexural stress, (top right) effect on flexural strain-at-failure, (bottom left) effect on energy to failure, (bottom right) effect on flexural modulus (Mean ± SD).

Lastly, the flexural modulus decreased from a value of 98 GPa for samples with no silicone to 48 GPa for samples soaked in a 5% silicone solution. Overall, it was observed that silicone treatment, and thus the reduction of fiber-matrix adhesion, had mixed effects on flexural properties. Interestingly, the results seemed to suggest that flexural strain at failure can increase

with the reduction of interfacial adhesion. This property may be used to advantage for systems where flexibility needs to be increased, and ultimate strengths are less important.

For tensile and flexural testing, fiber tows with no silicone produced abrupt failure events. Pieces of the testing often would fully separate and have clean fractures. Conversely, fiber tows with high amounts of silicone failed in a much more gradual manner. Often, they would not separate at all, but rather remain intact with a dramatic drop in flexural modulus. The tradeoff between strain-rate dependent and independent properties through the modulation of interfacial adhesion should be considered when designing a composite.

4.4.7 *Rheological testing*

An initial amplitude sweep showed that at up to 2.3% strain, the specimens remained within the linear visco-elastic range, so the subsequent oscillatory frequency sweep was confined to this amplitude range. The results of the subsequent frequency sweep up to 500 Hz are shown in Figure 4.13. Both storage and loss moduli, G' and G", respectively, increased with frequency up to 300Hz, beyond which the loss modulus, and hence tanδ, decreased slightly. The relatively high value of tanδ at approximately 0.3 for high strain rates suggested that the silicone polymer may aid in impact absorption.

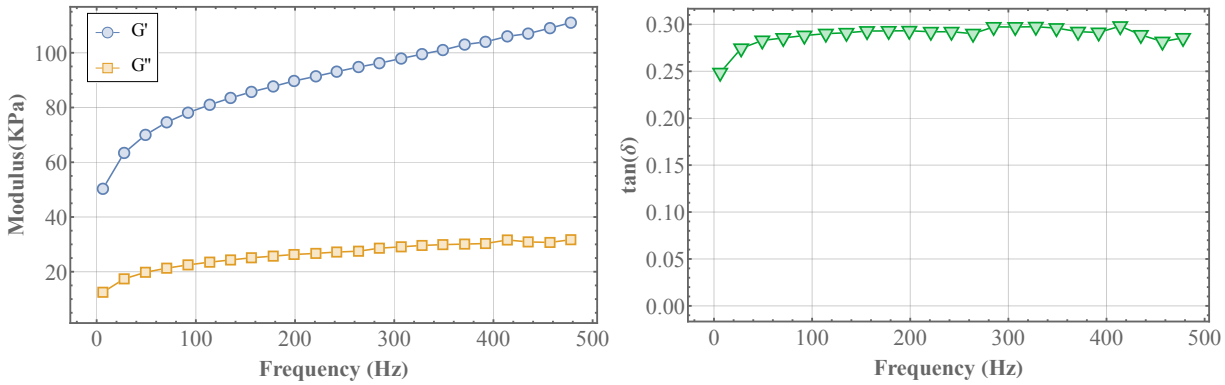

Figure 4.13: Frequency sweep for cured silicone puck. Frequency values ramp linearly from 6Hz to 500Hz at a rate of 83Hz/min and an amplitude of 1% strain. (Left): Storage modulus, G' (blue circles), and Loss modulus, G" (orange squares); (Right): tanδ = G"/G'.

In addition, although higher G" values have been theorized to correlate with impact toughness for composites, it has been shown[198] that higher G' values are also important for the structural integrity of a polymer. In the present case, both the G' and G" exhibit growth with strain rates, suggesting the suitability of the silicone coating used.

4.5 CONCLUSIONS

This work contributes to a method for modulating interfacial adhesion in carbon-fiber reinforced polymeric composites simply and predictably by creating fiber-matrix interphases of varying amounts of an inexpensive silicone sealant (Liquid Nails, Akzo Nobel Paints LLC, Strongsville, OH) dispersed in the paraffinic hydrocarbon solvent Isopar™ L (ExxonMobil Chemical, Irving, TX). The sealant is composed of a cross-linking agent (methyltri (2-butanoneoximyl) silane), a polymer (dimethyl polysiloxane), and a silica filler. Cross-linking and hardening of the thermoset occur when the silane (cross-linking agent) reacts with water from the atmosphere and hydrolyzes to form silanol groups followed by silane-siloxane condensation causing chain linking and extension[176].

Single fiber-matrix adhesion tests were conducted using Hexcel IM7 fibers with a matrix of EPON862 and Epikure W hardener. The silicone interphase was applied layer-by-layer to achieve different levels of coating. With each increasing layer of silicone, the interfacial adhesion (IFFS) decreased linearly from 101MPa for untreated fibers, to near zero for ten layers. Direct optical observation showed the structure of the fiber breaks also changed as the number of silicone coatings increased. The untreated fibers, when fractured, produced long and thick dumbbell shaped cracks, but as the adhesion was reduced (amount of silicone increased), the fractures became smaller and less prominent, suggesting energy dispersal through fiber/matrix delamination rather than crack propagation perpendicular to the fiber direction.

The effect of controlled adhesion reduction on the impact toughness of composite samples made from the same materials as used in the single fiber tests was investigated. Tows of 12,000 fibers treated with solutions of the silicone sealant of varying concentration at a fiber volume fraction of approximately 40 vol% were tested using a modified ASTM E2248 − 18, "Standard Test Method for Determining the Charpy Impact Resistance of Notched Specimens of Plastics." A testing apparatus constructed and used to break through composite specimens found that the energy absorbed (proportional to impact toughness) increased linearly by more than a factor of two as the level of fiber silicone treatment increased. These results were consistent with the findings from rheological testing which found that the silicone interphase material, over a wide range of frequencies, maintained a significant value of its loss modulus, indicating an ability to absorb and dissipate energy.

The tensile properties, such as ultimate stress, strain at failure, energy to failure, and modulus of the fiber tows described above show a linear decrease with the level of silicone fiber surface treatment, and flexural properties of the tow composites had mixed results where the

ultimate flexural stress, and flexural modulus decreased in value, the energy to fracture stayed constant, and the strain to failure slightly increased.

Chapter 5. ISOCONVERSIONAL METHOD FOR THE MODELING OF COMPLEX REACTION SYSTEMS

5.1 INTRODUCTION

5.1.1 *Background*

The modeling of chemical reactions has long been employed to predict the behavior of chemical systems and has proven to be useful in a variety of applications. Overall, the process uses previously gathered empirical reaction data to deduce a set of constants fundamental to the nature of the chemical system. Therefore, once all constants have been identified, they can in theory, be used to predict the reaction rate and system behavior for any arbitrarily chosen condition, such as temperature and pressure. This information can be particularly useful for calculating the viability of conditions for desired reactions and aid in reducing economic costs by removing the need to use any physical materials.

In general, the time dependency of reaction progression, α, is defined as the product of two parameters, seen in Eq. (5.1)[199]

$$\frac{d\alpha}{dt} = k(T)f(\alpha) \tag{5.1}$$

Where the first function, known as the Arrhenius expression[200], and can be seen in Eq. (5.2).

$$k(T) = Ae^{\left(-\frac{E_a}{RT}\right)} \tag{5.2}$$

Where T is temperature, A is the pre-exponential frequency factor, E_a is the activation energy of the reaction, R is the gas constant, and T is the temperature of the system. The other part of Eq. (5.1), called the reaction function, $f(\alpha)$, is related to the concentration of reactants, and can take many theoretical or empirical forms given the system dynamics.

Traditionally, reaction progression for relatively elementary systems can be modeled using rate-law relationships. Additional tables for other common reaction models have been compiled and used with some success[201–204]. The accuracy of these models to predict hypothetical reaction behavior ultimately depends on the accuracy of the parameters for the system, namely the reaction model, $f(\alpha)$, the Arrhenius pre-exponential factor, A, and the activation energy, E_A. Finding these values consists of using empirical reaction data gathered through experimentation, and then fitting the parameters in Eq. (5.2) until the model best represents empirical data. This method was originally completed by Borchardt and Daniels[204]. An overlaying assumption of this method requires that the activation energy, E_A, remains constant and independent of the reaction progress, $\alpha(t)$. Thus, for complex and multi-step reaction systems, multiple models must be generated and solved numerically as a system of equations, which can rapidly become difficult to complete. In addition, as stated by Kandelbauer et al.[205], the assumption of Arrhenius parameters and activation energy remaining constant is often valid only for straightforward reaction systems. Whereas for more complex, and realistic processes, the overall E_A may also incorporate contributions from other parts in a web on reactions.

Most often, generalized reaction models are used to encapsulate entire series of reactions. So even though each individual reaction may have a defined set of constant Arrhenius parameters, the generalized reaction model can become too complex to flatten into one single relationship. Therefore, in most scenarios, the assumption of the overall activation energy, E_A , remaining constant for the entire process becomes unrealistic. Additionally, for complex systems the reaction model, $f(\alpha)$ itself, can become difficult or impossible to define analytically even with precise knowledge of the system itself.

To circumvent the drawbacks of these traditional methods, current techniques, named "model-free kinetics" attempt to bypass the need of a reaction model, $f(\alpha)$, and relax the assumption of activation energy remaining constant throughout the entire reaction. This can be useful for multi-step and complex reactions such as combustion and polymerization.

5.1.2 *Use in thermoset curing*

Thermosets are a subset of polymers that harden by chemical linkage, otherwise known as cross-linking[2]. Many thermoset systems are comprised of two separate chemicals but can reach three or more elements. Some common examples of thermosets are epoxy, amine, phenol, and even bio-based cross-linking agents and resins[53,206,207]. Curing takes place when enough energy is added to the system by means of heat or electromagnetic radiation to overcome the activation energy for cross-linking to initiate. Given the wide array of chemical compositions, curing times for thermoset systems can range from the order of minutes to hours and even days[208–213].

However, from an outside perspective, curing schedules seen in literature or manuals can appear to be arbitrarily chosen, consequently making it difficult for researchers to determine the extent of cure completion for a system without external knowledge. Therefore, modeling of such systems has been employed in an attempt to predict the extent of cure as a function of time, $\alpha(t)$, for any given curing schedule.

However, due to complex reaction mechanisms that take place during the cross-linkage of thermoset monomers, simplistic modeling becomes less feasible for more accurate use. This chapter will attempt to discuss the past and current "model-free" methods used for such systems. Additionally, it will thoroughly explain the theory and treatment of data using the most current method known as the "advanced isoconversional integral method."

5.1.3 *The isoconversional principle*

In the proceeding section, underlying assumptions of "model-free" kinetics will be discussed. Even though these principles will not directly be used when employing the *advanced isoconversional method*, it may be found useful for some readers who find that the current corpus of literature lacks sufficient explanations of all aspects and underpinnings in the background of model-free kinetics.

Overall, model-free reaction kinetic methods rely on the isoconversional principle[199,203,205,214–217], which was originally put forth by Dr. Sergey Vyazovkin. In its most simplistic form, the principle assumes that when multiple different reactions of the same system are completed by following different heating paths, all the reaction rates for each experiment, $(d\alpha/dt)$, at a constant conversion value (hence isoconversional), will depend solely on the temperate at which the chosen level of conversion was reached. Furthermore, the change of isoconversional reaction rates across different experiments will vary with temperature by a value proportional to the activation energy for that isoconversional value.

Using the isoconversional principle, instead of relying on a single reaction model, Eq. (5.1), to be valid for the entire span of the reaction (i.e. $\alpha = 0 \rightarrow \alpha = 1$), it is assumed that multiple variations of Eq. (5.1) , can be transformed into a set of relations for all conversion values[218] in the form of Eq. (5.3).

$$\left[\frac{d\alpha}{dt} = A_\alpha e^{\left(-\frac{E_\alpha}{RT}\right)} f(\alpha)\right]_{\alpha=0,\alpha_1,\alpha_2,\ldots,1} \tag{5.3}$$

Where A_α is the isoconversion Arrhenius pre-exponential factor. And E_α is the isoconversional the activation energy. The utility of this method becomes evident by not requiring any previous knowledge of the system's reaction model, $f(\alpha)$, as it will only be a numerical value for each conversional step.

A mathematical derivation of the isoconversional principle goes as follows[205]. Eq. (5.1) can be simplified into Eq. (5.4) by substituting Eq. (5.2) into Eq. (5.1).

$$\frac{d\alpha}{dt} = A_\alpha \, e^{\left(-\frac{E_\alpha}{RT}\right)} f(\alpha) \tag{5.4}$$

Then, by taking the natural log on both sides and expanding using log rules, Eq. (5.5) is obtained.

$$\ln\left(\frac{d\alpha}{dt}\right) = \ln(A_\alpha) - \frac{E_\alpha}{RT} + \ln\big(f(\alpha)\big) \tag{5.5}$$

Next, partially differentiate each side by T^{-1} while holding α constant to obtain Eq. (5.6)

$$\left[\frac{\partial\left(\ln\left(\frac{d\alpha}{dt}\right)\right)}{\partial T^{-1}}\right]_\alpha = \left[\frac{\partial(\ln(A_\alpha))}{\partial T^{-1}}\right]_\alpha - \frac{E_\alpha}{R} + \left[\frac{\partial\big(\ln\big(f(\alpha)\big)\big)}{\partial T^{-1}}\right]_\alpha \tag{5.6}$$

Because α is held constant, and because they are not a function of temperature, $f(\alpha)$ and A_α will reduce to zero when partially differentiated by T^{-1}. However, given that the reaction rate, $(d\alpha/dt)$, does vary with temperature across different experiments, it does not reduce to zero. Leaving the final expression as Eq. (5.7).

$$\left[\frac{\partial\left(\ln\left(\frac{d\alpha}{dt}\right)\right)}{\partial T^{-1}}\right]_\alpha = -\frac{E_\alpha}{R} \tag{5.7}$$

It should also be noted that the reaction rate with dependence to time can also be transformed into the reaction rate with dependence to temperature by following Eq. (5.9). During experimentation, the same chemical system is split into multiple sets where each is tested by following different heating paths, shown in Eq. (5.8).

$$T(t) = \beta t + T_0 \tag{5.8}$$

Where $T(t)$ is the temperature profile as a function of time, β is the ramping rate, and T_0 is the initial temperature. After differentiation and substitution to the left-hand side of Eq. (5.1), the relationship between both differentials is presented below.

$$\frac{d\alpha}{dt} = \beta \frac{d\alpha}{dT} \tag{5.9}$$

5.1.4 *Example of the isoconversional principle*

The following segment will illustrate the isoconversional principle. While not necessary for use in the *Advanced Isoconversional Method*, it may prove helpful for some readers. For this example, a thermoset resin was used.

Initially, the resin was prepared and separated into five different differential scanning calorimetry (DSC) pans. Then, each sample temperature was ramped and reacted until completion at different, heating rates, β (K/min). Typical heating rates range from 1 to 15 (K/min). After solving for the extent of conversion as a function of temperature (refer to section 5.2.1) plots similar to Figure 5.1 can be produced.

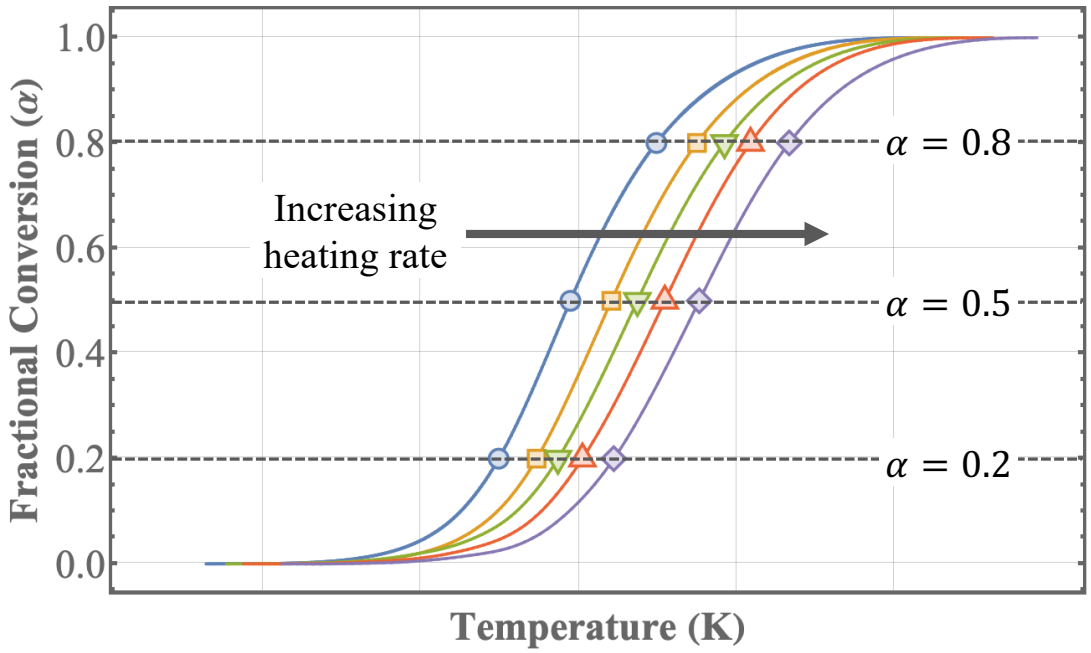

Figure 5.1: Plot of the extent of reaction (fractional conversion) versus temperature for five separate tests of a thermoset system. The dashed lines represent isoconversional values, and the five points represent their intersection with each experimental DSC ramp.

In the above figure, different isoconversional lines are drawn, and the five points represent their intersection with each DSC temperature ramp. According to the isoconversional principle as explained in the section above, the difference in slopes at each point should be related to their corresponding temperature and activation energy.

After reformatting and calculating all necessary values, Figure 5.2 can be produced.

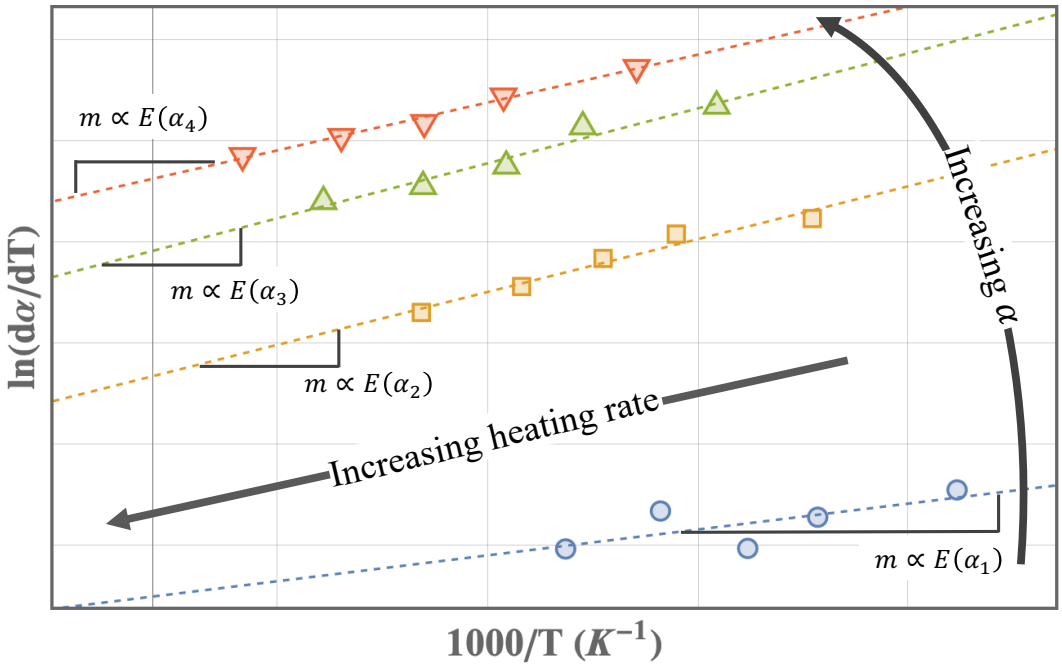

Figure 5.2: Relationship between $\ln(d\alpha/dT)$ and $1000/T$ plotted along isoconversional lines. Each point for each set represents a separate experiment with a different heating rate.

As shown above, the natural log of the reaction rate with respect to temperature (keeping in mind that a transformation from temperature to time can be made using Eq. (5.9)) is inversely dependent on temperature. Additionally, the slope of each line is proportional to the activation energy of the reaction for that specific fractional conversion. This result shows excellent agreement with the isoconversional principle and Eq. (5.7).

Overall, the above example, which uses experimental data, may be useful for readers who are new to model-free kinetics and require additional material to fully grasp the isoconversional principle.

5.1.5 *Previously used isoconversional method models*

Initial model-free methods closely followed the derivation to Eq. (5.7) above to calculate the activation energy and are classified as "differential methods." Friedman[219] was among the

first to publish on this method and used a combination of Eq. (5.5) and (5.9) to obtain Eq. (5.10).

$$\ln\left(\beta\frac{d\alpha}{dT}\right) = \ln\left(A_\alpha f(\alpha)\right) - \frac{E_\alpha}{RT} \tag{5.10}$$

For this method, different temperature ramps are run in the DSC and isoconversional values are linearly interpolated and plotted. The y-intercept of the linear regression for each isoconversional set is proportional to the product of the reaction model and Arrhenius pre-exponential factor, $\ln\left(A_\alpha f(\alpha)\right)$, and the slope is proportional to the conversion-dependent activation energy.

Unfortunately, this method has some drawbacks as detailed by Vyazovkin and Golekeri and Luss[220,221], namely that derivative methods may be unstable due to the use of instantaneous rates. As a result, integral techniques have become more popular due to their inherent stability[205]. The basis of such techniques can be seen below in Eq. (5.11)

$$g(\alpha) = \int_0^\alpha \frac{d\alpha}{f(\alpha)} = \int_0^t A_\alpha \exp\left(\frac{-E_\alpha}{RT}\right) dt \tag{5.11}$$

Where $g(\alpha)$ is regarded as the integral form for the reaction model. Methods such as Flynn-Wall-Ozawa[222,223] (FWO), Coats and Redfern[224] (CD), and Kissinger-Akahira-Sunose[225,226] (KAS) all use Eq. (5.11) as the basis of their methods used to solve for isoconversional activation energies, E_α. While useful, these methods have been less adopted than the *Advanced Isoconversional Technique*, which will be discussed below.

5.2 Obtaining Advanced Isoconversional Method Parameters

5.2.1 *Solving for degree of cure*

Generally, the extent or reaction or completion for any system is denoted with the symbol α. While there any many methods to deduce the extent of reaction, the two primary methods used in the analytical techniques, differential scanning calorimetry (DSC) and thermogravimetric analysis (TGA), can be seen in Eq. (5.12))[80] and Eq. (5.13)[227], respectively.

$$\alpha(t) = \frac{\Delta H(t_i)}{\Delta H_{total}} = \frac{\int_0^{t_i} H(t)dt}{\int_0^{t_{final}} H(t)dt} \tag{5.12}$$

$$\alpha(t) = \frac{\Delta m(t_i)}{\Delta m_{total}} = \frac{m_{initial} - m(t_i)}{m_{intial} - m_{final}} \tag{5.13}$$

Where $\Delta H(t_i)$ is the enthalpy of reaction from time zero up to time t_i (J), ΔH_{total} is the total enthalpy released for the entire reaction (J), and $H(t_i)$ is the heat flow at time t_i (J/s). Secondly, $\Delta m(t_i)$ is the mass loss of a sample during heating from time zero up to time t_i, and Δm_{total} is the total mass loss the entire heating.

5.2.2 *Solving for E_α*

The following subsection will elucidate the methods to solve for E_α by referencing, expanding, and adding additional context to work by Campbell et al.[199]. The general form for any reaction can be described in Eq. (5.4) as the product between $k(T)$, the temperature-dependent kinetic constant, and $f(\alpha)$, the unknown reaction model.

$$\frac{d\alpha}{dt} = k(T)f(\alpha) = A_\alpha\, e^{\left(-\frac{E_\alpha}{RT}\right)} f(\alpha) \tag{5.4}$$

It is assumed that for small slices of reaction conversion, E_α A_α and $f(\alpha)$ all remain constant, therefore, $k(T)$ and $f(\alpha)$ are independent and can be integrated through separation of variables. The integral form of this function, referred to as $g(\alpha)$, can be seen in Eq. (5.14).

$$g(\alpha) = \int_{\alpha-\Delta\alpha}^{\alpha} \frac{d\alpha}{f(\alpha)} = A_\alpha \int_{t_{\alpha-\Delta\alpha}}^{t_\alpha} e^{\left[\frac{-E_\alpha}{RT(t)}\right]} dt \tag{5.14}$$

Furthermore, the right-hand side can be shortened by using Eq. (5.15) to achieve the final form of Eq. (5.16).

$$J_\alpha = \int_{t_{\alpha-\Delta\alpha}}^{t_\alpha} e^{\left[\frac{-E_\alpha}{RT(t)}\right]} dt \tag{5.15}$$

$$g(\alpha) = A_\alpha J_\alpha \tag{5.16}$$

Because $g(\alpha)$ is independent of the temperature path required to reach a specific reaction conversion, then it can be stated that all $g(\alpha_i)$ are equal, and therefore, $g(\alpha_i)_{\beta_1} = g(\alpha_i)_{\beta_2} = g(\alpha_i)_{\beta_3} = g(\alpha_i)_{\beta_i} = const.$, where β_i represents a specific heating path. By substituting J_α into the above equations, then $A_\alpha J_{\alpha,\,\beta_1} = A_\alpha J_{\alpha,\,\beta_2} = const.$ and can be rearranged into the form of $\frac{J_{\alpha,\,\beta_1}}{J_{\alpha,\,\beta_2}} = const.$ From prior knowledge, because the minimum of the sum of any variable and its reciprocal will always be equal to two, $min\left|x + \frac{1}{x}\right| = 2$ (see Figure 5.3), then it must also be true that $min\left|\frac{J_{\alpha,\,\beta_1}}{J_{\alpha,\,\beta_2}} + \frac{J_{\alpha,\,\beta_2}}{J_{\alpha,\,\beta_1}}\right| \cong 2$. Given the above information, the activation energy, E_α, will finally be solved for through error minimization until the relationship above is closest to two.

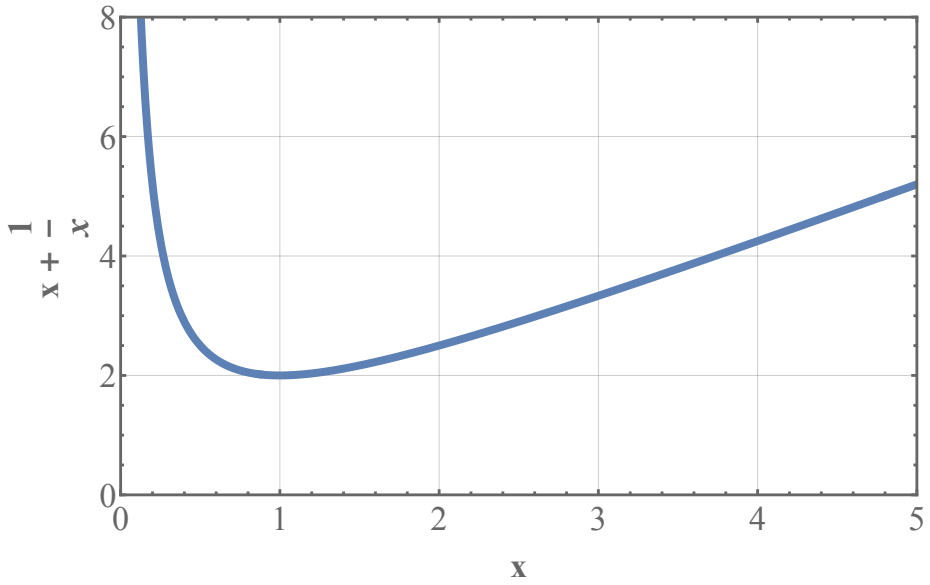

Figure 5.3: Plot showing that the global minimum of $x + \frac{1}{x}$ is equal to 2

As seen above, this analysis requires at least two different ramping rates, β_i, to be valid. However, to increase the model accuracy, three to five different ramping rates are often used for analysis. Therefore, the minimization function ultimately takes the form of Eq. (5.17).

$$\phi_\alpha(n) = n(n-1) \cong min \left| \sum_{i=1}^{n} \sum_{j \neq i}^{n} \frac{J_{\alpha,\beta_i}}{J_{\alpha,\beta_j}} \right| \tag{5.17}$$

Where n is the number of different ramping rates. For example, if three separate ramping rates are used (e.g., $\beta = 3{,}5{,}7\ K/min$), then Eq. (5.17) will become $\phi_\alpha(3) = 6 \cong min \left| \frac{J_{\alpha,\beta_1}}{J_{\alpha,\beta_2}} + \frac{J_{\alpha,\beta_2}}{J_{\alpha,\beta_1}} + \frac{J_{\alpha,\beta_1}}{J_{\alpha,\beta_3}} + \frac{J_{\alpha,\beta_3}}{J_{\alpha,\beta_1}} + \frac{J_{\alpha,\beta_2}}{J_{\alpha,\beta_3}} + \frac{J_{\alpha,\beta_3}}{J_{\alpha,\beta_2}} \right|$, where ϕ_α is the function to be minimized closest to a value of six by modulating its corresponding E_α value.

This minimization process will occur for every conversional step, where the typical step size is $\Delta\alpha = 0.05\ or\ 0.10$. After completion, a final array of all activation energies, (α_i, E_{α_i}) for $(\alpha_{1\Delta\alpha}, \alpha_{2\Delta\alpha}, \alpha_{3\Delta\alpha}, \dots, \alpha_1)$, can be compiled and used for predictions in the next section. It should

be noted that the activation energy corresponding to $\alpha = 0$ cannot be calculated given mathematical constraints and can be taken as equal to $E_{1\Delta\alpha}$.

5.3 KINETIC PREDICTIONS

The goal of the previous section was to perform three to five different DSC or TGA heating ramps on the same system and compile an array of activation energies with their corresponding extent of conversion, $\left(\alpha_i, E_{\alpha_i}\right)_{\alpha=0\rightarrow1}$.

Recall from the previous section, since $g(\alpha_i)_{\beta_1} = g(\alpha_i)_{\beta_2}$ and $J_{\alpha_i,\beta_1} = J_{\alpha_i,\beta_2}$, then it must also be true that $J_{\alpha_i,\beta_i} = J_{\alpha_i,T(t)}$, where $T(t)$ is any chosen temperature path in which the ultimate goal is to acquire (α, t) predictions. Fully expanded, this takes the form of Eq. (5.18).

$$\int_{t_{\alpha-\Delta\alpha,exp.}}^{t_{\alpha,\,exp.}} e^{\left[\frac{-E_\alpha}{RT(t)_{exp.}}\right]}dt = \int_{t_{\alpha-\Delta\alpha,\,pred.}}^{t_{\alpha,pred.}} e^{\left[\frac{-E_\alpha}{RT(t)_{chosen}}\right]}dt \tag{5.18}$$

Where, n is the number of steps, $\Delta\alpha$ is n^{-1}, $t_{\alpha,pred.}$ is the time at percent cure, α_i, for desired temperature profile, $t_{\alpha,exp.}$ is the time at percent cure, α_i, from a previously recorded empirical experiment. $T(t)_{chosen}$ temperature profile for the desired kinetic prediction, and $T(t)_{exp.}$ is the temperature profile of any previously recorded experiment. All E_α values were determined in the previous section. Note that the LHS of Eq. (5.18) can be data from any of the temperature sweeps.

In practice, all the above values are known or defined except for $t_{\alpha,pred.}$. Therefore, a system of n equations with n unknowns, following the form of Eq. (5.18) can be set up and solved (assuming that $t_{\alpha=0} = 0$), where the limits of integration are the variables are to be numerically calculated. The result is an array of kinetic predictions for the time required to reach a specific degree of cure.

5.4 Overall Summary of the Advanced Isoconversional Method

The following is a condensed set of instructions to be referred to when completing the *Advanced Isoconversional Technique* for making kinetic predictions. They are not meant to stand alone and require the theoretical background described in the sections above.

1. Using DSC or TGA to gather preliminary data:
    A. On the system to be tested, create three to five identical samples, and run them through a temperature sweep in a DSC/TGA using different, linear ramping rates
    B. For DSC, gather the heat flow (W/g) vs. time data. For TGA, gather mass loss vs. time
    C. Using Eq. (5.12) or Eq. (5.13), compile $\alpha \; vs. time$ data for all temperature sweeps
2. Solving for the $E_\alpha \; vs. \alpha$ array:
    A. Use Eq. (5.15) to create a minimization function in the form of Eq. (5.17) for each conversional step, $(\alpha = 0, \Delta\alpha, 2\Delta\alpha, 3\Delta\alpha, \dots, 1)$
        - Note that typically $\Delta\alpha = 0.05 \; or \; 0.10$
    B. Solve for E_{α_i} through modulation to minimize each equation in the form of Eq. (5.17)
    C. Compile a list of all $\left(\alpha_i, E_{\alpha_i}\right)_{\alpha=0\rightarrow1}$
3. Using activation energy data to perform kinetic predictions:
    A. Choose any desired temperature profile for kinetic predictions, $T(t)_{chosen}$
    B. Compile a system of *n* equations *n* unknown t_{α_i} values in the form of Eq. (5.18)
        - Note that $t_{\alpha=0} = 0$
        - Any previous empirical experiment can be used for the LHS of Eq. (5.18)
        - Use previously recorded E_{α_i} for each corresponding isoconversional step
    C. Solve the system of equations for all t_{α_i} values

D. Use t_{α_i} values to create an array of $(\alpha, t)_{pred}$ for the chosen temperature profile

Chapter 6. FUTURE WORK

6.1 Experiment 1: Polyynyl Butyral For The Modulation of Interfacial Adhesion

6.1.1 *Motivation*

As discussed in Chapter 4, the tailoring of interfacial adhesion can play a critical role when designing composites to most optimally fit loading conditions. This was completed through the addition of discrete amounts of silicone polymer into the interphase region of a carbon fiber-reinforced epoxy composite. While this technique showed promising results, it has one notable drawback. Namely, some key industries regard silicone as an unusable component for composite production because it can cause contamination and affect adhesive properties in other parts. Due to this, silicone is often avoided near some composite production facilities. Thus, the motivation of this project is to expand the dip-coating or layer-by-layer technique for the tailoring of interfacial adhesion to all industries by choosing a new adhesion-tailoring coating polymer.

The interfacial adhesion modification techniques discussed in Chapter 4 can still be used in certain settings if the polymers used for the interface coating are viewed as more acceptable for such applications. Therefore, the polymer chosen for future experimentation should meet the following criteria. 1) The polymer should be acceptable to use in high-performance composite manufacturing facilities. 2) The polymer should be low enough molecular weight to easily dissolve in an inert solvent, such as paraffins, ethanol, toluene, or xylene. 3) Should have meaningfully different properties compared to the bulk matrix as to allow for the modulation of properties through the deposition of discrete amounts. 4) Should be able to adhere to the fiber surface.

6.1.2 *Setup*

While many polymers may satisfy the above criteria, an appealing option is Polyvinyl Butyral (PVB) and can be seen in Figure 6.1. This includes many reasons, such as its high adhesion to most substrates, high impact resistance, flexibility, ease of dissolving in solvents, ability to form thin films, and its availability to purchase with differing amounts of vinyl alcohol groups which can modulate acid functionality.

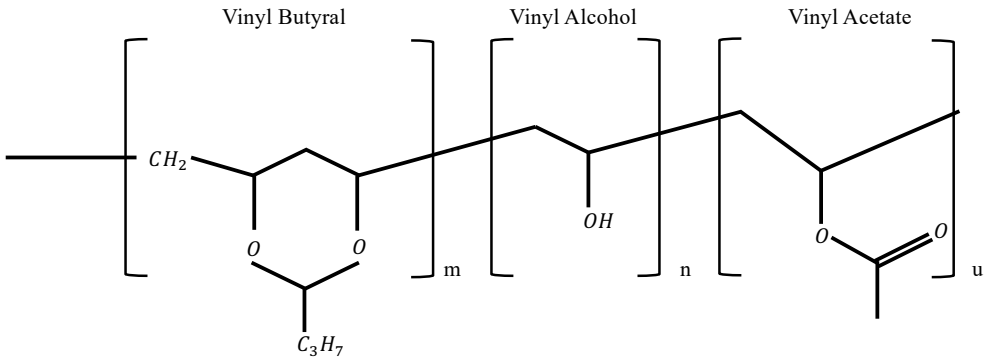

Figure 6.1: Chemical structure of Polyvinyl Butyral block-copolymer, which is composed of vinyl butyral groups, vinyl alcohol groups, and vinyl acetate groups.

As seen above, PBV is a versatile polymer because it can be acquired with differing ratios of each copolymer, shown as *m, n,* and *u* above. Given this, the interfacial properties of composites can be changed though not only the amount of PBV added to the interphase but also the ratios of each copolymer.

For experimentation, it is first recommended to study the micromechanics of the system with and without the addition of PBV. As a control, it is recommended to determine the baseline adhesion of pristine fibers with the surrounding matrix. Next, successively higher quantities of the polymer can be added to the interphase region (either through layer-by-layer painting or dip

coating) to determine the degree of adhesion modulation of the system as a function of the polymer coating amount. Secondly, it will also be of interest to determine how the fiber-matrix adhesion responds to the type of PBV used for interfacial modification. For example, the amount of polyvinyl alcohol and total polymer molecular weight.

After mapping the responsiveness of the system to both the amount and type of PVB, it would next be of importance to determine how PBV would affect the macro tensile, flexural, and impact properties. Therefore, new larger composite samples can be created in the same fashion as in 0, through the winding of panels, or through interlamellar deposition for composite layups.

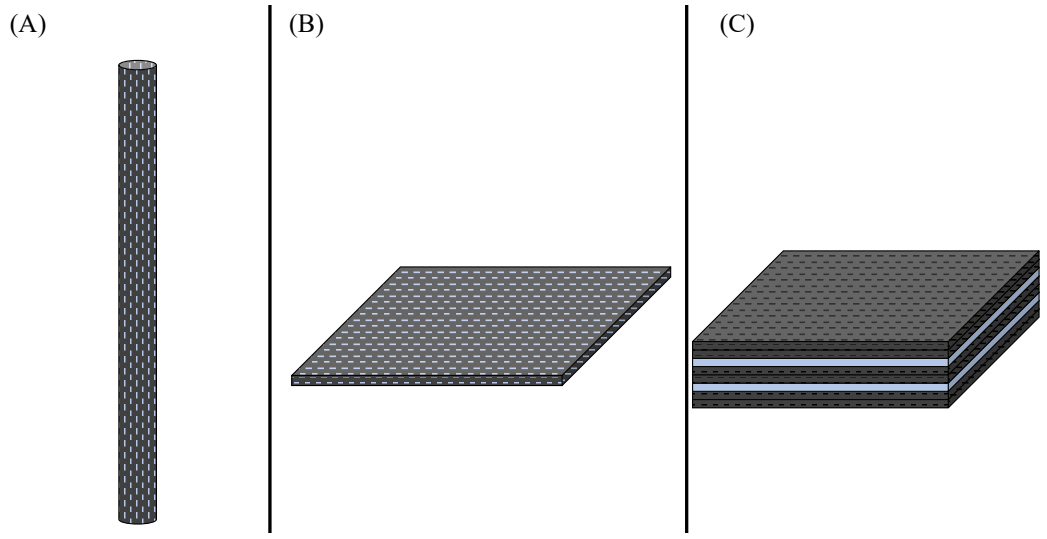

Figure 6.2: Possible testing systems for the addition of PVB to fiber-reinforced polymer composites. (A) Addition of PVB to unidirectional fiber tow composites through dip coating. (B) Addition of PVB through fiber dip coating to a carbon fiber composite panel. (C) Interlamellar addition of PBV to pristine composite panels. Black and gray sections represent carbon fiber composite, and blue sections represent the addition of PVB.

As discussed in previous sections, impact toughness and static strength properties are inversely correlated in most cases. In other words, the promotion of one of the properties

generally leads to the degradation of the other. However, because PBV is an adhesion promotor as well as a shock absorber, there is an interesting opportunity for increases in both impact and static strength properties. All possible testing systems shown above in Figure 6.2 will vary slightly with the addition of PVB. System "A" is the least complex and will best show how unidirectional composite properties are affected by the addition of PVB to the interphase. System "B" also shows how the addition of PVB to the interphase will affect certain properties but will additionally allow for more design complexity that can more accurately represent composite structures used for practical purposes. System "C" is of most interest because it can be employed as a method to increase impact toughness through the addition of thin layers of PVB between sheets of carbon fiber composite panels – which is already popular in certain fields, such as producing impact-resistant windshields[228]. Additionally, this method will have no direct effect on fiber-matrix adhesion because it does not require the pre-coating of fibers with PVB. Lastly, a combination of "B" and "C" can be used for even more degrees of control.

Overall, the process of using PVB to enhance carbon fiber polymer composites has many possible iterations, such as changing the molecular weight of PVB used, polyvinyl alcohol content, the amount of PVB used to coat fibers, and the amount of PVB to add in interlaminar layers.

6.2 Experiment 2: Relating Matrix Curing Speed and Interphase Properties Through Atomic Force Microscopy

6.2.1 *Motivation*

As discussed in Chapter 2 and Chapter 6, the modulus and thickness of the interphase region play a vital role in the overall performance of composite materials. Therefore, the study of interphase properties is critical to describe composite micromechanics mechanics more

completely. Previous studies[229,230] have used atomic force microscopy (AFM) to examine the stiffness and depth of the interphase region. Specifically, Qi et al.[229] studied how curing speed affects interphase stiffness and thickness through AFM measurements. In their experiment, bisphenol A diglycidyl ether (DGEBA) was mixed with either a conventional hardener or a quick-curing hardener, where the difference in curing times was roughly a factor of 16x. The group then used two different AFM techniques (adhesion and stiffness force) to measure the depth of the interphase region and ultimately suggested that shorter curing times resulted in shorter interphase regions. According to their paper, no other groups had yet studied how curing times affected interphase properties. Even though they showed that two different types of measurements can successfully measure interphase depth with little disagreement, however, the cause of the shortened interphase depth was less clearly elucidated. This is because a different hardener was used for each experiment, thus causing a different chemical makeup for the matrix. Therefore, this experiment makes it difficult to determine the influence that chemical makeup and curing time each had on the interphase depth. Perhaps, a more conclusive study would use the same epoxy-hardener system and alter curing time solely through changes in curing temperature.

As discussed in Chapter 2 shorter curing times caused by increasing curing temperatures resulted in higher levels of interfacial shear strength. Even though the overall phenomenon was observed, only inferences of the causal mechanism were made, such as differences in time above the glass transition temperature and in thermal expansion mismatch paired with curing shrinkage from cross-linking. It is suspected, but not proven that the interphase depth itself may be influential in interfacial shear strength. Therefore, an important study would be to further build

where both pieces of research could use more detail, namely, by measuring the interphase depth as a function of cure time/temperature and then relating it to interfacial shear strength.

6.2.2 *Setup*

The goal of this project would be to determine the relationship between fiber-matrix interphase properties (depth and modulus), speed of resin curing, and interfacial adhesion. Ultimately, a correlation of interphase depth and modulus with interfacial shear strength can be created, which will give a deeper understanding to fiber-matrix micromechanics for constitutive models.

To start, a resin-hardener system must be selected, and curing times must be mapped for three to five different isothermal curing temperatures (as done in section 2.3.1 or section 5.2.1). To ensure that all other variables are held constant, samples should be cured to the same degree of conversion, $\alpha = 0.99$. After curing, the oven will be shut off with the door slightly ajar to allow for slow cooling back to room temperature.

Next, single fiber samples will be fabricated consistent with the steps taken in section 2.3.5. Afterwards, interfacial adhesion tests can be completed with the single fiber fragmentation technique as described in sections 2.3.8 and 2.3.9. To study the interphase depth and properties, gauge section segments of single fiber fragmentation dog-bone samples can be cut and polished, creating a small sample through the cross-section of the fiber. Before cutting, dog-bone samples may also be soaked in liquid nitrogen to promote brittle fracture and a clean surface. Once prepared, an AFM scan can be completed across the fiber into the matrix. A sample AFM scan through the cross-section of the fiber into the matrix can be seen in Figure 6.3. As shown below, the depth and modulus of the interphase region can be scanned for each sample and then used to observe its relation to interfacial shear strength.

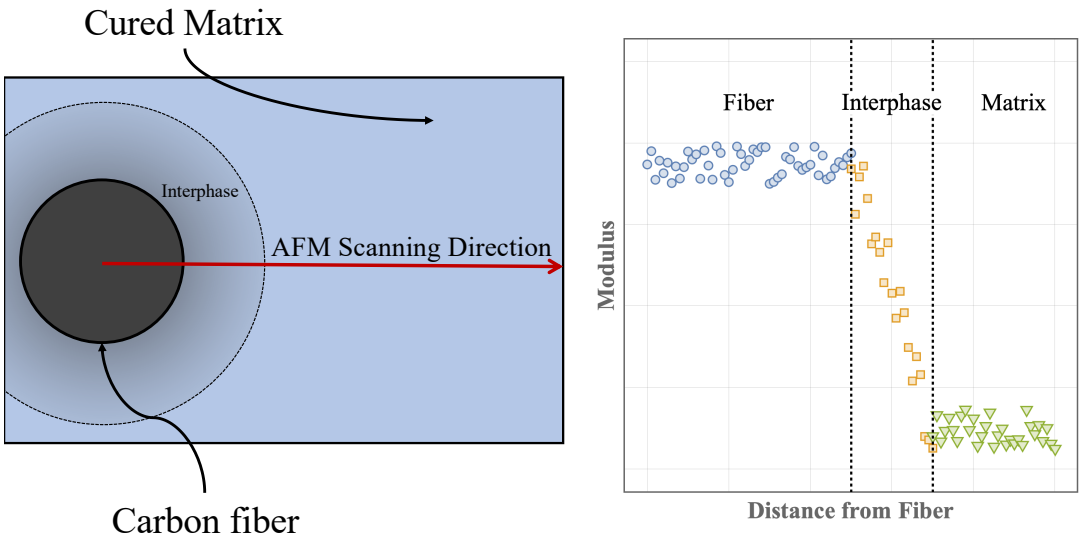

Figure 6.3: (Left) Cross-section AFM scan of single fiber composite sample. (Right) Corresponding graph of modulus as the AFM scan goes from fiber to interphase to matrix.

In summary, work in Chapter 2 observed the relationship between curing speed and interfacial adhesion when the chemistry of a system was held constant. Work by Qi et al.[229] determined the relation between curing speed and interphase depth for two separate resin systems. In an attempt to connect the conclusions of each paper, the goal of this project is to describe the relation between interfacial shear strength, interphase depth, and curing speed.

6.3 Experiment 3: Measuring Mode-1 Fiber-Matrix Adhesion

6.3.1 *Motivation*

As discussed throughout all sections above, interfacial adhesion plays a critical role for the performance of fiber-reinforced polymer composites. Consequently, several tests have been created to measure interfacial adhesion, such as single fiber fragmentation, fiber pull-out, fiber push-out, and micro-droplet. All such testing methods are thoroughly described by Rutz[91].

However, even though these strategies are well known and show some utility, they only measure shear, or mode-II, adhesion which can be seen in Figure 6.4.

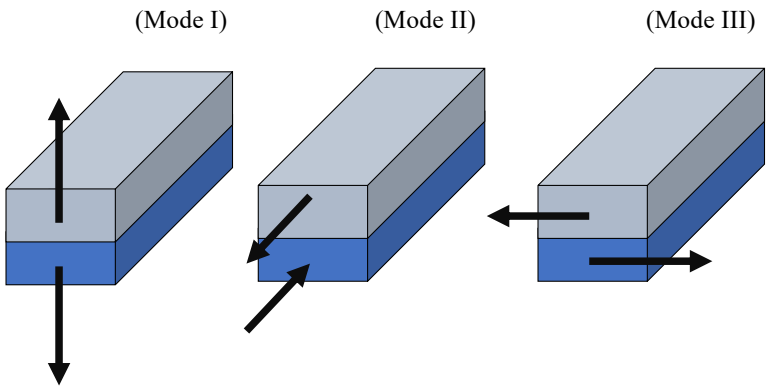

Figure 6.4: Animation describing different modes of loading conditions

While the degree of mode-II adhesion is important for describing certain fiber-matrix properties, such as delamination, it does not fully encapsulate all loading and failure conditions that fiber reinforcements may encounter. Namely, when fibers are subjected to transverse stress. More commonly, fiber-reinforced composites encounter mixed mode loading conditions (such as pulling and shearing at the same time) in which the measurement of interfacial shear strength (mode-II) is not sufficient to fully describe the mechanics of the system. Currently, there appears to be a deficit of mode-I fiber-matrix adhesion tests throughout academic literature, and the realization of such a test can prove to be helpful in trying to fully understand the micromechanics of composites.

6.3.2 *Peel testing setup*

In theory, there are multiple ways to measure mode-I adhesion. Among them, peel tests have been popular and may come in many forms. Two possible tests that can be transferred to

use for micromechanics are 90° peel tests (ASTM D6862-11)[231] and 180° peel tests (ASTM D903 − 98)[232]. Even though the accompanying ASTM manuals describe usage cases where testing samples are larger materials such as flat plates and strips of plastic, their general principles can still be used as a guide while crafting a new mode-I micromechanics test. Figure 6.5 below shows a possible design for the *single fiber peel test.*

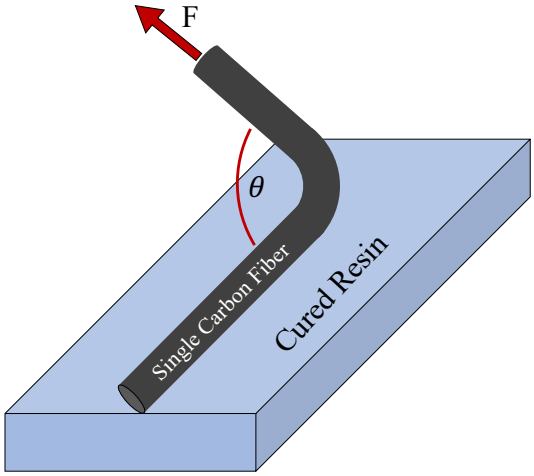

Figure 6.5: Schematic of single fiber peel test. Image not drawn to scale.

In the schematic above, a single carbon fiber will be partially embedded on a slab of cured resin and then pulled at an angle, θ, with force F to slowly peel it away from the resin. In theory, this test will measure the required peeling force for the interfacial area, which can then be related to mode-I adhesion values. However, there are a few key factors that may impact the feasibility of such a test. First, the adhesive strength between the fiber and the resin may not exceed the ultimate tensile strength of the carbon fiber itself. Second, the fiber must be precisely stationed on top of the resin as to be only partially submerged. Otherwise, the resin would fully surround the fiber, and peel tests will measure cohesive rather than adhesive failure.

Additionally, the level of fiber submersion in resin must be precise so the contact area can be reliably measured when used for adhesion calculations.

6.3.3 *Transverse tension test*

Given the difficulties of the methods above, a separate test must be used that is neither limited by the ultimate tensile strength of the fiber nor the extreme precision needed. A viable alternative to measure mode-I interfacial adhesive strength would be to embed a single fiber in cured resin where its orientation is perpendicular to the loading direction. A sample of this testing setup can be seen in Figure 6.6.

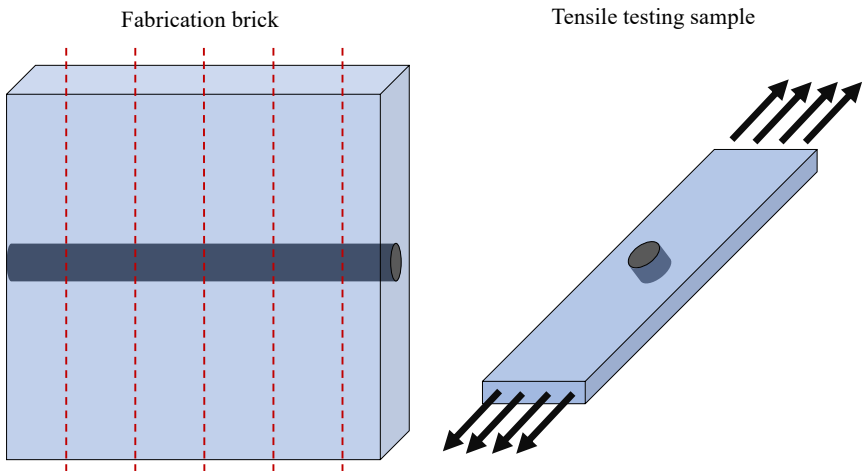

Figure 6.6: (Left) Gauge section of single fiber embedded in a large block of cured resin – referred to as fabrication brick. Red dashed lines represent where cuts would be made in the brick to create single fiber tensile samples. (Right) Gauge section of single fiber tensile samples. Note that the entire testing sample will have the shape of a dog-bone tensile specimen, as seen in Figure 2.2. Image not drawn to scale.

To perform a mode-I adhesive strength test, as shown in the figure above, multiple fabrication and testing steps must be completed. To start, a two-part inverse mold should be

machined for making the “fabrication brick” in Figure 6.6. To avoid adhering to the walls of the inverse mold, it should be made of metal coated with a releasing agent or Teflon. Additionally, the inverse of the mold should have the shape of an elongated dog-bone tensile testing specimen, where the dimensions of the gauge section should be proactively calculated to allow for proper adhesion testing to occur (i.e., the cross-sectional area should be designed to achieve needed tensile stress for testing and delamination). Finally, the two-part mold must have two small holes in the center for single fibers to be strung across, as well as have a water-tight seal to curb leakage of the liquid thermoset while curing.

For sample creation, the mold will be filled halfway with the thermoset resin, then a single fiber will be placed across and through the two small holes. Then, the top half of the mold will be placed above and filled with the rest of the resin. High-temperature tape or sealant can be used to stop resin flow and plug the two small holes where the fiber protrudes.

After the sample is cured and released from the mold, it will then be cut across its length (seen as red dotted lines in Figure 6.6) to create multiple small testing slabs. Each slab must be carefully polished on each side to ensure smoothness, optical clarity, and a uniform gauge section.

For testing, the carbon fiber segment in each sample will be viewed under a microscope while being strained at each end. The tabs of the tensile sample will be attached to a straining device, and similar to previously completed work[233,234], the stress or strain at which the sample delaminates from the cured matrix (coupled with the relevant stresses from thermal shrinkage) can later be related to the work of adhesion. Failure events can be located either by acoustic analysis, or by direct viewing under cross-polarized light. For acoustic analysis, debonding events may be perceptible, as shown in work by Nguyen and Berg[234]. Additionally, debonding

events may be perceptible under cross-polarized light through birefringence patterns located at the poles of each fiber.

In conclusion, devising a micromechanics test on single fibers to determine mode-I (sometimes referred to as transverse) adhesion may be helpful for future researchers and engineers because composites often undergo mixed mode loading conditions, and knowledge solely of mode-II adhesive strength may not fully encapsulate such loading conditions. Therefore, the more commonly tested interfacial shear strength (mode-II) may not correlate as well to the overall performance of the composite. Overall, having mode-I and mode-II adhesive strength values will give composite engineers a more detailed portrayal of composite systems and can contribute to more accurate designs.

BIBLIOGRAPHY

1. Pascault J-P, Williams RJJ. Thermosetting Polymers. In: *Handbook of Polymer Synthesis, Characterization, and Processing*. Hoboken, New Jersey: John Wiley & Sons, Ltd, pp. 519–533.
2. Gotro J, Prime RB. Thermosets. In: *Encyclopedia of Polymer Science and Technology*. Hoboken, New Jersey: John Wiley & Sons, Ltd, pp. 1–75.
3. Adabbo HE, Williams RJJ. The evolution of thermosetting polymers in a conversion–temperature phase diagram. *Journal of Applied Polymer Science* 1982; 27: 1327–1334.
4. Barton J, Hamerton I, Howlin H, et al. Studies of cure schedule and final property relationships of a commercial epoxy resin using modified imidazole curing agents. *Polymer* 1998; 39: 1929–1937.
5. Post W, Susa A, Blaauw R, et al. A Review on the Potential and Limitations of Recyclable Thermosets for Structural Applications. *Polymer Reviews* 2020; 60: 359–388.
6. Paipa-Álvarez HO, Alvarado WP, Delgado BM. Biodegradable thermosets polymers as an alternative solution to pollution generated by plastics. *J Phys: Conf Ser* 2020; 1672: 012013.
7. Ma S, Li T, Liu X, et al. Research progress on bio-based thermosetting resins. *Polymer International* 2016; 65: 164–173.
8. Liu J, Zhang L, Shun W, et al. Recent development on bio-based thermosetting resins. *Journal of Polymer Science* 2021; 59: 1474–1490.
9. Spontak RJ, Patel NP. Thermoplastic elastomers: fundamentals and applications. *Current Opinion in Colloid & Interface Science* 2000; 5: 333–340.
10. Izunobi JU, Higginbotham CL. Polymer Molecular Weight Analysis by 1H NMR Spectroscopy. *J Chem Educ* 2011; 88: 1098–1104.
11. Polymer Molecular Weight Distribution and Definitions of MW Averages, https://www.agilent.com/cs/library/technicaloverviews/Public/5990-7890EN.pdf (2015, accessed 4 February 2023).
12. Stepto RFT. Dispersity in polymer science (IUPAC Recommendations 2009). *Pure and Applied Chemistry* 2009; 81: 351–353.
13. Valente M, Rossitti I, Sambucci M. Different Production Processes for Thermoplastic Composite Materials: Sustainability versus Mechanical Properties and Processes Parameter. *Polymers* 2023; 15: 242.
14. Garofalo J, Walczyk D. In situ impregnation of continuous thermoplastic composite prepreg for additive manufacturing and automated fiber placement. *Composites Part A: Applied Science and Manufacturing* 2021; 147: 106446.

15. Jespersen ST, Wakeman MD, Michaud V, et al. Film stacking impregnation model for a novel net shape thermoplastic composite preforming process. *Composites Science and Technology* 2008; 68: 1822–1830.
16. Murray RE, Beach R, Barnes D, et al. Structural validation of a thermoplastic composite wind turbine blade with comparison to a thermoset composite blade. *Renewable Energy* 2021; 164: 1100–1107.
17. Stewart R. Thermoplastic composites — recyclable and fast to process. *Reinforced Plastics* 2011; 55: 22–28.
18. Nash NH, Young TM, McGrail PT, et al. Inclusion of a thermoplastic phase to improve impact and post-impact performances of carbon fibre reinforced thermosetting composites — A review. *Materials & Design* 2015; 85: 582–597.
19. Huang X. Fabrication and Properties of Carbon Fibers. *Materials* 2009; 2: 2369–2403.
20. The Society of Fiber Science and Techno J. Carbon Fiber. In: *High-Performance and Specialty Fibers: Concepts, Technology and Modern Applications of Man-Made Fibers for the Future*. Tokyo, JAPAN: Springer Japan, pp. 326–371.
21. Peijs T, Kirschbaum R, Lemstra PJ. Chapter 5: A critical review of carbon fiber and related products from an industrial perspective. *Advanced Industrial and Engineering Polymer Research* 2022; 5: 90–106.
22. Paris O, Loidl D, Peterlik H. Texture of PAN- and pitch-based carbon fibers. *Carbon* 2002; 40: 551–555.
23. Li D, Wang H, Wang X. Effect of microstructure on the modulus of PAN-based carbon fibers during high temperature treatment and hot stretching graphitization. *J Mater Sci* 2007; 42: 4642–4649.
24. Wazir AH, Kakakhel L. Preparation and characterization of pitch-based carbon fibers. *New Carbon Materials* 2009; 24: 83–88.
25. Naito K, Tanaka Y, Yang J-M, et al. Tensile properties of ultrahigh strength PAN-based, ultrahigh modulus pitch-based and high ductility pitch-based carbon fibers. *Carbon* 2008; 46: 189–195.
26. Vicki M. The making of carbon fiber. *Composites World*, https://www.compositesworld.com/articles/the-making-of-carbon-fiber (2008, accessed 6 February 2023).
27. Liu L, Jia C, He J, et al. Interfacial characterization, control and modification of carbon fiber reinforced polymer composites. *Composites Science and Technology* 2015; 121: 56–72.
28. Dai Z, Shi F, Zhang B, et al. Effect of sizing on carbon fiber surface properties and fibers/epoxy interfacial adhesion. *Applied Surface Science* 2011; 257: 6980–6985.
29. Drzal LT, Rich MJ, Koenig MF, et al. Adhesion of Graphite Fibers to Epoxy Matrices: II. The Effect of Fiber Finish. *The Journal of Adhesion* 1983; 16: 133–152.

30. Giraud I, Franceschi-Messant S, Perez E, et al. Preparation of aqueous dispersion of thermoplastic sizing agent for carbon fiber by emulsion/solvent evaporation. *Applied Surface Science* 2013; 266: 94–99.

31. Xiaojun M, Guangjie Z. Preparation of carbon fibers from liquefied wood. *Wood Sci Technol* 2010; 44: 3–11.

32. Wu Y, Gao X, Nguyen TT, et al. Green and Low-Cost Natural Lignocellulosic Biomass-Based Carbon Fibers—Processing, Properties, and Applications in Sports Equipment: A Review. *Polymers* 2022; 14: 2591.

33. Qiao WM, Huda M, Song Y, et al. Carbon Fibers and Films Based on Biomass Resins. *Energy Fuels* 2005; 19: 2576–2582.

34. Baker DA, Rials TG. Recent advances in low-cost carbon fiber manufacture from lignin. *Journal of Applied Polymer Science* 2013; 130: 713–728.

35. Lacombe R. Introduction. In: *Adhesion Measurement Methods: Theory and Practice*. Boca Raton, FL: CRC Press, 2005, pp. 1–6.

36. Butt MA, Chughtai A, Ahmad J, et al. Theory of adhesion and its practical implications. *Journal of Faculty of Engineering & Technology* 2008; 2007: 21–45.

37. Mittal KL. Adhesion Measurement of Thin Films. *Active and Passive Electronic Components* 1975; 3: 21–42.

38. Packham DE. Work of adhesion: contact angles and contact mechanics. *International Journal of Adhesion and Adhesives* 1996; 16: 121–128.

39. Hull T, Colligon J, Hill A. Measurement of thin film adhesion. *Vacuum* 1987; 37: 327–330.

40. Berg JC. Solid-Liquid Interactions. In: *An Introduction to Interfaces & Colloids: The Bridge to Nanoscience*. Singapore: World Scientific, 2010, pp. 214–338.

41. Wu G, Ma L, Jiang H, et al. Improving the interfacial strength of silicone resin composites by chemically grafting silica nanoparticles on carbon fiber. *Composites Science and Technology* 2017; 153: 160–167.

42. Liu F, Shi Z, Dong Y. Improved wettability and interfacial adhesion in carbon fibre/epoxy composites via an aqueous epoxy sizing agent. *Composites Part A: Applied Science and Manufacturing* 2018; 112: 337–345.

43. Meuler AJ, Smith JD, Varanasi KK, et al. Relationships between Water Wettability and Ice Adhesion. *ACS Appl Mater Interfaces* 2010; 2: 3100–3110.

44. Wenzel RN. Resistance of solid surfaces to wetting by water. *Industrial & Engineering Chemistry* 1936; 28: 988–994.

45. Cioffi MOH, Voorwald HJC, Mota RP. Surface energy increase of oxygen-plasma-treated PET. *Materials Characterization* 2003; 50: 209–215.

46. Chirila V, Marginean G, Brandl W. Effect of the oxygen plasma treatment parameters on the carbon nanotubes surface properties. *Surface and Coatings Technology* 2005; 200: 548–551.

47. Joseph K, Varghese S, Kalaprasad G, et al. Influence of interfacial adhesion on the mechanical properties and fracture behaviour of short sisal fibre reinforced polymer composites. *European Polymer Journal* 1996; 32: 1243–1250.

48. Liu Y, Zhang X, Song C, et al. An effective surface modification of carbon fiber for improving the interfacial adhesion of polypropylene composites. *Materials & Design* 2015; 88: 810–819.

49. Tiwari S, Bijwe J. Surface Treatment of Carbon Fibers - A Review. *Procedia Technology* 2014; 14: 505–512.

50. Stojcevski F, Randall JD, Henderson LC. Using variable interfacial adhesion characteristics within a composite to improve flexural strength and decrease fiber volume. *Composites Science and Technology* 2018; 165: 250–258.

51. Chen P, Lu C, Yu Q, et al. Influence of fiber wettability on the interfacial adhesion of continuous fiber-reinforced PPESK composite. *Journal of Applied Polymer Science* 2006; 102: 2544–2551.

52. Nguyen T-C, Bai Y, Zhao X-L, et al. Curing effects on steel/CFRP double strap joints under combined mechanical load, temperature and humidity. *Construction and Building Materials* 2013; 40: 899–907.

53. Lascano D, Quiles-Carrillo L, Torres-Giner S, et al. Optimization of the Curing and Post-Curing Conditions for the Manufacturing of Partially Bio-Based Epoxy Resins with Improved Toughness. *Polymers* 2019; 11: 1354.

54. Czaderski C, Martinelli E, Michels J, et al. Effect of curing conditions on strength development in an epoxy resin for structural strengthening. *Composites Part B: Engineering* 2012; 43: 398–410.

55. Min B-G, Hodgkin JH, Stachurski ZH. The dependence of fracture properties on cure temperature in a DGEBA/DDS epoxy system. *Journal of Applied Polymer Science* 1993; 48: 1303–1312.

56. Shokrieh MM, Safarabadi M. Effects of imperfect adhesion on thermal micro-residual stresses in polymer matrix composites. *International Journal of Adhesion and Adhesives* 2011; 31: 490–497.

57. Paipetis AS. Room vs. temperature studies of model composites: modes of failure of carbon fibre/epoxy interfaces. *Composite Interfaces* 2012; 19: 135–158.

58. Khoun L, Hubert P. Cure shrinkage characterization of an epoxy resin system by two in situ measurement methods. *Polymer Composites* 2010; 31: 1603–1610.

59. Haider M, Hubert P, Lessard L. Cure shrinkage characterization and modeling of a polyester resin containing low profile additives. *Composites Part A: Applied Science and Manufacturing* 2007; 38: 994–1009.

60. Zarrelli M, Skordos AA, Partridge IK. Investigation of cure induced shrinkage in unreinforced epoxy resin. *Plastics, Rubber and Composites* 2002; 31: 377–384.

61. Wang H-B, Yang Y-G, Yu H-H, et al. Assessment of residual stresses during cure and cooling of epoxy resins. *Polymer Engineering and Science* 1995; 35: 1895–1899.

62. Jakobsen J, Jensen M, Andreasen JH. Thermo-mechanical characterisation of in-plane properties for CSM E-glass epoxy polymer composite materials – Part 1: Thermal and chemical strain. *Polymer Testing* 2013; 32: 1350–1357.

63. Parlevliet PP, Bersee HEN, Beukers A. Measurement of (post-)curing strain development with fibre Bragg gratings. *Polymer Testing* 2010; 29: 291–301.

64. Shokrieh MM (ed). Understanding Residual Stresses in Polymer Matrix Composites. In: *Residual Stresses in Composite Materials*. Cambridge, UK: Woodhead Publishing, pp. 197–232.

65. Bhalerao MS. *On process-induced fiber waviness in composites: Theory and experiments*. Ph.D., The University of Texas at Austin, 1996.

66. Javid Kalantar. *The Bonding Mechanisms of Aramid Fibers to Epoxy Matrices*. Master's, Michigan State University, 1988.

67. Chang S-S. Effect of curing history on ultimate glass transition temperature and network structure of crosslinking polymers. *Polymer* 1992; 33: 4768–4778.

68. Gupta VB, Drzal LT, Lee CY-C, et al. The temperature-dependence of some mechanical properties of a cured epoxy resin system. *Polymer Engineering & Science* 1985; 25: 812–823.

69. Wang X, Xu D, Liu H-Y, et al. Effects of thermal residual stress on interfacial properties of polyphenylene sulphide/carbon fibre (PPS/CF) composite by microbond test. *J Mater Sci* 2016; 51: 334–343.

70. Pérez-Pacheco E, Moreno-Chulim MV, Valadez-González A, et al. Effect of the interphase microstructure on the behavior of carbon fiber/epoxy resin model composite in a thermal environment. *J Mater Sci* 2011; 46: 4026–4033.

71. Mostovoy S, Ripling EJ. Fracture toughness of an epoxy system. *Journal of Applied Polymer Science* 1966; 10: 1351–1371.

72. Fu K, Xie Q, Lü F, et al. Molecular Dynamics Simulation and Experimental Studies on the Thermomechanical Properties of Epoxy Resin with Different Anhydride Curing Agents. *Polymers* 2019; 11: 975.

73. Rahul R, Kitey R. Effect of cross-linking on dynamic mechanical and fracture behavior of epoxy variants. *Composites Part B: Engineering* 2016; 85: 336–342.

74. Fernandez-Nograro F, Valea A, Llano-Ponte R, et al. Dynamic and mechanical properties of DGEBA/poly(propylene oxide) amine based epoxy resins as a function of stoichiometry. *European Polymer Journal* 1996; 32: 257–266.

75. d'Almeida JRM, Menezes GW de, Monteiro SN. Ageing of the DGEBA/TETA epoxy system with off-stoichiometric compositions. *Mat Res* 2003; 6: 415–420.

76. Petersen HN, F. Minty R, Thomason JL, et al. The amine:epoxide ratio at the interface of a glass fibre/epoxy matrix system and its influence on the interfacial shear strength. *Composite Interfaces* 2019; 26: 493–505.

77. Minty RF, Yang L, Thomason JL. The influence of hardener-to-epoxy ratio on the interfacial strength in glass fibre reinforced epoxy composites. *Composites Part A: Applied Science and Manufacturing* 2018; 112: 64–70.

78. Sawicz-Kryniger K, Popielarz R. Comparison of the effectiveness of epoxy cure accelerators using a fluorescent molecular probe. *Polymer Testing* 2013; 32: 1558–1564.

79. Rich MJ, Drzal LT, Hunston DL, et al. Round Robin Assessment of the Single Fiber Fragmentation Test, https://www.nist.gov/publications/round-robin-assessment-single-fiber-fragmentation-test (2002, accessed 17 May 2021).

80. Menczel JD, Judovits L, Prime RB, et al. Differential Scanning Calorimetry (DSC). Hoboken, NJ: John Wiley & Sons, Ltd, pp. 7–239.

81. Rao V, Drzal LT. The dependence of interfacial shear strength on matrix and interphase properties. *Polymer Composites* 1991; 12: 48–56.

82. EPIKURE W Curing Agent | Aromatic Amine Curing Agent | Hexion. *Miller-Stephenson Chemicals*, https://miller-stephenson.com/product/epikure-w/ (2016, accessed 22 April 2021).

83. Burton B. Acceleration of Amine-Cured Epoxy Resin Systems. Newport, Rhode Island, 2013.

84. Evonik Resource Efficiency GmbH - Crosslinkers Product Finder, https://www.productfinder.crosslinkers.com/productCenter/productdetails.php?code=Anchor_1115 (accessed 28 June 2021).

85. EPIKURE™ Curing Agent 3253, https://www.hexion.com/en-GB/product/epikure-curing-agent-3253 (accessed 28 June 2021).

86. Nelson WB. Weibull Distribution. In: *Applied Life Data Analysis*. Hoboken, NJ: John Wiley & Sons, 2003, pp. 36–43.

87. Feih S, Wonsyld K, Minzari D, et al. *Testing Procedure for the Single Fiber Fragmentation Test*. Risø National Laboratory, https://orbit.dtu.dk/en/publications/testing-procedure-for-the-single-fiber-fragmentation-test (2004, accessed 5 February 2021).

88. Kelly A, Tyson WR. Tensile properties of fibre-reinforced metals: Copper/tungsten and copper/molybdenum. *Journal of the Mechanics and Physics of Solids* 1965; 13: 329–350.

89. Detassis M, Pegoretti A, Migliaresi C. Effect of temperature and strain rate on interfacial shear stress transfer in carbon/epoxy model composites. *Composites Science and Technology* 1995; 53: 39–46.

90. Ohsawa T, Nakayama A, Miwa M, et al. Temperature dependence of critical fiber length for glass fiber-reinforced thermosetting resins. *Journal of Applied Polymer Science* 1978; 22: 3203–3212.

91. Rutz BH. *Improvement of Mechanical Properties of Polymeric Composites*. University of Washington, 2014.

92. Tripathi D, Jones FR. Single fibre fragmentation test for assessing adhesion in fibre reinforced composites. *Journal of Materials Science* 1998; 33: 1–16.

93. Graciani E, Mantič V, París F, et al. Numerical analysis of debond propagation in the single fibre fragmentation test. *Composites Science and Technology* 2009; 69: 2514–2520.

94. Sørensen BF. Micromechanical model of the single fiber fragmentation test. *Mechanics of Materials* 2017; 104: 38–48.

95. Lacroix Th, Tilmans B, Keunings R, et al. Modelling of critical fibre length and interfacial debonding in the fragmentation testing of polymer composites. *Composites Science and Technology* 1992; 43: 379–387.

96. Feillard P, Désarmot G, Favre JP. Theoretical aspects of the fragmentation test. *Composites Science and Technology* 1994; 50: 265–279.

97. Yilmaz YI. Analyzing Single Fiber Fragmentation Test Data by Using Stress Transfer Model. *Journal of Composite Materials* 2002; 36: 537–551.

98. Drzal LT, Rich MJ, Camping JD, et al. *Interfacial Shear Strength and Failure Mechanisms in Graphite Fiber Composites.* ADA097050, Air Force Wright Aeronautical Labs., Wright-Patterson AFB, OH., https://ntrl.ntis.gov/NTRL/dashboard/searchResults/titleDetail/ADA097050.xhtml (1981, accessed 31 January 2023).

99. Kim BW, Nairn JA. Experimental verification of the effects of friction and residual stress on the analysis of interfacial debonding and toughness in single fiber composites. *Journal of Materials Science* 2002; 37: 3965–3972.

100. Luo W, Zhang B, Zou H, et al. Enhanced interfacial adhesion between polypropylene and carbon fiber by graphene oxide/polyethyleneimine coating. *Journal of Industrial and Engineering Chemistry* 2017; 51: 129–139.

101. Product Selector Guides | Hexcel, https://hexcel.com/Resources/Product-Selector-Guides/ (accessed 29 April 2021).

102. A.R. Plepys, R.J. Farris. Evolution of residual stresses in three-dimensionally constrained epoxy resins. *Polymer* 1990; 31: 1932–1936.

103. Di Landro L, Pegoraro M. Evaluation of residual stresses and adhesion in polymer composites. *Composites Part A: Applied Science and Manufacturing* 1996; 27: 847–853.

104. Jang J, Yang H. The effect of surface treatment on the performance improvement of carbon fiber/polybenzoxazine composites. *Journal of Materials Science* 2000; 35: 2297–2303.

105. Aldridge M, Wineman A, Waas A, et al. In Situ Analysis of the Relationship between Cure Kinetics and the Mechanical Modulus of an Epoxy Resin. *Macromolecules* 2014; 47: 8368–8376.

106. Zarrelli M, Skordos AA, Partridge IK. Toward a constitutive model for cure-dependent modulus of a high temperature epoxy during the cure. *European Polymer Journal* 2010; 46: 1705–1712.

107. Hale A, Macosko CW, Bair HE. Glass transition temperature as a function of conversion in thermosetting polymers. *Macromolecules* 1991; 24: 2610–2621.

108. Venditti RA, Gillham JK. A relationship between the glass transition temperature (Tg) and fractional conversion for thermosetting systems. *Journal of Applied Polymer Science* 1997; 64: 3–14.

109. Pang KP, Gillham JK. Competition between cure and thermal degradation in a high Tg epoxy system: Effect of time and temperature of isothermal cure on the glass transition temperature. *Journal of Applied Polymer Science* 1990; 39: 909–933.

110. Zhang M, Sun B, Gu B. Accelerated thermal ageing of epoxy resin and 3-D carbon fiber/epoxy braided composites. *Composites Part A: Applied Science and Manufacturing* 2016; 85: 163–171.

111. Ekbrant BEF, Skov AL, Daugaard AE. Epoxy-Rich Systems with Preference for Etherification over Amine-Epoxy Reactions for Tertiary Amine Accelerators. *Macromolecules*. Epub ahead of print 2 May 2021. DOI: 10.1021/acs.macromol.0c02630.

112. Thomason JL. Dependence of interfacial strength on the anisotropic fiber properties of jute reinforced composites. *Polymer Composites* 2010; 31: 1525–1534.

113. Zhang G, Latour RA. FRP Composite Compressive Strength and Its Dependence upon Interfacial Bond Strength, Fiber Misalignment, and Matrix Nonlinearity. *Journal of Thermoplastic Composite Materials* 1993; 6: 298–311.

114. Pukánszky B. Influence of interface interaction on the ultimate tensile properties of polymer composites. *Composites* 1990; 21: 255–262.

115. Mathijsen D. Long fiber thermoplastics are a key technology in expanding existing markets for composites. *Reinforced Plastics* 2019; 63: 267–272.

116. Ewart PaulD, Verbeek CJR. Prediction of the Flexural Modulus of Fibre Reinforced Thermoplastics for use as Kayak Paddle Blades. In: Moritz EF, Haake S (eds) *The Engineering of Sport 6*. New York, NY: Springer, 2006, pp. 107–112.

117. Starkweather HW. The surface tension of polyethylene. *Polymer Engineering & Science* 1965; 5: 5–6.

118. Xie Y, Hill CAS, Xiao Z, et al. Silane coupling agents used for natural fiber/polymer composites: A review. *Composites Part A: Applied Science and Manufacturing* 2010; 41: 806–819.

119. Park J-M, Kim P-G, Jang J-H, et al. Interfacial evaluation and durability of modified Jute fibers/polypropylene (PP) composites using micromechanical test and acoustic emission. *Composites Part B: Engineering* 2008; 39: 1042–1061.

120. Felix JM, Gatenholm P. The nature of adhesion in composites of modified cellulose fibers and polypropylene. *Journal of Applied Polymer Science* 1991; 42: 609–620.

121. Bikiaris D, Matzinos P, Larena A, et al. Use of silane agents and poly(propylene-g-maleic anhydride) copolymer as adhesion promoters in glass fiber/polypropylene composites. *Journal of Applied Polymer Science* 2001; 81: 701–709.

122. Palanikumar K. 6 - Analyzing surface quality in machined composites. In: Hocheng H (ed) *Machining Technology for Composite Materials*. Cambridge, UK: Woodhead Publishing, pp. 154–182.

123. Situ SF, Cao J, Chen C, et al. Reactive Extrusion Strategies to Fabricate Magnetite–Polyethylene Nanocomposites with Enhanced Mechanical and Magnetic Hyperthermia Properties. *Macromolecular Materials and Engineering* 2016; 301: 1525–1536.

124. Favre J, Merienne M. Characterization of fibre/resin bonding in composites using a pull-out test. *International Journal of Adhesion and Adhesives* 1981; 1: 311–316.

125. Sobczak L, Brüggemann O, Putz RF. Polyolefin composites with natural fibers and wood-modification of the fiber/filler–matrix interaction. *Journal of Applied Polymer Science* 2013; 127: 1–17.

126. He JM, Huang YD. Effect of silane-coupling agents on interfacial properties of CF/PI composites. *Journal of Applied Polymer Science* 2007; 106: 2231–2237.

127. Nachtigall SMB, Stedile FC, Felix AHO, et al. Polypropylene functionalization with vinyltriethoxysilane. *Journal of Applied Polymer Science* 1999; 72: 1313–1319.

128. Sirisinha K, Boonkongkaew M, Kositchaiyong S. The effect of silane carriers on silane grafting of high-density polyethylene and properties of crosslinked products. *Polymer Testing* 2010; 29: 958–965.

129. Maldas D, Kokta BV, Daneault C. Influence of coupling agents and treatments on the mechanical properties of cellulose fiber–polystyrene composites. *Journal of Applied Polymer Science* 1989; 37: 751–775.

130. Wu Z, Pittman CU, Gardner SD. Nitric acid oxidation of carbon fibers and the effects of subsequent treatment in refluxing aqueous NaOH. *Carbon* 1995; 33: 597–605.

131. Song W, Gu A, Liang G, et al. Effect of the surface roughness on interfacial properties of carbon fibers reinforced epoxy resin composites. *Applied Surface Science* 2011; 257: 4069–4074.

132. Jin Z, Zhang Z, Meng L. Effects of ozone method treating carbon fibers on mechanical properties of carbon/carbon composites. *Materials Chemistry and Physics* 2006; 97: 167–172.

133. Karsli NG, Aytac A. Effects of maleated polypropylene on the morphology, thermal and mechanical properties of short carbon fiber reinforced polypropylene composites. *Materials & Design* 2011; 32: 4069–4073.

134. Li S-C, Lu L-N, Zeng W. Thermostimulative shape-memory effect of reactive compatibilized high-density polyethylene/poly(ethylene terephthalate) blends by an ethylene–butyl acrylate–glycidyl methacrylate terpolymer. *Journal of Applied Polymer Science* 2009; 112: 3341–3346.

135. Jasso M, Hampl R, Vacin O, et al. Rheology of conventional asphalt modified with SBS, Elvaloy and polyphosphoric acid. *Fuel Processing Technology* 2015; 140: 172–179.

136. Coleman L, Bork J, Dunn H. Notes. Reaction of Primary Aliphatic Amines with Maleic Anhydride. *J Org Chem* 1959; 24: 135–136.

137. Li LC, Wang LL, Hao H, et al. Study of Surface Characteristics of T700 Carbon Fibers and Interfacial Properties of their Reinforced Epoxy Composites. *Applied Mechanics and Materials* 2013; 364: 706–710.

138. Li Y, Dong X, Liu Y, et al. Improvement of decay resistance of wood via combination treatment on wood cell wall: Swell-bonding with maleic anhydride and graft copolymerization with glycidyl methacrylate and methyl methacrylate. *International Biodeterioration & Biodegradation* 2011; 65: 1087–1094.

139. Li YF, Liu YX, Wang XM, et al. Improvement of Durability of Wood by Maleic Anhydride. *International Journal of Materials and Metallurgical Engineering* 2010; 4: 281–284.

140. Plueddemann EP. *Silane Coupling Agents*. Berlin, Germany: Springer Science & Business Media, 1982.

141. Salvatore J. Monte. Why Titanates and Zirconates are Different Than Silanes, https://4kenrich.com/wp-content/uploads/2020/05/CAMX-2020-why-titanates-zirconates-are-differeent-than-silanes.pdf (2021, accessed 6 August 2021).

142. Salvatore J. Monte. Why Titanates and Zirconates May Be Better Adhesion Promoters Than Silanes, https://www.pcimag.com/articles/104001-why-titanates-and-zirconates-may-be-better-adhesion-promoters-than-silanes?v=preview (2017, accessed 23 August 2021).

143. Igwe IO, Ewulonu CM, Igboanugo I. Studies on the diffusion characteristics of some aromatic solvents into polypropylene film. *Journal of Applied Polymer Science* 2006; 102: 1985–1989.

144. Bahar E, Ucar N, Onen A, et al. Thermal and mechanical properties of polypropylene nanocomposite materials reinforced with cellulose nano whiskers. *Journal of Applied Polymer Science* 2012; 125: 2882–2889.

145. Karger-Kocsis J, Mahmood H, Pegoretti A. Recent advances in fiber/matrix interphase engineering for polymer composites. *Progress in Materials Science* 2015; 73: 1–43.

146. Deng S, Ye L. Influence of Fiber-Matrix Adhesion on Mechanical Properties of Graphite/Epoxy Composites: I. Tensile, Flexure, and Fatigue Properties. *Journal of Reinforced Plastics and Composites* 1999; 18: 1021–1040.

147. Debnath S, Ranade R, Wunder SL, et al. Interface effects on mechanical properties of particle-reinforced composites. *Dental Materials* 2004; 20: 677–686.

148. Jiang D, Liu L, Long J, et al. Reinforced unsaturated polyester composites by chemically grafting amino-POSS onto carbon fibers with active double spiral structural spiralphosphodicholor. *Composites Science and Technology* 2014; 100: 158–165.

149. Lee SM. Influence of fiber/matrix interfacial adhesion on composite fracture behavior. *Composites Science and Technology* 1992; 43: 317–327.

150. Kessler A, Bledzki A. Correlation between interphase-relevant tests and the impact-damage resistance of glass/epoxy laminates with different fibre surface treatments. *Composites Science and Technology* 2000; 60: 125–130.

151. Peijs AAJM, Catsman P, Govaert LE, et al. Hybrid composites based on polyethylene and carbon fibres Part 2: influence of composition and adhesion level of polyethylene fibres on mechanical properties. *Composites* 1990; 21: 513–521.

152. Jensen RE, McKnight SH, Flanagan DP, et al. *Hybrid Fiber Sizings for Enhanced Energy Absorption in Glass-Reinforced Composites*. ARMY RESEARCH LAB ABERDEEN PROVING GROUND MD, https://apps.dtic.mil/sti/citations/ADA425481 (1 July 2004, accessed 3 March 2022).

153. Kim J-K, Sham M-L. Impact and delamination failure of woven-fabric composites. *Composites Science and Technology* 2000; 60: 745–761.

154. Cantwell WJ, Morton J. The impact resistance of composite materials — a review. *Composites* 1991; 22: 347–362.

155. Kim J-K, Sham M-L, Sohn M-S, et al. Effect of hybrid layers with different silane coupling agents on impact response of glass fabric reinforced vinylester matrix composites. *Polymer* 2001; 42: 7455–7460.

156. Carrillo-Baeza JG, Cantwell WJ, Gamboa-Castellanos RA. *Advantages of Low Energy Adhesion PP for Ballistics*. London, UK: IntechOpen. Epub ahead of print 28 March 2012. DOI: 10.5772/34995.

157. Chen S, Cao Y, Feng J. Polydopamine As an Efficient and Robust Platform to Functionalize Carbon Fiber for High-Performance Polymer Composites. *ACS Appl Mater Interfaces* 2014; 6: 349–356.

158. Chamochin R, de Santayana MC, Abenojar J, et al. The Effect of Surface Treatment on the Behavior of Toughened Acrylic Adhesive/GRP(epoxy) Composite Joints. *Journal of Adhesion Science & Technology* 2010; 24: 1903–1916.

159. Leonard GC, Hosseinpour D, Berg JC. Modulus-Graded Interphase Modifiers in E-Glass Fiber/Thermoplastic Composites. *Journal of Adhesion Science & Technology* 2009; 23: 2031–2046.

160. Nguyen FN, Saks AM, Berg JC. Use of polyethyleneimine dendrimer as a novel graded-modulus interphase material in polymeric composites. *Journal of Adhesion Science and Technology* 2007; 21: 1375–1393.

161. Ramrus DA, Berg JC. Characterization and adhesion testing of mixed silane-treated surfaces. *Journal of Adhesion Science and Technology* 2004; 18: 1395–1414.

162. De Greef N, Zhang L, Magrez A, et al. Direct growth of carbon nanotubes on carbon fibers: Effect of the CVD parameters on the degradation of mechanical properties of carbon fibers. *Diamond and Related Materials* 2015; 51: 39–48.

163. Qin W, Vautard F, Askeland P, et al. Modifying the carbon fiber–epoxy matrix interphase with silicon dioxide nanoparticles. *RSC Adv* 2014; 5: 2457–2465.

164. Javanshour F, Prapavesis A, Pärnänen T, et al. Modulating impact resistance of flax epoxy composites with thermoplastic interfacial toughening. *Composites Part A: Applied Science and Manufacturing* 2021; 150: 106628.

165. Gassan J, Dietz T, Bledzki AK. Effect of silicone interphase on the mechanical properties of flax--polyurethane composites. *Composite Interfaces* 2000; 7: 103.

166. Koolen G, Soete J, van Vuure AW. Interface modification and the influence on damage development of flax fibre – Epoxy composites when subjected to hygroscopic cycling. *Materials Today: Proceedings* 2020; 31: S273–S279.

167. Pavlidou S, Mai S, Zorbas T, et al. Mechanical properties of glass fabric/polyester composites: Effect of silicone coatings on the fabrics. *Journal of Applied Polymer Science* 2004; 91: 1300–1308.

168. Varelidis PC, McCullough RL, Papaspyrides CD. The effect on the mechanical properties of carbon/epoxy composites of polyamide coatings on the fibers. *Composites Science and Technology* 1999; 59: 1813–1823.

169. Skourlis T, Duvis T, Papaspyrides CD. The role of a polyamide interphase on carbon fibres reinforcing an epoxy matrix. *Composites Science and Technology* 1993; 48: 119–125.

170. Gerard J-F. Characterization and role of an elastomeric interphase on carbon fibers reinforcing an epoxy matrix. *Polymer Engineering & Science* 1988; 28: 568–577.

171. Labronici M, Ishida H. Toughening composites by fiber coating: a review. *Composite Interfaces* 1994; 2: 199–234.

172. Hancox NL, Wells H. The effects of fibre surface coatings on the mechanical properties of CFRP. *Fibre Science and Technology* 1977; 10: 9–22.

173. Broutman LJ, Agarwal BD. A theoretical study of the effect of an interfacial layer on the properties of composites. *Polymer Engineering & Science* 1974; 14: 581–588.

174. Barry Arkles. Silane Coupling Agents: Connecting Across Boundaries (3rd Edition), https://www.gelest.com/themencode-pdf-viewer/?file=https://www.gelest.com/wp-content/uploads/Goods-PDF-brochures-couplingagents.pdf (2014, accessed 10 August 2021).

175. Han SH, Oh HJ, Kim SS. Evaluation of fiber surface treatment on the interfacial behavior of carbon fiber-reinforced polypropylene composites. *Composites Part B: Engineering* 2014; 60: 98–105.

176. Schneberger GL (ed). Adhesives in Manufacturing. In: *Adhesives in Manufacturing*. New York: Routledge, 2018, pp. 387–392.

177. Kant ME, Crabtree JD, Young S, et al. Concept of limit stress for the tensile behavior of carbon fiber composite tows. *Composites Part B: Engineering* 2020; 201: 108384.

178. Marston C, Gabbitas B, Adams J, et al. Measurement of stress concentration around fibre breaks in carbon-fibre/epoxy-resin composite tows. *Composites Science and Technology* 1997; 57: 913–923.

179. Lee B, Leong KH, Herszberg I. Effect of Weaving on the Tensile Properties of Carbon Fibre Tows and Woven Composites. *Journal of Reinforced Plastics and Composites* 2001; 20: 652–670.

180. Cilley E, Roylance D, Schneider N. Methods of Fiber and Void Measurement in Graphite/Epoxy Composites. In: *Composite Materials: Testing and design*. Baltimore, MD: American Society for Testing and Materials, pp. 237–249.

181. Grund D, Orlishausen M, Taha I. Determination of fiber volume fraction of carbon fiber-reinforced polymer using thermogravimetric methods. *Polymer Testing* 2019; 75: 358–366.

182. Yee RY, Stephens TS. A TGA technique for determining graphite fiber content in epoxy composites. *Thermochimica Acta* 1996; 272: 191–199.

183. Kim Y, Choi C, Kumar SKS, et al. Thermo-gravimetric analysis method to determine the fiber volume fraction for PAN-based CFRP considering oxidation of carbon fiber and matrix. *Composites Part A: Applied Science and Manufacturing* 2017; 102: 40–47.

184. Carbon Fiber DataSheet | Hexcel, https://www.hexcel.com/Resources/DataSheets/Carbon-Fiber (accessed 11 February 2021).

185. Standard Test Method for Impact Testing of Miniaturized Charpy V-notch Specimens, https://www.astm.org/e2248-18.html (2018, accessed 13 September 2022).

186. ASTM D4018-17 Standard Test Methods for Properties of Continuous Filament Carbon and Graphite Fiber Tows, https://www.astm.org/d4018-17.html (2017, accessed 9 August 2022).

187. ASTM D7264/D7264M-21 Standard Test Method for Flexural Properties of Polymer Matrix Composite Materials, https://www.astm.org/Standards/D7264.htm (2021, accessed 22 July 2022).

188. Sheikhi MR, Gürgen S. Anti-impact design of multi-layer composites enhanced by shear thickening fluid. *Composite Structures* 2022; 279: 114797.

189. Khodadadi A, Liaghat G, Taherzadeh-Fard A, et al. Impact characteristics of soft composites using shear thickening fluid and natural rubber–A review of current status. *Composite Structures* 2021; 271: 114092.

190. Talreja K, Ghosh A, Arora S, et al. Tailoring the Rheology of Shear Thickening Fluids by Regulating the Particle Size of Dispersed Phase for Enhancing the Impact Resistance of Aramid Fabrics. *Fibers Polym* 2022; 23: 1300–1308.

191. Jafari SH, Gupta AK. Impact strength and dynamic mechanical properties correlation in elastomer-modified polypropylene. *Journal of Applied Polymer Science* 2000; 78: 962–971.

192. Kim BW, Nairn JA. Observations of Fiber Fracture and Interfacial Debonding Phenomena Using the Fragmentation Test in Single Fiber Composites. *Journal of Composite Materials* 2002; 36: 1825–1858.

193. Pupurs A, Goutianos S, Brondsted P, et al. Interface debond crack growth in tension–tension cyclic loading of single fiber polymer composites. *Composites Part A: Applied Science and Manufacturing* 2013; 44: 86–94.

194. Nishikawa M, Okabe T, Takeda N, et al. Micromechanics of the fragmentation process in single-fiber composites. *Modelling Simul Mater Sci Eng* 2008; 16: 055009.

195. Dronamraju N, Solass J, Hildebrand J. Studies of fiber-matrix debonding. *Front Struct Civ Eng* 2015; 9: 448–456.

196. Zhuang L. *Fiber/matrix interface crack propagation in polymeric unidirectional composite*. Luleå University of Technology, Department of Engineering Sciences and Mathematics, Material Science., http://urn.kb.se/resolve?urn=urn:nbn:se:ltu:diva-17391 (2016, accessed 2 August 2022).

197. Drzal LT, Madhukar M. Fibre-matrix adhesion and its relationship to composite mechanical properties. *J Mater Sci* 1993; 28: 569–610.

198. Álvarez-García S, Martín-Martínez JM. Effect of the carbon black content on the thermal, rheological and mechanical properties of thermoplastic polyurethanes. *Journal of Adhesion Science & Technology* 2015; 29: 1136–1154.

199. Campbell JS, Grace JR, Lim CJ, et al. A new diagnostic when determining the activation energy by the advanced isoconversional method. *Thermochimica Acta* 2016; 636: 85–93.

200. Laidler KJ. The development of the Arrhenius equation. *J Chem Educ* 1984; 61: 494.

201. Brown ME, Galwey AK. The distinguishability of selected kinetic models for isothermal solid-state reactions. *Thermochimica Acta* 1979; 29: 129–146.

202. Brown ME, Dollimore D, Galwey AK. *Reactions in the Solid State*. Elsevier, 1980.

203. Vyazovkin S, Wight CA. Kinetics in solids. *Annu Rev Phys Chem* 1997; 48: 125–149.

204. Borchardt HJ, Daniels F. The Application of Differential Thermal Analysis to the Study of Reaction Kinetics1. *ACS Publications*. Epub ahead of print 1 January 1957. DOI: 10.1021/ja01558a009.

205. Kandelbauer A, Wuzella G, Mahendran A, et al. Model-free kinetic analysis of melamine–formaldehyde resin cure. *Chemical Engineering Journal* 2009; 152: 556–565.

206. Wan J, Zhao J, Zhang X, et al. Epoxy thermosets and materials derived from bio-based monomeric phenols: Transformations and performances. *Progress in Polymer Science* 2020; 108: 101287.

207. Ng F, Couture G, Philippe C, et al. Bio-Based Aromatic Epoxy Monomers for Thermoset Materials. *Molecules* 2017; 22: 149.

208. Zhang S, Wang Z, Rafique I, et al. Room-temperature fast-curing polybenzoxazine hybrid thermosets via UV irradiation. *European Polymer Journal* 2022; 162: 110871.

209. Odom MGB, Sweeney CB, Parviz D, et al. Rapid curing and additive manufacturing of thermoset systems using scanning microwave heating of carbon nanotube/epoxy composites. *Carbon* 2017; 120: 447–453.

210. Mgbemena CO, Li D, Lin M-F, et al. Accelerated microwave curing of fibre-reinforced thermoset polymer composites for structural applications: A review of scientific challenges. *Composites Part A: Applied Science and Manufacturing* 2018; 115: 88–103.

211. Thostenson ET, Chou T-W. Microwave and conventional curing of thick-section thermoset composite laminates: Experiment and simulation. *Polymer Composites* 2001; 22: 197–212.

212. Naik TP, Singh I, Sharma AK. Processing of polymer matrix composites using microwave energy: A review. *Composites Part A: Applied Science and Manufacturing* 2022; 156: 106870.

213. Antonucci V, Giordano M, Cusano A, et al. Real time monitoring of cure and gelification of a thermoset matrix. *Composites Science and Technology* 2006; 66: 3273–3280.

214. Vafayan M, Hosain Beheshty M, Ghoreishy MHR, et al. Advanced integral isoconversional analysis for evaluating and predicting the kinetic parameters of the curing reaction of epoxy prepreg. *Thermochimica Acta* 2013; 557: 37–43.

215. Vyazovkin S. *Isoconversional Kinetics of Thermally Stimulated Processes*. Berlin, Germany: Springer, 2015.

216. Vyazovkin S, Sbirrazzuoli N. Isoconversional Kinetic Analysis of Thermally Stimulated Processes in Polymers. *Macromolecular Rapid Communications* 2006; 27: 1515–1532.

217. Vyazovkin S, Burnham AK, Criado JM, et al. ICTAC Kinetics Committee recommendations for performing kinetic computations on thermal analysis data. *Thermochimica Acta* 2011; 520: 1–19.

218. Vyazovkin S. Model-free kinetics: Staying free of multiplying entities without necessity. *Journal of Thermal Analysis and Calorimetry* 2006; 83: 45–51.

219. Friedman HL. Kinetics of thermal degradation of char-forming plastics from thermogravimetry. Application to a phenolic plastic. *Journal of Polymer Science Part C: Polymer Symposia* 1964; 6: 183–195.

220. Vyazovkin S. Modification of the integral isoconversional method to account for variation in the activation energy. *Journal of Computational Chemistry* 2001; 22: 178–183.

221. Golikeri SV, Luss D. Analysis of activation energy of grouped parallel reactions. *AIChE Journal* 1972; 18: 277–282.

222. Flynn JH, Wall LA. General Treatment of the Thermogravimetry of Polymers. *J Res Natl Bur Stand A Phys Chem* 1966; 70A: 487–523.

223. Ozawa T. A New Method of Analyzing Thermogravimetric Data. *BCSJ* 1965; 38: 1881–1886.

224. Coats AW, Redfern JP. Kinetic Parameters from Thermogravimetric Data. *Nature* 1964; 201: 68–69.

225. Kissinger HE. Reaction Kinetics in Differential Thermal Analysis. *Anal Chem* 1957; 29: 1702–1706.

226. Zheng C, Li D, Ek M. Mechanism and kinetics of thermal degradation of insulating materials developed from cellulose fiber and fire retardants. *Journal of Thermal Analysis and Calorimetry* 2019; 135: 3015–3027.

227. Fox DM, Gilman JW, De Long HC, et al. TGA decomposition kinetics of 1-butyl-2,3-dimethylimidazolium tetrafluoroborate and the thermal effects of contaminants. *The Journal of Chemical Thermodynamics* 2005; 37: 900–905.

228. Liu B, Xu T, Xu X, et al. Energy absorption mechanism of polyvinyl butyral laminated windshield subjected to head impact: Experiment and numerical simulations. *International Journal of Impact Engineering* 2016; 90: 26–36.

229. Qi Y, Jiang D, Ju S, et al. Determining the interphase thickness and properties in carbon fiber reinforced fast and conventional curing epoxy matrix composites using peak force atomic force microscopy. *Composites Science and Technology* 2019; 184: 107877.

230. Niu Y-F, Yang Y, Gao S, et al. Mechanical mapping of the interphase in carbon fiber reinforced poly(ether-ether-ketone) composites using peak force atomic force microscopy: Interphase shrinkage under coupled ultraviolet and hydro-thermal exposure. *Polymer Testing* 2016; 55: 257–260.

231. Standard Test Method for 90 Degree Peel Resistance of Adhesives, https://compass.astm.org/document/?contentCode=ASTM%7CD6862-11R21%7Cen-US (2021, accessed 25 January 2023).

232. Standard Test Method for Peel or Stripping Strength of Adhesive Bonds, https://compass.astm.org/document/?contentCode=ASTM%7CD0903-98R17%7Cen-US (2017, accessed 25 January 2023).

233. Harding PH, Berg JC. The characterization of interfacial strength using single-particle composites. *Journal of Adhesion Science and Technology* 1997; 11: 1063–1076.

234. Nguyen FN, Berg JC. The effect of vinyl alcohol content on adhesion performance in poly(vinyl butyral)/glass systems. *Journal of Adhesion Science & Technology* 2004; 18: 1011–1026.

VITA

Luke Georges El Khoury was born and raised in Long Beach, California. He has two brothers, Dimitri, and Constantino, and his parents are Rebecca and Georges. From 2010-2014, he attended Woodrow Wilson Classical high school in Long Beach, California and concurrently competed as a varsity rower on the local crew team. During that time, he won the 2013 youth men's 4+ at the Head of the Charles regatta, the 2014 youth men's 8+ national championship title. Additionally, he joined the USA junior men's national rowing team in 2013 and 2014 to compete at the youth world championship race in Trakai, Lithuania, and Hamburg, Germany, respectively.

Afterwards he attended University of Washington for his undergraduate degree in Chemical Engineering. As in high school, he also joined the D1 varsity men's crew team at UW where he competed all four years. During his time as an athlete, he won three PAC-12 titles, and two national championship titles. Moreover, senior year of his undergraduate degree, he explored his love for science and experimentation by joining Dr. John C. Berg's research group.

For graduate school, he decided to join Dr. Berg's research team once again, but as a PhD student – where composite materials, adhesion, and interfaces were the central themes of his thesis. On top of research, he taught CHEME 455," Surface and Colloid Science Laboratory" a total of five separate times. Teaching and interacting with undergraduate students were some of the highlights of his time in graduate school.

Other activities that Luke enjoys outside of school are reading (favorite book, *East of Eden* by John Steinbeck), exercising, teaching, long walks on the beach, discussing philosophy, eating spicy food, traveling the world, and learning foreign languages.